January 2009

Investigations into Building Block Structure and Method of Preparation on the Properties of Nanomaterials

Zicheng Li
Washington University in St. Louis

WASHINGTON UNIVERSITY IN ST. LOUIS

Department of Chemistry

Dissertation Examination Committee:
Karen L. Wooley, Chair
William E. Buhro
John-Stephen A. Taylor
André d'Avignon
Jeffrey R. Leonard
Sheila A. Stewart

Investigations into Building Block Structure and Method of Preparation on the Properties of Nanomaterials

by

Zicheng Li

A dissertation presented to the
Graduate School of Arts and Sciences
of Washington University in
partial fulfillment of the
requirements for the degree
of Doctor of Philosophy

August 2009

Saint Louis, Missouri

ABSTRACT OF THE DISSERTATION

Investigations into Building Block Structure and Method of Preparation on the Properties of Nanomaterials

By

Zicheng Li

Doctor of Philosophy in Chemistry

Washington University in Saint Louis, 2009

Professor Karen L. Wooley, Chairperson

This dissertation research is primarily focused on the preparation of polymer-based nanostructures as potential diagnostic agents and therapeutics delivery vehicles. Various polymers, nanoparticles and conjugation techniques were developed to meet the specific requirements of each application.

Shell crosslinked nanoparticles (SCKs) are characterized by their structural integrity and available functionality to attach multiple agents on the shell, such as receptor-recognizing or receptor-specific ligands, .imaging agents, Cell transduction components, etc. In this work, SCKs derived from amphiphilic poly(acrylic acid)-*block*-polystyrene (PAA-*b*-PS) have been studied as potential diagnostic and therapeutic agent delivery vehicles (Chapters 2 and 4). SCK nanoparticles bearing a cyclic KCRGDC peptide which specifically binds to $\alpha_v\beta_3$ integrin receptor were developed as potential delivery system for treatment of acute vascular injuries. Methods were developed to

afford “clean” nanoparticles with significant binding abilities. Nanoscale contrast agents for magnetic resonance imaging were also developed based on SCKs derived from PAA-*b*-PS and a Gadolinium-DOTA complex to achieve high relaxivity contrast agents. Our results showed that SCKs may serve well as potential diagnostic and therapeutic agent delivery vehicles Meanwhile, these SCKs were also studied as the template for mineralization of silver nanoparticles, along with a nuleating peptide, AG-P35, as a co-template (Chapter 5). Various morphologies of silver nanoparticles were obtained and it’s found that the morphology was highly dependent on polymer and peptide concentrations and incubation time.

Micelles from a novel hyperbranched fluoropolymer with small sizes able to pass the blood brain barrier were synthesized (Chapter 3). After conjugation with F3 peptide which targets to nucleolin in most tumor cells, and loaded with doxorubicin as the drug to kill the tumor cells, both *in vitro* and *in vivo* studies were performed. It was found that F3-peptide conjugated nanoparticle not only specifically bind to the tumor-associated angiogenic endothelial cells, doxorubicin carried by these nanoparticles also caused apoptotic effects on the targeted tumor cells.

To my grandfather, Daoyin Li

ACKNOWLEDGEMENTS

I wish to thank my advisor Professor Karen L. Wooley for leading me to the wonderful world of macromolecules and offering me the opportunity to explore freely in a huge research space. Her scientific guidance and encouragement helped me walking through the barriers in my journey, without which I would not have been able to finish this dissertation. Her passion for science has been passed onto me and those before me. I thank Karen for serving as my advisor in the past five years and teaching me beyond science as well.

I would also like to express my gratitude to my Ph. D. advisory committee members Professor William E. Buhro and Professor John-Stephen A. Taylor for their invaluable suggestions in guiding my work to a final destination. I am very grateful to Professor Sheila A. Stewart, Professor Jeffrey R. Leonard and Dr. André d'Avignon for serving on my defense committee and spending their precious time reading my dissertation.

My work at Wash U was not alone and was accompanied by wonderful group members. I would like to thank all the former and current Wooley group members, Dr. Jinqi Xu, Dr. Guorong Sun, Dr. Wenjun Du, Dr. Yali Li, Dr. Andreas Nyström, Mr. Jun Ma, Mr. Ke Zhang, Mr. Nam Lee, Mr. Jeremy W. Bartels, not to mention all, for their kind help and for creating a joyful environment to work in. Collaboration has been throughout my work, it’s my great pleasure to work with Ms. Ashley L. Fiamengo, Dr. Debasish Banerjee, Dr. Jie Zheng and all other collaborators. Many thanks to Professor

Joseph J.H. Ackerman and Dr. Joel R. Garbow for their helpful suggestions with the development of MRI contrast agents. I would also like to thank Dr. Ed Hiss, Dr. Kit Mao, Ms. Norma Taylor for their kind help in the past few years..

Finally, I would like to say a huge thank you to my parents for their endless love and support. Also, my brother and sister deserve recognition and I thank them for the love and support to me and to the family.

TABLE OF CONTENTS

List of Figures

Chapter 2.

List of Schemes

List of Tables

Chapter 2.

Chapter 3.

$AgNO_3$ addition. For experiments 1 - 5, the final volumes were adjusted to 8 mL by addition of nanopure water. For experiment 6, the final volume was adjusted to 5 mL by addition of nanopure water.

GLOSSARY OF TERMS AND ABBREVIATIONS

AFM	Atomic force microscopy
ATRP	Atom transfer radical polymerization
DLS	Dynamic light scattering
DOTA	1,4,7,10-Tetraazacyclodecane-N,N’,N”,N”’-tetraacetic acid
DSC	Differential scanning calorimetry
DTPA	Diethylenetriaminepentaacetic acid
EDCI	1-[3’(Dimethylamino)propyl]-3-ethylcarbodiimide methiodide
FPLC	Fast protein liquid chromatography
GPC	Gel permeation chromatography
ICP-MS	Inductively-coupled plasma-mass spectroscopy
MHz	Megaherz
MRI	Magnetic resonance imaging
MWCO	Molecular weight cut-off
NNLS	Non-negatively linear least squares
PAA	Poly(acrylic acid)
PBS	Phosphate buffer saline
PDI	Polydispersity index
PEG	Poly(ethylene glycol)
PET	Positron emission tomography
PMA	Poly(methyl acrylate)

PS	Polystyrene
P*t*BA	Poly(*tert*-butyl acrylate)
SCKs	Shell crosslinked (knedel-like) nanoparticles
SEM	Scanning electron microscopy
TEM	Transmission electron microscopy
TFA	Trifluoacetic acid
TGA	Thermogravimetric analysis
UV-vis	Ultraviolet-*visible*

Chapter 1

Introduction

Nanotechnologies are materials and devices that have a functional organization in at least one dimension on the nanometer scale, ranging from a few to about 100 nanometers.[1] Nature has given us numerous examples of building complex supramolecular structures using nanoscale objects to achieve a variety of efficient functions. Metallo-porphyrins, a class of small molecules that are involved in the photosynthesis of plants, have sizes around 1 nm; DNA, the material containing all the genetic information of life, has a size around 2 nm; proteins have size around 10 nm. The essence of chemical science finds its full expression in the words of that epitome of the artist-scientist Leonardo da Vinci: "Where Nature finishes producing its own species, man begins, using natural things and with the help of this nature, to create an infinity of species".[2] The elegance of nature in building complex structure has stimulated many scientists to construct man-made materials and devices that mimic nature, and with potential for sensing, catalysis, transport, and other applications in medicinal or engineering science.[3-9] Unique properties were found not only in inorganic nanomaterials, but also in organic/polymeric nanomaterials. The discovery of crown ether,[10, 11] and the subsequent studies in designing more complex cyclic molecules to

recognize positive ions are the first demonstrations of man-made organic materials that can self-assemble into complex structures, known as host-guest chemistry[12] or supramolecular chemistry[13], and the size of the building blocks is at the molecular level (less than 2 nm).

Self-assembly, defined as "the autonomous organization of components into patterns or structures without human intervention",[14] is a very common process occurring in nature, such as the self-assembly of amphiphilic poly-peptides into proteins with complex supramolecular structures and functionalities and biomineralization processes.[15] Inspired by this, material mimics have been synthesized using natural or unnatural building blocks to form supramolecular assemblies with unique optical, electric, catalytic and biological properties, such as synthetic polypeptide,[16] peptides amphiphiles,[17] giant amphiphiles,[18] DNA assemblies,[19] and synthetic oligomers or polymers.[20, 21]

Amphiphilic block copolymers are among the synthetic amphiphiles for the construction of supramolecular assemblies.[22] The self-assembly of amphiphilic block copolymers can generate a variety of morphologies, such as spheres, rod, vesicles, lamellas and toroids,[23] which offers a broad selection of building blocks for the construction of nanostructured materials as well as their use in biomedical applications.[24]

Since its first development for drug delivery purposes and for vaccines in the late 1960s,[25] nanoparticles for pharmaceutical and medical application were studied intensively, taking advantage of the enhanced permeability and retention effect (EPR

effect).[26-28] Nanoparticles were demonstrated to be able to improve the delivery of anticancer drugs,[29] antiinfective drugs,[30-32] as well as nucleic acids, DNA fragments and genes,[33-35] and for the treatment of AIDS.[36, 37] Among all these, the most important application of nanoparticles is considered to be their employment for cancer therapy.

Current cancer therapy usually involves intrusive processes including application of catheters to allow chemotherapy, initial chemotherapy to shrink any cancer present, surgery to then remove the tumor(s) if possible, followed by more chemotherapy and radiation. The purpose of the chemotherapy and radiation is to kill the tumor cells as these cells are more susceptible to the actions of these drugs and methods because of their growth at a much faster rate than healthy cells, at least in adults.[38] Current research areas include development of carriers to allow alternative dosing routes, new therapeutics targeting blood vessels fueling tumor growth and targeted therapeutics that are more specific in their activity. In all cases, the effectiveness of the treatment is directly related to the treatment's ability to target and to kill the cancer cells while affecting as few healthy cells as possible. Nanoparticles will usually be taken up by the liver, spleen and other parts of the reticuloendothelial system (RES) mainly depending on their surface characteristics.[39, 40] Usually, particles with long circulation times, and hence greater ability to target to the site of interest, should be 100 nm or less in diameter and have a hydrophilic surface in order to reduce clearance by macrophages.[41] Angiogenesis is a physiological process involving the growth of new blood vessels from existing

vasculature,[42] and is especially vital to the continued development of a tumor mass from a dormant state to a malignant one.[43-45] Angiogenesis is a multi-step, invasive process, characterized by endothelial cell proliferation, modulation of the extracellular matrix (ECM), and cell adhesion/migration. Among the many angiogenic factors, integrin $\alpha_v\beta_3$ has been found to be necessary for the formation, survival, and maturation of new blood vessels.[46] The tripeptide sequence arginine-glycine-aspartic acid (RGD) is common to various ECM proteins, e.g. vitronectin, fibronectin, fibrinogen, thrombospondin, and von-Willebrand factor, involved in cell-matrix adhesion.[47, 48] High-affinity $\alpha_v\beta_3$ selective ligands containing RGD have been identified by phage display.[49] Targeted chemotherapy has been investigated using RGD peptides to deliver doxorubicin[50] and proapoptotic peptides[51] to tumor vasculature. In vivo imaging of sites of angiogenesis has been demonstrated using RGD-containing peptides.[52, 53] Since the RGD-sequence is conserved in all native ligands, differences in binding affinities and specificity can be obtained from slight modifications of the peripheral structure of the RGD motif. The flanking amino acid residues, especially the two positions following the aspartic acid, are known to change binding affinity both by direct interaction of the residues with the integrin as well as influencing peptide folding.[54] Cyclization is a common technique to improve binding properties because it confers rigidity on the structure.[55] All selective RGD peptides have at least one ring structure. Linear RGD peptides are highly susceptible to degradation, due to reaction of the aspartic acid residue with the peptide

backbone.[56] Non-natural peptide modifications, such as the introduction of D-amino acids and replacement with peptidomimetic structures, have yielded RGD peptide ligands with greater specificity and nanomolar or higher affinities.[57] Multivalent RGD-protein conjugates demonstrate subnanomolar affinity for $\alpha_v\beta_3$-expressing human umbilical vein endothelial cells (HUVEC), a 250-fold increase verses the monomer.[58] Furthermore, multivalency has been shown to facilitate internalization.[59] Carrier systems like liposomes, nanoparticles, and proteins bearing multiple RGD peptides are, therefore, more likely to be internalized *via* receptor-mediated endocytosis than single peptide constructs.

Shell cross-linked nanoparticles (SCKs), a class of well-defined, polymeric, nanostructured materials, constitute a unique class of materials with amphiphilic core-shell morphology.[60-62] SCKs are characterized by their structural integrity and available functionality to attach receptor-recognizing or receptor-specific ligands on the shell. Studies have been reported on incorporating bioactive molecules, such as biotin and folate, for imaging and radiotherapy purposes.[63, 64]

In this dissertation work, SCKs prepared from the amphiphilic block copolymer, poly(acrylic acid)-*b*-polystyrene (PAA-*b*-PS) have been selected as the carrier for a cyclic peptide KCRGDC, to act as the nano-agent to target $\alpha_v\beta_3$ integrin receptors for treatment of acute vascular injuries (Chapter 2). These SCKs were functionalized with poly(ethylene glycol) (PEG) as a means to achieve prolonged blood retention time.

DOTAlysine (a derivative of DOTA, 1,4,7,10-tetraazacyclodecane-N,N',N",N"'-tetraacetic acid, with a lysine arm attached, chemical structure available in Chapter 2) was also labeled onto the SCKs as the chelator for radionuclide for position emission tomography (PET) imaging. Methods have been developed to afford clean RGD-labeled SCKs (in terms of contamination of free KCRGDC peptide) with significantly enhanced in. $\alpha_v\beta_3$. Cell internalization studies with U87MG glioma cells showed significant internalization of these RGD-labeled nanoparticles.

One of the most promising applications of nanoparticles is their use for the transport of drugs across the blood-brain barrier (BBB). The central nervous system (CNS) is the most common site of primary solid tumors in children.[65-68] Glioblastoma multiforme (GBM) is a highly malignant tumor in central nerve system.[69, 70] Patients diagnosed with GBM usually live less than one year after surgery despite intensive chemotherapy and radiation.[71] One of the biggest challenges for treating these patients is lack of effective therapeutics that could efficiently pass BBB and specifically target to the tumor site.[72-75] It's reported that nanoparticles with certain targeting ligands can gain access in the brain via a number of possible mechanisms, such as adsorption, receptor mediated endocytosis, transcytosis, membrane permeabilization effect, or disrupting the BBB.[76]. In Chapter 3, micelles from a novel star-like amphiphilic fluorinated block copolymer[77] with hydrodynamic diameters around 30 nm have been conjugated with an F3 peptide

(specifically targets to nucleolin) and loaded with doxorubicin as the drug to treat tumor cells in the brain of U87MG xenograft mice. Specific targeting to U87MG glioma cells were observed for these micelles. In vivo studies with U87MG mice indicated the ability of these micelles to cross the BBB. It was found that F3-peptide conjugated nanoparticle not only specifically bind to the tumor-associated angiogenic endothelial cells, doxorubicin carried by these nanoparticles also caused apoptotic effects on the targeted tumor cells. PEGylation was found to enhance the biodistribution of these materials by affording an improved blood retention time. This system showed potential to not only provide a novel approach to efficiently deliver therapeutics to the targeted tumor site, it can also potentially attenuate systemic side effects caused by free doxorubicin.

Besides targeting and therapeutic agents, imaging modalities such as contrast agents for magnetic resonance imaging (MRI) were also labeled to PAA-*b*-PS based SCKs. MRI measures the NMR signals of nuclei, mainly protons of water. The differences in signal intensity can create contrast in the images, thereby enabling differentiation of the types of tissues and detection of disease states.[78] MRI has been advanced by the development of contrast agents that enable more specific and clearer images and enlargements of detectable organs and systems, leading to a wide scope of applications of MRI not only for diagnostic radiology but also for therapeutic medicine.[79] The ability of the contrast agent to enhance the longitudinal relaxation rate ($1/T_1$) of the solvent (mostly water) is referred to as the longitudinal relaxivity, R. Current

T_1 MRI contrast agents are mainly in the form of paramagnetic metal complexes.[80] A common approach to enhance the T_1 relaxivities is to attach the complex to slow tumbling macromolecules.[81] In Chapter 4, gadolinium (Gd) based nanoscale CAs were developed from attaching the complex of Gd with DOTAlysine to achieved enhanced relaxivities. Methods have been developed to afford nanoparticles without the highly toxic free Gd^{3+} ions. The results indicated enhanced relaxivities compared to the small Gd-DOTAlysine complex. It is found that T_1 relaxivities increased as the extent of crosslinking of the micelles increased. With the good blood pool imaging capabilities, and potential for active targeting (as described in previous chapters), as well as the enhanced T_1 relaxivities, SCKs have the potential to serve as a promising candidate for *in vivo* MRI imaging.

In this work, SCK nanoparticles were also studied as the template for the growth of silver nanoparticles. Because of their intriguing optical, electronic, magnetic and mechanical properties,[82-85] silver nanoparticles have been intensively studied. Controlling the size of nanocrystals is of particular interest because of the effect these parameters have on the observed properties of the nanocrystals. Various macromolecules and their assemblies, such as viruses and proteins, polymers, porous polymer matrices, microemulsions, starch vermicelli and cellulose, have been studied as templates to grow inorganic nanoparticles.[86-90] Synthetic peptides binding to certain faces of inorganic nanocrystals are also being developed to direct the growth of inorganic nanoparticles.[91, 92] In Chapter 5, SCKs prepared from poly(acrylic acid)-*b*-poly(methyl

acrylate) and peptide AG-35 (binds to (111) of silver) were studied as the template to grow silver nanoparticles. Silver nanospheres, nanoplates, nano-flowers were obtained under varied conditions.

.

References

1. Silva, G., Nanotechnology approaches to crossing the blood-brain barrier and drug delivery to the CNS. *BMC Neuroscience* **2008,** *9* (Suppl 3), S4.

2. Christof, M. N., Nanoparticles, Proteins, and Nucleic Acids: Biotechnology Meets Materials Science. *Angew. Chem. Int. Ed.* **2001,** *40* (22), 4128-4158.

3. Stankic, S.; Sterrer, M.; Hofmann, P.; Bernardi, J.; Diwald, O.; Knozinger, E., Novel Optical Surface Properties of Ca^{2+}-Doped MgO Nanocrystals. *Nano Lett.* **2005,** *5* (10), 1889-1893.

4. Daniel, M.-C.; Astruc, D., Gold Nanoparticles: Assembly, Supramolecular Chemistry, Quantum-Size-Related Properties, and Applications toward Biology, Catalysis, and Nanotechnology. *Chem. Rev.* **2004,** *104* (1), 293-346.

5. Hu, M.; Chen, J.; Li, Z.-Y.; Au, L.; Hartland, G. V.; Li, X.; Marquez, M.; Xia, Y., Gold nanostructures: engineering their plasmonic properties for biomedical applications. *Chem. Soc. Rev.* **2006,** *35* (11), 1084-1094.

6. Zheng, N.; Stucky, G. D., A General Synthetic Strategy for Oxide-Supported Metal Nanoparticle Catalysts. *J. Am. Chem. Soc.* **2006,** *128* (44), 14278-14280.

7. Alan, G. M., "Synthetic Metals": A Novel Role for Organic Polymers (Nobel Lecture) *Angew. Chem. Int. Ed.* **2001,** *40* (14), 2581-2590.

8. Huang, C.-C.; Chang, H.-T., Selective Gold-Nanoparticle-Based "Turn-On" Fluorescent Sensors for Detection of Mercury(II) in Aqueous Solution. *Anal. Chem.* **2006,** *78* (24), 8332-8338.

9. Yu, H.; Li, J.; Loomis, R. A.; Wang, L.-W.; Buhro, W. E., Two- versus three-dimensional quantum confinement in indium phosphide wires and dots. *Nat. Mater.* **2003,** *2* (8), 517-520.

10. Pedersen, C. J., Cyclic polyethers and their complexes with metal salts. *J. Am. Chem. Soc.* **1967,** *89* (10), 2495-2496.

11. Pedersen, C. J., Cyclic polyethers and their complexes with metal salts. *J. Am. Chem. Soc.* **1967,** *89* (26), 7017-7036.

12. Cram, D. J. C. a. J. M., Host-Guest Chemistry: Complexes between organic compounds simulate the substrate selectivity of enzymes *Science* **1974,** *183* (4127), 803-809.

13. Lehn, J.-M., Toward complex matter: Supramolecular chemistry and self-organization. *Proc. Natl. Acad. Sci. U. S. A.* **2002,** *99* (8), 4763-4768.

14. Whitesides, G. M.; Grzybowski, B., Self-Assembly at All Scales. *Science* **2002,** *295*

(5564), 2418-2421.

15. Douglas, P.; Stoddart, J. F., Self-Assembly in Natural and Unnatural Systems. *Angew. Chem. Int. Ed.* **1996,** *35* (11), 1154-1196.

16. Nowak, A. P.; Breedveld, V.; Pakstis, L.; Ozbas, B.; Pine, D. J.; Pochan, D.; Deming, T. J., Rapidly recovering hydrogel scaffolds from self-assembling diblock copolypeptide amphiphiles. *Nature* **2002,** *417* (6887), 424-428.

17. Hartgerink, J. D.; Beniash, E.; Stupp, S. I., Peptide-amphiphile nanofibers: A versatile scaffold for the preparation of self-assembling materials. *Proc. Natl. Acad. Sci. U. S. A.* **2002,** *99* (8), 5133-5138.

18. Velonia, K.; Rowan, A. E.; Nolte, R. J. M., Lipase Polystyrene Giant Amphiphiles. *J. Am. Chem. Soc.* **2002,** *124* (16), 4224-4225.

19. Seeman, N. C.; Belcher, A. M., Emulating biology: Building nanostructures from the bottom up. *Proc. Natl. Acad. Sci. U. S. A.* **2002,** *99* (Suppl 2), 6451-6455.

20. Percec, V.; Dulcey, A. E.; Balagurusamy, V. S. K.; Miura, Y.; Smidrkal, J.; Peterca, M.; Nummelin, S.; Edlund, U.; Hudson, S. D.; Heiney, P. A.; Duan, H.; Magonov, S. N.; Vinogradov, S. A., Self-assembly of amphiphilic dendritic dipeptides into helical pores. *Nature* **2004,** *430* (7001), 764-768.

21. Rint P. Sijbesma, F. H. B., Luc Brunsveld, Brigitte J. B. Folmer, J. H. K. Ky Hirschberg, Ronald F. M. Lange, Jimmy K. L. Lowe, E. W. Meijer, Reversible Polymers Formed from Self-Complementary Monomers Using Quadruple Hydrogen Bonding.

Science **1997,** *278* (5343), 1601-1604.

22. Förster, S.; Thomas, P., From Self-Organizing Polymers to Nanohybrid and Biomaterials. *Angew. Chem. Int. Ed.* **2002,** *41* (5), 688-714.

23. Pochan, D. J.; Chen, Z.; Cui, H.; Hales, K.; Qi, K.; Wooley, K. L., Toroidal Triblock Copolymer Assemblies. *Science* **2004,** *306* (5693), 94-97.

24. Discher, D. E.; Eisenberg, A., Polymer Vesicles. *Science* **2002,** *297* (5583), 967-973.

25. Khanna, S. C., Speiser, P., Epoxy resin beads as a pharmaceutical dosage form I: Methods of preparation. *J. Pharm. Sci.* **1969,** *58* (9), 1114-1117.

26. Grislain, L., Couvreur, P., Lenaerts, V., Roland, M., Deprez-De Campenere, D., Speiser, P., Pharmacokinetics and distribution of a biodegradable drug-carrier. *Int. J. Pharm.* **1983,** *15* (3), 335-345.

27. Maeda, H., Matsumura, Y., Tumoritropic and lymphotropic principles of macromolecular drugs. *Crit. Rev. Ther. Drug Carrier Syst.* **1989,** *6* (3), 193–210.

28. Chiannilkulchai, N., Driouich, Z., Benoit, J.P., Parodi, A.L., Couvreur, P., Doxorubicin-loaded nanoparticles: Increased efficiency in murine hepatic metastases. *Sel. Cancer Ther.* **1989,** *5* (1), 1-11.

29. Kattan, J.; Droz, J.-P.; Couvreur, P.; Marino, J.-P.; Boutan-Laroze, A.; Rougier, P.; Brault, P.; Vranckx, H.; Grognet, J.-M.; Morge, X.; Sancho-Garnier, H., Phase I clinical trial and pharmacokinetic evaluation of doxorubicin carried by polyisohexylcyanoacrylate nanoparticles. *Invest. New Drugs* **1992,** *10* (3), 191-199.

30. Henry-Michelland, S.; Alonso, M. J.; Andremont, A.; Maincen, P.; Sauzières, J.; Couvreur, P., Attachment of antibiotics to nanoparticles: preparation, drug-release and antimicrobial activity in vitro. *Int. J. Pharm.* **1987,** *35* (1-2), 121-127.

31. Youssef, M.; Fattal, E.; Alonso, M. J.; Roblot-Treupel, L.; Sauzieres, J.; Tancrede, C.; Omnes, A.; Couvreur, P.; Andremont, A., Effectiveness of nanoparticle-bound ampicillin in the treatment of Listeria monocytogenes infection in athymic nude mice. *Antimicrob. Agents Chemother.* **1988,** *32* (8), 1204-1207.

32. Fattal, E.; Youssef, M.; Couvreur, P.; Andremont, A., Treatment of experimental salmonellosis in mice with ampicillin-bound nanoparticles. *Antimicrob. Agents Chemother.* **1989,** *33* (9), 1540-1543.

33. Bertling, W. M.; Gareis, M.; Paspaleeva, V.; Zimmer, A.; Kreuter, J.; Nurnberg, E.; Harrer, P., Use of liposomes, viral capsids, and nanoparticles as DNA carriers. *Biotech. Appl. Biochem.* **1991,** *13* (3), 390-405.

34. Chavany, C.; Doan, T. L.; Couvreur, P.; Puisieux, F.; Hélèna, C., Polyalkylcyanoacrylate Nanoparticles as Polymeric Carriers for Antisense Oligonucleotides. *Pharm. Res.* **1992,** *9* (4), 441-449.

35. Cun, D.; Jensen, L. B.; Nielsen, H. M.; rck; Moghimi, M.; Foged, C., Polymeric Nanocarriers for siRNA Delivery: Challenges and Future Prospects. *J. Biomed. Nanotechnol.* **2008,** *4* (3), 258-275.

36. Lobenberg, R., Kreuter, J., Macrophage Targeting of Azidothymidine: A Promising

Strategy for AIDS Therapy*. *AIDS Res. Hum. Retroviruses* **1996,** *12* (18), 1709-1715.

37. Raimar Löbenberg, L. A., Hagen von Briesen, Emily Rodgers, Jörg Kreuter, Body distribution of azidothymidine bound to hexyl-cyanoacrylate nanoparticles after i.v. injection to rats. *J. Controlled Release* **1998,** *50* (1-3), 21-30.

38. Brannon-Peppas, L.; Blanchette, J. O., Adv. Drug Delivery Rev. *Adv. Drug Delivery Rev.* **2004,** *56* (11), 1649-1659.

39. Irène Brigger, C. D. a. P. C., Nanoparticles in cancer therapy and diagnosis. *Adv. Drug Delivery Rev.* **2002,** *54* (5), 631-651.

40. Gaur, U.; Sahoo, S. K.; De, T. K.; Ghosh, P. C.; Maitra, A.; Ghosh, P. K., Biodistribution of fluoresceinated dextran using novel nanoparticles evading reticuloendothelial system. *Int. J. Pharm.* **2000,** *202* (1-2), 1-10.

41. Storm, G.; Belliot, S. O.; Daemen, T.; Lasic, D. D., Surface modification of nanoparticles to oppose uptake by the mononuclear phagocyte system. *Adv. Drug Delivery Rev.* **1995,** *17* (1), 31-48.

42. Brooks, P. C.; Clark, R. A.; Cheresh, D. A., Requirement of vascular integrin $\alpha_v\beta_3$ for angiogenesis. *Science* **1994,** *264* (5158), 569-571.

43. Creamer, D.; Sullivan, D.; Bicknell, R.; Barker, J., Angiogenesis in psoriasis. *Angiogenesis* **2002,** *5* (4), 231-236.

44. Bishop, G. G.; McPherson, J. A.; Sanders, J. M.; Hesselbacher, S. E.; Feldman, M. J.; McNamara, C. A.; Gimple, L. W.; Powers, E. R.; Mousa, S. A.; Sarembock, I. J.,

Selective αvβ3-Receptor Blockade Reduces Macrophage Infiltration and Restenosis After Balloon Angioplasty in the Atherosclerotic Rabbit. *Circulation* **2001,** *103* (14), 1906-1911.

45. Wilder, R. L., Integrin $\alpha_v\beta_3$ as a target for treatment of rheumatoid arthritis and related rheumatic diseases. *Ann. Rheum. Dis.* **2002,** *61* (90002), 96-99.

46. Jens Gille, R. A. S., Integrins: Role in Cell Adhesion and Communication. *Ann. N. Y. Acad. Sci.* **1996,** *797* (Microbial Pathogenesis and Immune Response II), 93-106.

47. Plow, E. F.; Haas, T. A.; Zhang, L.; Loftus, J.; Smith, J. W., Ligand Binding to Integrins. *J. Biol. Chem.* **2000,** *275* (29), 21785-21788.

48. Ruoslahti, E.; Pierschbacher, M. D., New perspectives in cell adhesion: RGD and integrins. *Science* **1987,** *238* (4826), 491-497.

49. Pasqualini, R.; Koivunen, E.; Ruoslahti, E., αv Integrins as receptors for tumor targeting by circulating ligands. *Nat. Biotech.* **1997,** *15* (6), 542-546.

50. Arap, W.; Pasqualini, R.; Ruoslahti, E., Cancer Treatment by Targeted Drug Delivery to Tumor Vasculature in a Mouse Model. *Science* **1998,** *279* (5349), 377-380.

51. Ellerby, H. M.; Arap, W.; Ellerby, L. M.; Kain, R.; Andrusiak, R.; Rio, G. D.; Krajewski, S.; Lombardo, C. R.; Rao, R.; Ruoslahti, E.; Bredesen, D. E.; Pasqualini, R., Anti-cancer activity of targeted pro-apoptotic peptides. *Nat. Med.* **1999,** *5* (9), 1032-1038.

52. Cai, W.; Niu, G.; Chen, X., Imaging of Integrins as Biomarkers for Tumor Angiogenesis. *Curr. Pharm. Design* **2008,** *14*, 2943-2973.

53. Lim, E. H.; Danthi, N.; Bednarski, M.; Li, K. C. P., A review: Integrin $\alpha_v\beta_3$-targeted molecular imaging and therapy in angiogenesis. *Nanomedicine* **2005,** *1* (2), 110-114.

54. Pierschbacher, M. D.; Ruoslahti, E., Influence of stereochemistry of the sequence Arg-Gly-Asp-Xaa on binding specificity in cell adhesion. *J. Biol. Chem.* **1987,** *262* (36), 17294-17298.

55. Hautanen, A.; Gailit, J.; Mann, D. M.; Ruoslahti, E., Effects of modifications of the RGD sequence and its context on recognition by the fibronectin receptor. *J. Biol. Chem.* **1989,** *264* (3), 1437-1442.

56. Susan, J. B. K.; Soma, C.; Teruna, J. S.; Todd, D. W.; Robert, K. D., Solution stability of linear vs. cyclic RGD peptides. *J. Pept. Res.* **1999,** *53* (5), 530-541.

57. Goodman, S. L.; Holzemann, G.; Sulyok, G. A. G.; Kessler, H., Nanomolar Small Molecule Inhibitors for αvβ6, αvβ5, and αvβ3 Integrins. *J. Med. Chem.* **2002,** *45* (5), 1045-1051.

58. Kok, R. J.; Schraa, A. J.; Bos, E. J.; Moorlag, H. E.; Asgeirsdottir, S. A.; Everts, M.; Meijer, D. K. F.; Molema, G., Preparation and Functional Evaluation of RGD-Modified Proteins as $\alpha_v\beta_3$ Integrin Directed Therapeutics. *Bioconjugate Chem.* **2002,** *13* (1), 128-135.

59. Boturyn, D.; Coll, J.-L.; Garanger, E.; Favrot, M.-C.; Dumy, P., Template Assembled Cyclopeptides as Multimeric System for Integrin Targeting and Endocytosis. *J. Am. Chem. Soc.* **2004,** *126* (18), 5730-5739.

60. Karen, L. W., From Dendrimers to Knedel-like Structures. *Chem. Eur. J.* **1997,** *3* (9), 1397-1399.

61. Thurmond Ii, K. B.; Huang, H.; Clark Jr, C. G.; Kowalewski, T.; Wooley, K. L., Shell cross-linked polymer micelles: stabilized assemblies with great versatility and potential. *Colloids Surf., B* **1999,** *16* (1-4), 45-54.

62. Karen, L. W., Shell crosslinked polymer assemblies: Nanoscale constructs inspired from biological systems. *J. Polym. Sci. Part A* **2000,** *38* (9), 1397-1407.

63. Pan, D.; Turner, J. L.; Wooley, K. L., Shell Cross-Linked Nanoparticles Designed To Target Angiogenic Blood Vessels via $\alpha_v\beta_3$ Receptor-Ligand Interactions. *Macromolecules* **2004,** *37* (19), 7109-7115.

64. Pan, D.; Turner, J. L.; Wooley, K. L., Folic acid-conjugated nanostructured materials designed for cancer cell targeting. *Chem. Commun.* **2003,** (19), 2400-2401.

65. Shaker Abdullah, I. Q. E. B., Advances in the Management of Pediatric Central Nervous System Tumors. *Ann. N. Y. Acad. Sci.* **2008,** *1138* (Recent Advances in Clinical Oncology), 22-31.

66. Buckner, J. C.; Brown, P. D.; O'Neill, B. P.; Meyer, F. B.; Wetmore, C. J.; Uhm, J. H., Central Nervous System Tumors. *Mayo Clin. Proc.* **2007,** *82* (10), 1271-1286.

67. Hargrave, D. R.; Zacharoulis, S., Pediatric CNS tumors: current treatment and future directions. *Expert Rev. Neurother.* **2007,** *7* (8), 1029-1042.

68. Wilne, S.; Collier, J.; Kennedy, C.; Koller, K.; Grundy, R.; Walker, D., Presentation

of childhood CNS tumours: a systematic review and meta-analysis. *Lancet Oncol.* **2007,** *8* (8), 685-695.

69. Kostianovsky, A. M.; Maier, L. M.; Anderson, R. C.; Bruce, J. N.; Anderson, D. E., Astrocytic Regulation of Human Monocytic/Microglial Activation. *J. Immunol.* **2008,** *181* (8), 5425-5432.

70. Zhu, H.; Acquaviva, J.; Ramachandran, P.; Boskovitz, A.; Woolfenden, S.; Pfannl, R.; Bronson, R. T.; Chen, J. W.; Weissleder, R.; Housman, D. E.; Charest, A., Oncogenic EGFR signaling cooperates with loss of tumor suppressor gene functions in gliomagenesis. *Proc. Natl. Acad. Sci. U. S. A.* **2009,** *106* (8), 2712-2716.

71. Leighton, C.; Fisher, B.; Bauman, G.; Depiero, S.; Stitt, L.; MacDonald, D.; Cairncross, G., Supratentorial low-grade glioma in adults: an analysis of prognostic factors and timing of radiation. *J. Clin. Oncol.* **1997,** *15* (4), 1294-1301.

72. Larramendy-Gozalo, C.; Barret, A.; Daudigeos, E.; Mathieu, E.; Antonangeli, L.; Riffet, C.; Petit, E.; Papy-Garcia, D.; Barritault, D.; Brown, P.; Deslys, J.-P., Comparison of CR36, a new heparan mimetic, and pentosan polysulfate in the treatment of prion diseases. *J. Gen. Virol.* **2007,** *88* (3), 1062-1067.

73. Riemer, C.; Burwinkel, M.; Schwarz, A.; Gultner, S.; Mok, S. W. F.; Heise, I.; Holtkamp, N.; Baier, M., Evaluation of drugs for treatment of prion infections of the central nervous system. *J. Gen. Virol.* **2008,** *89* (2), 594-597.

74. Kocisko, D. A.; Morrey, J. D.; Race, R. E.; Chen, J.; Caughey, B., Evaluation of new

cell culture inhibitors of protease-resistant prion protein against scrapie infection in mice. *J. Gen. Virol.* **2004,** *85* (8), 2479-2483.

75. Trevitt, C. R.; Collinge, J., A systematic review of prion therapeutics in experimental models. *Brain* **2006,** *129* (9), 2241-2265.

76. Agarwal, A.; Lariya, N.; Saraogi, G.; Dubey, N.; Agrawal, H.; Agrawal, G. P., Nanoparticles as Novel Carrier for Brain Delivery: A Review. *Curr. Pharm. Des.* **2009,** *15* (8), 917-925.

77. Du, W.; Nystrom, A. M.; Zhang, L.; Powell, K. T.; Li, Y.; Cheng, C.; Wickline, S. A.; Wooley, K. L., Amphiphilic Hyperbranched Fluoropolymers as Nanoscopic 19F Magnetic Resonance Imaging Agent Assemblies. *Biomacromolecules* **2008,** *9* (10), 2826-2833.

78. Tatjana, N. P.-V.; Luce Vander, E.; Kristof, K.; Sophie, L.; Carmen, B.; Feng, C.; Rik Van, D.; Yicheng, N.; Robert, N. M.; Koen, B., Pharmacokinetic and in vivo evaluation of a self-assembled gadolinium(III)-iron(II) contrast agent with high relaxivity. *Contrast Med. Mol. Imaging* **2006,** *1* (6), 267-278.

79. Sabrina, L.; Robert, R.; Tóth, É.; Merbach, A. E., Gd^{III} Complexes with Fast Water Exchange and High Thermodynamic Stability: Potential Building Blocks for High-Relaxivity MRI Contrast Agents. *Chem. Eur. J.* **2003,** *9* (15), 3555-3566.

80. Hifumi, H.; Yamaoka, S.; Tanimoto, A.; Citterio, D.; Suzuki, K., Gadolinium-Based Hybrid Nanoparticles as a Positive MR Contrast Agent. *J. Am. Chem. Soc.* **2006,** *128* (47),

15090-15091.

81. Lin, Y.-S.; Hung, Y.; Su, J.-K.; Lee, R.; Chang, C.; Lin, M.-L.; Mou, C.-Y., Gadolinium(III)-Incorporated Nanosized Mesoporous Silica as Potential Magnetic Resonance Imaging Contrast Agents. *J. Phys. Chem. B* **2004,** *108* (40), 15608-15611.

82. He, J.; Kunitake, T.; Watanabe, T., Porous and nonporous Ag nanostructures fabricated using cellulose fiber as a template. *Chem. Commun.* **2005,** (6), 795-796.

83. Deshmukh, R. D.; Composto, R. J., Surface Segregation and Formation of Silver Nanoparticles Created In situ in Poly(methyl Methacrylate) Films. *Chem. Mater.* **2007,** *19* (4), 745-754.

84. Evanoff, D. D.; Chumanov, G., Size-Controlled Synthesis of Nanoparticles. 2. Measurement of Extinction, Scattering, and Absorption Cross Sections. *J. Phys. Chem. B* **2004,** *108* (37), 13957-13962.

85. He, J.; Kunitake, T., Formation of Silver Nanoparticles and Nanocraters on Silicon Wafers. *Langmuir* **2006,** *22* (18), 7881-7884.

86. Flynn, C. E.; Lee, S.-W.; Peelle, B. R.; Belcher, A. M., Viruses as vehicles for growth, organization and assembly of materials. *Acta Mater.* **2003,** *51* (19), 5867-5880.

87. Chairam, S.; Poolperm, C.; Somsook, E., Starch vermicelli template-assisted synthesis of size/shape-controlled nanoparticles. *Carbohydr. Polym.* **2009,** *75* (4), 694-704.

88. Rifai, S.; Breen, C. A.; Solis, D. J.; Swager, T. M., Facile in Situ Silver Nanoparticle

Formation in Insulating Porous Polymer Matrices. *Chem. Mater.* **2006,** *18* (1), 21-25.

89. Brott, L. L.; Naik, R. R.; Pikas, D. J.; Kirkpatrick, S. M.; Tomlin, D. W.; Whitlock, P. W.; Clarson, S. J.; Stone, M. O., Ultrafast holographic nanopatterning of biocatalytically formed silica. *Nature* **2001,** *413* (6853), 291-293.

90. Sun, Y.; Xia, Y., Shape-Controlled Synthesis of Gold and Silver Nanoparticles. *Science* **2002,** *298* (5601), 2176-2179.

91. Naik, R. R.; Jones, S. E.; Murray, C. J.; McAuliffe, J. C.; Vaia, R. A.; Stone, M. O., Peptide Templates for Nanoparticle Synthesis Derived from Polymerase Chain Reaction-Driven Phage Display. *Adv. Funct. Mater.* **2004,** *14* (1), 25-30.

92. Hartgerink, J. D.; Beniash, E.; Stupp, S. I., Self-Assembly and Mineralization of Peptide-Amphiphile Nanofibers. *Science* **2001,** *294* (5547), 1684-1688.

Chapter 2

RGD-conjugated Shell Crosslinked Nanoparticles (RGD-SCKs) for $\alpha_v\beta_3$ Binding Affinity Studies

Abstract

In this work, micelles and shell crosslinked nanoparticles (SCKs), prepared from poly(acrylic acid)-*b*-polystyrene block copolymer precursors, were functionalized with the cyclic peptide KCRGDC to generate nanoscale agents for targeted imaging and drug delivery. The peptide contained a tripeptide arginine-glycine-aspartic acid (RGD) sequence as the recognition motif for the $\alpha_v\beta_3$ integrin receptor, which is highly expressed in tumors, cardiovascular sites, and other areas where angiogenesis occurs. Our specific interest in these nanomaterials includes their development as agents for the selective imaging and treatment of acute vascular injury. The work within this chapter focuses upon rigorous studies to develop methods for the synthesis of nanoparticles functionalized with covalently-attached and ready-to-bind KCRGDC peptides. Special attention is paid to the need for the peptides to be presented from the surface of the nanoparticles and to be available for binding with their protein receptors. The binding affinities of these peptide-labeled nanoparticles were, therefore, evaluated by means of IC_{50} values to $\alpha_v\beta_3$, and those data were used to guide the synthetic efforts further. Targeting to the $\alpha_v\beta_3$ integrin, with selectivity against other integrins such as $\alpha_v\beta_5$, was also demonstrated. The best affinities to $\alpha_v\beta_3$ receptors was achieved by

post-conjugation strategy that involved pre-assembly of nanostructures functionalized with reactive groups on the ends of grafted poly(ethylene glycol) (PEG) chains followed by attaching the KCRGDC peptide, with the highest affinity being observed for nanoscopic polymer micelles assembled from HOOC-PEG3000$_4$-*g*-DOTAlysine$_{3.2}$-*g*-PAA$_{58.8}$-*b*-PS$_{71}$, which gave an IC_{50} value of 0.49 nM. Compared with the unconjugated KCRGDC peptide having an IC_{50} value of 10.5 nM to $\alpha_v\beta_3$, the RGD-nanoparticles exhibited a considerable binding affinity enhancement of *ca.* 20-fold. Also, a *pre-conjugation strategy* was explored, which involved the attachment of the KCRGDC peptide to the block graft copolymer prior to micellar assembly, but this approach seemed to allow for inward folding of the grafted chains and burying of peptides within the inner portions of the nanoparticles, giving lower binding affinities to $\alpha_v\beta_3$. Interest in these materials also for cancer imaging and therapeutic delivery was explored, from which *in vitro* cell assay experiments demonstrated significant binding and internalization of these nanoparticles with a glioma cell line.

Introduction

Angiogenesis is a physiological process involving the growth of new blood vessels from existing vasculature.[1] It is a normal process involved in many biological processes, *e.g.* embryogenesis, wound healing, and tissue remodeling. It is also a fundamental step in the transition of tumors from a dormant state to a malignant one. Several disorders are characterized by either an excess or insufficient number of blood vessels, *e.g.* rheumatoid arthritis[2], psoriasis[3], restenosis[4], and diabetic retinopathy[5].

Being essential for the proliferation and metastatic properties of human tumors, angiogenesis is a multi-step and invasive process, as characterized by the endothelial cell proliferation, the modulation of extracellular matrix (ECM), and the cell adhesion/migration. Among the many angiogenic factors, integrin $\alpha_v\beta_3$ has been found to be necessary for the formation, survival, and maturation of new blood vessels.[6] In human melanoma cells, the expression of $\alpha_v\beta_3$ is correlated with malignancy grade, collagenase production, and cell growth.[7, 8] Due to the key roles of integrin $\alpha_v\beta_3$ in many physiological processes, it has been evaluated extensively as target. The tripeptide sequence arginine-glycine-aspartic acid (RGD) is common to various ECM proteins, *e.g.* vitronectin, fibronectin, fibrinogen, thrombospondin, and von-Willebrand factor, involved in cell-matrix adhesion.[9, 10] High-affinity $\alpha_v\beta_3$ selective ligands containing RGD have been identified by phage display.[11] Targeted chemotherapy has been investigated using RGD peptides to deliver doxorubicin[12] and proapoptotic peptides[13] to tumor vasculatures. *In vivo* imaging of sites of angiogenesis has been demonstrated using RGD-containing peptides.[14, 15]

Although the RGD-sequence is conserved in all native ligands, slight modifications

still can provide differences in both binding affinities and specificities. The flanking amino acid residues, especially the two positions following the aspartic acid, are known to change binding affinity by direct interaction of the residues with the integrin as well as influencing the peptide folding.[9] Cyclization is a common technique to improve binding properties because it confers rigidity on the structure.[16] All selective RGD peptides have at least one ring moiety. It has been recently reported that multimeric RGD peptides could enhance the binding affinity of receptor-ligand interactions through either multivalent binding or statistical rebinding. Polyvalency affords better targeting capability and higher cellular uptake because of the increased apparent ligand concentration.[17] The unique structural properties of nanoscale materials provide the ability for them to carry therapeutic agents and to present numerous targeting moieties as well. Furthermore, multivalency has been shown to facilitate internalization.[18] Carrier systems like liposomes,[19] polymers,[20-22] nanoparticles,[23] and proteins[24] bearing multiple RGD peptides are, therefore, more likely to be internalized *via* receptor-mediated endocytosis than single peptide constructs.

In this work, the cyclic KCRGDC peptide was selected as the antagonist to $\alpha_v\beta_3$. Shell crosslinked nanoparticles (SCKs) were used as the carrier system. SCKs are self-assembled core-shell nanomaterials, originating from the crosslinking of the shell domain of micelles assembled from amphiphilic block copolymers (poly(acrylic acid)-*b*-polystyrene (PAA-*b*-PS) in this work). The SCKs obtained have a robust structure due to the covalent crosslinking reaction, and have controllable sizes ranging from 10 to 200 nm.[25, 26] SCKs conjugated with KCRGDC peptide were synthesized *via* various methods and were tested for binding affinities to $\alpha_v\beta_3$ *via* in vitro plate-based

assays (in collaboration with A. L. Fiamengo and C. J. Anderson). Improved binding affinities were achieved, compared to the KCRGDC peptide as a small molecule that is capable only of monovalent binding. KCRGDC-conjugated SCKs also showed good binding and internalization to U87MG glioma cells (studied in collaboration with Z. Xu and J. R. Leonard). Such particles were found to be both non-toxic to mammalian cells and non-immunogenic within mice. With the enhanced blood circulation times that can be achieved by grafting poly(ethylene glycol) from the nanoparticles,[27] these multi-functional materials could be good candidates as carrier systems for imaging and therapeutic agents, selectively to injured or diseased tissues that overexpress $\alpha_v\beta_3$.

Experimental Section

Materials

All solvents were purchased from Sigma-Aldrich and used without further purification unless otherwise noted. Trifluoroacetic acid (TFA; 95%; Aldrich), 2,2′-(ethylenedioxy)-bis(ethylamine) (97%; Aldrich), 1-(3′-dimethylaminopropyl)-3-ethylcarbo-diimide methiodide (EDCI; 98%; Aldrich), *N*-hydroxysuccinimide (NHS; 98%; Aldrich), *N*-Hydroxysulfosuccinimide sodium salt (sulfo-NHS; 98.5%; Aldrich), *N*,*N*′-Dicyclohexylcarbodiimide (DCC; 99%; Aldrich), Succinic anhydride (99%; Aldrich), were used as received. Supor 25 mm 0.1 μm Spectra/Por Membrane tubes (molecular weight cutoff (MWCO) 3,500 or 6-8000 Da), purchased from Spectrum Medical Industries Inc., were used for dialysis. Sodium phosphate monobasic (>99.0%), sodium phosphate dibasic (>99.0%), sodium chloride (>99.0%) were purchased from Sigma-Aldrich. Precursor of DOTAlysine was a gift from Dr. Dennis A. Moore at Covidien Inc., Saint Louis, MO. Nanopure water (18 MΩ·cm) was acquired by means of a Milli-Q water filtration system (Millipore Corp.; Bedford, MA). KCRGDC was custom synthesized by Tianma Pharma Co., Suzhou, China, and used as received. 5-FAM-KCRGDC was custom synthesized by Chengdu Kaijie Biopharmaceuticals Co. Ltd., Chengdu, China, and was used as received. Polyethylene glycol (PEG) and derivatives were purchased from Rapp Polymere GmbH, Germany, and used as received. Superfine Sephadex ® G75 resin (bead diameter: 20-50 μm; Fractionation range: 1000-50000 Da (Dextrans)) was purchased from GE Healthcare and was used to purify aqueous nanoparticle samples.

5 mM PBS (phosphate buffered saline, with 5 mM of phosphates and 5 mM of NaCl)

was prepared by mixing NaH_2PO_4 (0.76 g), Na_2HPO_4 (1.93 g) and NaCl (1.17 g) into 4 liters of nanopure water and was used as the solvent for dialysis. 150 mM PBS (phosphate buffered saline, with 150 mM of phosphates and 150 mM of NaCl) was prepared by mixing NaH_2PO_4 (22.7 g), Na_2HPO_4 (59.0 g) and NaCl (35.1 g) into 4 liters of nanopure water and was used as the solvent for running Sephadex® columns. Both buffers have pH values around 7.4.

PAA_{61}-*b*-PS_{34} and SCKs assembled from PAA_{61}-*b*-PS_{34} were prepared as reported *via* atom transfer radical polymerization (ATRP).[28] PAA_{64}-*b*-PS_{54} and its derivatives functionalized with NH_2-PEO_{113}-OCH_3 and DOTAlysine were prepared by Dr. Guorong Sun.[27] DOTAlysine$_{2.5}$-*g*-PAA_{68}-*b*-PS_{70}, which was synthesized *via* ATRP, was provided by Dr. Jinqi Xu.[28] PAA_{66}-*b*-PS_{71} was synthesized by Dr. Andreas Nyström *via* reversible addition-fragmentation chain transfer polymerization (RAFT).[34]

Instrumental

^{1}H NMR spectra were recorded on a Varian 300 MHz spectrometer interfaced to a UNIX computer using Mercury software. Chemical shifts are referred to the solvent proton resonance.

Transmission electron microscopy (TEM) was performed in bright-field mode with a JEOL 2000-FX at 150 kV accelerating voltage. Samples for TEM measurements were diluted with 1 wt% of phosphotungstic acid (PTA) stain solution (v/v, 1:1). Carbon grids were exposed to oxygen plasma treatment to increase the surface hydrophilicity. Micrographs were collected at 100,000 magnifications. The number average particle diameters (D_{av}) and standard deviations were generated from the analysis of a minimum of 150 particles from at least three different micrographs.

The average heights for the nanoparticles were determined by performing tapping-mode AFM under ambient conditions in air. The AFM instrumentation consisted of a Nanoscope III BioScope system (Digital Instruments, Veeco Metrology Group; Santa Barbara, CA) and standard silicon tips (type, OTESPA-70; L, 160 μm; normal spring constant, 50 N/m; resonance frequency, 246-282 kHz). Samples for AFM imaging analysis were prepared through spin-coating *ca*. 2.0 μL of the nanoparticle solution (typical concentration: 0.2 mg/mL) onto freshly cleaved mica plates (Ruby clear mica, New York Mica Co.) and allowed to dry freely in air. The number-average particle heights (H_{av}) values and standard deviations were generated from the sectional analysis of more than 150 particles from several different regions.

Hydrodynamic diameters (D_h) and size distributions for the SCKs in aqueous solutions were determined by dynamic light scattering (DLS). The DLS instrument consisted of a Brookhaven Instruments Limited (Worcestershire, U.K.) system, including a model BI-200SM goniometer, a model BI-9000AT digital correlator, a model EMI-9865 photomultiplier, and a model 95-2 Ar ion laser (Lexel Corp., Farmindale, NY) operated at 514.5 nm. Measurements were made at 20 °C. Prior to analysis, solutions were filtered through a 0.22 μm Millex GV PVDF membrane filter (Millipore Corp., Medford, MA) and then centrifuged in a model 5414 microfuge (Brinkman Instruments, Inc., Westbury, NY) for 10 minutes to remove dust particles. Scattered light was collected at a fixed angle of 90 °. The digital correlator was operated with 522 ratio spaced channels, and initial delay of 5 μs, a final delay of 100 ms, and a duration of 10 minutes. A photomultiplier aperture of 400 μm was used, and the incident laser intensity was adjusted to obtain a photon counting of between 200 and 300 kcps. Only measurements

in which the measured and calculated baselines of the intensity autocorrelation function agreed to within 0.1% were used to calculate particle sizes. The calculations of the particle size distributions and distribution averages were performed with the ISDA software package (Brookhaven Instruments Company), which employed single-exponential fitting, cumulants analysis, non-negatively constrained least-squares (NNLS) and CONTIN particle size distribution analysis routines. All determinations were made in triplicate.

Fast protein liquid chromatography (FPLC) was performed by Dr. Yongjian Liu in Prof. Michael J. Welch's laboratory at Washington University School of Medicine on an AKTA (GE) system, including a P-920 pump, Columns of Superose 12 10/300 GL, and a UV detector with 254 nm wavelength. The eluent was 20 mM HEPES with 150 mM NaCl and flow rate was 0.8 mL/min. The results were analyzed by UNICORN 3.10.11.

UV-*vis* spectra were acquired on a Varian Cary 1E UV-*vis* system (Varian, Inc., Palo Alto, CA) using polystyrene cuvettes.

Preparation of NH_2-PEO_{113}-5-FAM-KCRGDC. Three steps were involved to prepare NH_2-PEO_{113}-5-FAM-KCRGDC.

BocNH-PEO_{113}-NH_2 (300 mg, 0.0600 mmol), was dissolved in 13 mL of dichloromethane and stirred at room temperature for *c.a.* 0.5 h. Succinic anhydride (24.6 mg, 0.246 mmol) and DIPEA (21.0 μL, 15.5 mg, 0.120 mmol) were added. The reaction mixture was allowed to stir at room temperature for 24 h. The reaction mixture was then concentrated and precipitated into cold ether (40 mL) twice. The precipitate was dried under vacuum to afford 238 mg of white solid as BocNH-PEO_{113}-$NHCOCH_2CH_2COOH$ (yield 80%). ^1H NMR (CD_2Cl_2, 300 MHz, ppm):

δ1.43 (s, C(C***H***$_3$)$_3$ on the Boc protecting group), 2.5-2.65 (br, -C***H***$_2$C***H***$_2$- of the succinic anhydride unit), 3.3-3.8 (br, -C***H***$_2$C***H***$_2$- of the PEG repeating unit), 5.0-5.1 (br, amide proton), 6.8-6.9 (br, amide proton).

BocNH-PEO$_{113}$-NHCOCH$_2$CH$_2$COOH (201 mg, 0.0402 mmol) was dissolved in 10 mL of dichloromethane and stirred at room temperature for *c.a.* 0.5 h. *N*-hydroxysuccinimide (23.6 mg, 0.205 mmol) and *N*,*N*′-Dicyclohexylcarbodiimide (43.7 mg, 0.211 mmol) were added. The solution was allowed to stir at room temperature for 24 h before being concentrated and precipitated into cold ether (40 mL) twice. The precipitate was then dried under vacuum to afford a white solid, BocNH-PEO$_{113}$-NHCOCH$_2$CH$_2$CO-NHS (151 mg, yield: 73%). ^{1}H NMR (CD$_2$Cl$_2$, 300 MHz, ppm): δ1.43 (s, C(C***H***$_3$)$_3$ on the Boc protecting group), 2.5-2.65 (br, -C***H***$_2$C***H***$_2$- of the succinic anhydride unit), 2.8-2.9 (m, -C***H***$_2$C***H***$_2$- of the *N*-hydroxysuccinimide unit), 3.3-3.8 (br, -C***H***$_2$C***H***$_2$- of the PEG repeating unit), 5.0-5.1 (br, amide proton), 6.8-6.9 (br, amide proton).

5-FAM-KCRGDC (40.6 mg, 0.0390 mmol) was dissolved in 5 mL of anhydrous DMF, to this solution were also added BocNH-PEO$_{113}$-NHCOCH$_2$CH$_2$CO-NHS (104 mg, 0.0201 mmol) and DIPEA (10 μL, 7.3 mg, 0.057 mmol). The reaction mixture was allowed to stir at room temperature for 24 h. The reaction mixture was precipitated into cold ether (45 mL) once. The solid was then dissolved in DCM and precipitated into cold ether (45 mL) twice to afford a yellow solid as BocNH-PEO$_{113}$-NHCOCH$_2$CH$_2$CO-5-FAM-KCRGDC (100 mg, yield: 80%). The peptide coupling efficiency was determined to be 60% by UV-vis.

BocNH-PEO$_{113}$-NHCOCH$_2$CH$_2$CO-5-FAM-KCRGDC (100 mg, 15.9 μmol) was

dissolved in 6 mL of DCM. TFA (4.8 mL, 7.1 g, 62.3 mmol) was added. The reaction mixture was allowed to stir at room temperature for 12 h, concentrated and precipitated into cold ether. The precipitate was dried under vacuum to afford NH_2-PEO_{113}-5-FAM-KCRGDC as a yellow solid (80 mg, yield: 79%).

General procedures for the preparation of NH_2-PEO_{113}-5-FAM-KCRGDC-*g*-mPEG2000-*g*-DOTAlysine-*g*-PAA-*b*-PS Block Copolymers. The NH_2-PEO_{113}-5-FAM-KCRGDC was grafted onto mPEG2000-*g*-DOTAlysine-*g*-PAA-*b*-PS by following the procedures: to a solution of mPEG2000-*g*-DOTAlysine-*g*-PAA-*b*-PS in anhydrous DMF, 1-[3′-(dimethylamino)propyl]-3-ethylcarbodiimide methiodide (EDCI), and 1-hydroxybenzotriazole (HOBt) were added, and the reaction mixture was allowed to stir for 1 h at room temperature. Then DIPEA and a solution of NH_2-PEO_{113}-5-FAM-KCRGDC in anhydrous DMF were added and the reaction mixture was further stirred for 30 h at room temperature. The relative ratio of mPEG2000-*g*-DOTAlysine-*g*-PAA-*b*-PS block copolymer/EDCI/HOBt/mPEG-NH_2 was 1:20:20:4. Appropriate amount of DMF was added to the reaction mixture to adjust the polymer concentration to be 1.00 mg/mL. Micelle was directly prepared from the reaction mixture and was crosslinked into SCKs. The impurities were later removed by dialysis against nanopure water in MWCO 100 kDa dialysis tubings and/or by passing through a Sephadex® G75 SEM column.

Preparation of HOOC-$PEG3000_{4.0}$-*g*-$DOTAlysine_{3.2}$-*g*-$PAA_{58.8}$-*b*-PS_{71} Block Copolymer. Similar procedures were followed as mentioned above, except the attaching sequence.

PAA_{66}-*b*-PS_{71} (50.6 mg, 0.0041 mmol) was dissolved in 8.0 mL of N_2-flushed DMF. EDCI (37.3 mg, 0.125 mmol) and HOBt (17.2 mg, 0.127 mmol), both prepared as DMF solutions, were added into the polymer solution. The reaction mixture was stirred at room temperature for 1 h. DOTAlysine(tetra-*t*-butyl ester) (10.8 mg, 0.013 mmol) and DIPEA (100 μL, 0.57 mmol) were added to the reaction mixture as a DMF solution. The reaction mixture was allowed to stir at room temperature for 24 h, and was then transferred to MWCO 6-8000 Da dialysis tubing and dialyzed against nanopure water for 4 d. DOTAlysine(tetra-*t*-butyl ester)$_{3.2}$-*g*-$PAA_{62.8}$-*b*-PS_{71} was obtained after lyophilization as a white powder. Yield, 36.2 mg, 60%. The number of DOTAlysine(tetra-*t*-butyl ester) per polymer chain was determined by ^{1}H NMR (coupling efficiency 90%). ^{1}H NMR (DMSO-d_6, 300 MHz, ppm): δ 1.10-2.20 (br, C***H*****$_2$** of the polymer backbone), 1.40 (s, C(C***H*****$_3$)$_3$ of the *t*-butyl ester group), 2.20-2.64 (br, C***H*** of the polymer backbone), 2.40-3.05 (br, DOTAlysine macrocyclic protons), 6.35-7.20 (m, 5Ar-***H***).

DOTAlysine(tetra-*t*-butyl ester)$_{3.2}$-*g*-$PAA_{62.8}$-*b*-PS_{71} (28.5 mg, 0.0022 mmol) was dissolved in 7.0 mL of N_2-flushed DMF. EDCI (32.8 mg, 0.110 mmol) and HOBt (14.8 mg, 0.110 mmol), both prepared as DMF solutions, were added into the polymer solution. The reaction mixture was stirred at room temperature for 1 h. NH_2-PEG3000-COOH (21.9 mg, 0.0066 mmol) and DIPEA (100 μL, 0.57 mmol) were added to the reaction mixture as a DMF solution. The reaction mixture was allowed to stir at room temperature for 24 h, and was then transferred to MWCO 50 kDa dialysis tubing and dialyzed against 5 mM PBS (pH ~ 7.4) for 4 d. The polymer solution in 5 mM PBS was then passed through Sephadex® G50 SEC column with 150 mM PBS (pH ~7.4) as the

solvent. The polymer fractions were combined and desalted through dialysis against nanopure water, followed by lyophilization to afford a white polymer as HOOC-PEG3000$_{4.0}$-*g*-DOTAlysine(tetra-*t*-butyl ester)$_{3.2}$-*g*-PAA$_{58.8}$-*b*-PS$_{71}$. Yield, 43.2 mg, 82%. The number of HOOC-PEG3000 per polymer chain was determined by ^{1}H NMR (coupling efficiency, 80%). Yield, 29.3 mg, 95%. ^{1}H NMR (DMSO-d$_6$, 300 MHz, ppm): δ 1.10-2.20 (br, C***H*****$_2$** of the polymer backbone), 1.40 (s, C(C***H*****$_3$)$_3$ of the *t*-butyl ester group), 2.20-2.65 (br, C***H*** of the polymer backbone), 2.40-3.10 (br, DOTAlysine macrocyclic protons), 3.40-3.70 (br, mEEG backbone –OC***H***$_2$C***H***$_2$O- protons), (6.28-7.16 (m, 5Ar-***H***).

HOOC-PEG3000$_{4.0}$-*g*-DOTAlysine(tetra-*t*-butyl ester)$_{3.2}$-*g*-PAA$_{58.8}$-*b*-PS$_{71}$ (36.2 mg, 0.0015 mmol) was dissolved in 2.0 mL of DCM. TFA, 1 mL, was added to the polymer solution and the reaction mixture was allowed to stir at room temperature for 6 h. The solvent and TFA were removed by blowing N_2 to the surface of the reaction mixture and residual polymer was dissolved in DMF to afford an off-yellow solution. The solution was dialyzed in MWCO 6-8000 Da tubing against nanopure water for 4 d. A white was obtained after lyophilization of the solution in water as the HOOC-PEG3000$_{4.0}$-*g*-DOTAlysine$_{3.2}$-*g*-PAA$_{58.8}$-*b*-PS$_{71}$. Yield, 29.3 mg, 95%. ^{1}H NMR (DMSO-d$_6$, 300 MHz, ppm): δ 1.10-2.20 (br, C***H*****$_2$** of the polymer backbone), 2.20-2.65 (br, C***H*** of the polymer backbone), 2.40-3.10 (br, DOTAlysine macrocyclic protons), 3.40-3.70 (br, mEEG backbone –OC***H***$_2$C***H***$_2$O- protons), (6.28-7.16 (m, 5Ar-***H***).

General procedures for micelle assembly and SCK formation. To a solution of the amphiphilic block copolymer (PAA-*b*-PS, mPEG2000-*g*-DOTAlysine-*g*-PAA-*b*-PS, PEG113-5-FAM-KCRGDC-*g*-mPEG2000-*g*-DOTAlysine-*g*-PAA-*b*-PS, or

HOOC-PEG3000-*g*-DOTAlysine-*g*-PAA-*b*-PS) in THF or DMF, (*ca.* 1.0 mg/mL in polymer concentration), an equal volume of nanopure water was added dropwise *via* a syringe pump over 6 h. The reaction mixture was further stirred for *ca*. 16 h at room temperature before transferring to a presoaked dialysis tubing (MWCO. 6,000-8,000 Da for PAA-*b*-PS; MWCO 100000 Da for PEG113-5-FAM-KCRGDC-*g*-mPEG2000-*g*-DOTAlysine-*g*-PAA-*b*-PS), and dialyzed against nanopure water for 4 days, to afford a micelle solution with the final polymer concentration of 0.20-0.30 mg/mL.

General procedures for the PAA Block Crosslinking to Form SCKs. To a solution of micelle in nanopure water, was added dropwise a solution of 2,2'-(ethylenedioxy)bis(ethylamine) (*c. a.* 1.0 mg/mL) in nanopure water over 10 min. The reaction mixture was stirred for *c. a*. 2 h at room temperature. To this solution, was added dropwise *via* syringe pump over 30 min, a solution of 1-[3'-(dimethylamino)propyl]-3-ethylcarbodiimide methiodide in nanopure water. The reaction mixture was further stirred 20 h at room temperature before transferring to presoaked dialysis tubing, and dialyzed against nanopure water for 4 days, to remove all of the impurities and afford the SCK solution. The nominal crosslinking extent (20% and 50%) were based on the stoichiometry of the crosslinker (2,2'-(ethylenedioxy)bis(ethylamine)) to that of the carboxylic acids on the PAA domain. The general stoichiometry employed to achieve 20% nominal crosslinking was 9:2.2:1 for carboxylic acid units : EDCI : crosslinker, and to achieve 50% nominal crosslinking, the stoichiometry was 3.6:2.2:1.

General procedures for post-attaching

KCRGDC/5-FAM-KCRGDC/PEG-5-FAM-KCRGDC onto micelle/SCK nanoparticles. All micelle/SCK samples were pre-cooled to 4 °C. Sulfo-NHS aqueous solution was then added, and the containers were shaken for *c.a.* 30 min. Freshly prepared EDCI aqueous solution was added and the reaction containers were shaken for 1.5 h in a 4 °C refrigerator. Here, the pH values of the solutions were adjusted to around 7.4 with pH 9.2 0.2 M phosphate buffer. KCRGDC/5-FAM-KCRGDC/PEG-5-FAM-KCRGDC solutions were then added. The pH of the reaction solutions were finally adjusted to around 7.4 (optimal pH for the coupling reaction to occur) and the reaction mixtures were kept shaking at 4 °C for 24 h. All reaction mixtures were then dialyzed against pH 7.4 5 mM PBS (after treatment of Chelax 100 resin to removed heavy metals) for 5 d. The equivalence for the [COOH], [EDCI] and [sulfo-NHS] was controlled as 1:1.5:3.0, and the peptide amount was exactly based on stoichiometry.

Reduction of disulfide bond on KCRGDC-NP to thiol for Ellman's assay. Excess amount of DTT (DL-Dithiothreitol) was incubated with micelle/SCK nanoparticles labeled with the cyclic KCRGDC at 45 °C for 1h. The reaction mixture was then dialyzed against nanopure water in pre-soaked MWCO 6-8000 Da dialysis tubing to remove unreacted DTT and for later quantification of thiol groups by Ellman's assay.

Protocol for Ellman's assay

26.0 mg of cysteine (Sigma) is dissolved into 10.00 mL of reaction buffer (0.10 M Sodium Phosphate Buffer pH 8.0) to make the stock solution. 4.00 mg of Ellman's reagent (DTNB, Sigma) was dissolved into 1.00 mL of reaction buffer. A series of

cysteine standard solutions with different concentrations are then prepared from the stock solution, with cysteine concentrations being 15.0 mM, 1.50 mM, 1.25 mM, 1.00 mM, 1.00 mM, 0.75 mM, 0.50 mM, 0.25 mM and 0.05 mM. The Ellman's reagent solution was then mixed with the cysteine standard solutions and the samples to be measured using the following volumetric quantities

Blank: 983 μL rxn. Buffer + 18 μL Ellman's.

Standards/Samples: 938 μL rxn buffer + 18 μL of Ellman's + 45 μL sample.

After 15 min from the mixing, absorbances were measured at 412 nm. A standard curve can be generated and sample thiol concentrations can be determined.

Procedures for running Sephadex® G75 gravity SEC columns to purify aqueous nanoparticle samples. Sephadex® G75 resin (superfine) (10 g) was pre-soaked in boiling water for *c.a.* 30 min to form a gel. After cooling to room temperature, the resin was packed into a glass column (30 cm × 2 cm) equipped with a stopcock. About 200 mL of the eluent (150 mM PBS, pH ~ 7.4) was passed through the column prior to any sample loading. For each run, *c.a.* 4 mL of nanoparticle samples (with polymer concentration around 0.20-0.30 mg/mL) was loaded. The separation process was monitored by UV. Columns were reused after being flushed with plenty of the eluent. The desired fractions were collected and concentrated and solvent-exchanged into 5 mM PBS by using Centricon (MWCO 10000 Da, Millpore, MA) tubes.

Preparation of FITC-functionalized micelles

mPEG2000$_{2.4}$-*g*-DOTAlysine$_{2.0}$-*g*-PAA$_{59.6}$-*b*-PS$_{54}$ (15.9 mg, 0.99 μmol) was dissolved in 7.0 mL of anhydrous DMF and the solution was stirred for 1 h at room temperature. EDCI (1.23 mg, 4.1 μmol) and HOBt (0.56 mg, 4.2 μmol) were added as DMF solutions

into the polymer solution. The reaction mixture was allowed to stir at room temperature for 1 h. Fluorescein-5-thiosemicarbazide (1.0 mg, 2.36 μmol) was added as a DMF solution. The reaction mixture was further stirred at room temperature for 24 h. Proper amount of DMF was added to the reaction mixture to make the polymer concentration to be *c.a.* 1 mg/mL. Micelle was then directly prepared from the reaction mixture by dropwise addition of water over 6 h. The DMF/water mixture was transferred to MWCO 6-8000 Da tubing and dialysed against 5 mM PBS (pH ~7.4) to afford the final micelle solution in water with polymer concentration to be 0.262 mg/mL. The FITC attached to the polymer was quantified by measuring its UV absorbance at 492 nm and using a molar extinction coefficient of 63000 $M^{-1}cm^{-1}$. The average number of FITC per polymer chain was determined to be 0.2.

Procedures for integrin binding assay (Performed by Ms. Ashley L. Fiamengo in Prof. Carolyn J. Anderson's laboratory at Washington University School of Medicine): An isolated, competitive binding assay described previously[33, 37] is utilized here. Briefly, vitronectin (Chemicon CC080) was biotinylated with N-hydroxysuccinimide biotin (2 h at room temperature) before dialysis into PBS, pH 7.4. The wells of a 96-well plate (Nunc Immuno Plate with MaxiSorp) were coated with 100 μg integrin $\alpha_v\beta_3$ or $\alpha_v\beta_5$ (Chemicon CC1019 and CC1025, respectively) in coating buffer (20 mM Tris, pH 7.4, 150 mM NaCl, 2 mM $CaCl_2$, 1 mM $MgCl_2$, 10 μM $MnCl_2$). The plates were then blocked (1 h at 4 °C) with bovine serum albumin (BSA) (3% in coating buffer). After washing three times with binding buffer (0.1% BSA in coating buffer), biotinylated vitronectin (final concentration 14 nM) with and without serially diluted ligands was allowed to bind to the integrins (3 h at 37 °C). After washing (3 times in

binding buffer), bound biotinylated vitronectin was detected by binding ExtrAvidin alkaline phosphatase (Sigma) (1/35,000 dilution, 1 h at room temperature) using the p-nitrophenyl phosphate liquid substrate system (Sigma) as the chromogen. Each concentration data point was done in triplicate, and each binding experiment was performed at least twice. Nonlinear regression was used to fit binding curves and calculate inhibitory concentrations of 50% (IC_{50} values) (Prism, version 5.02; GraphPad).

Procedures for cell assay of 5-FAM-KCRGDC-labeled nanoparticles (Performed by Dr. Zhiqiang Xu in Prof. Jeffery R. Leonard's laboratory at Washington University School of Medicine): 5000 human U87MG glioma cells were seeded on glass coverslip in a 24-well plate at 37 °C for 12 h before the experiment. 5-FAM-KCRGDC-labeled nanoparticles were then added directly into the media (alpha-MEM(Gibco)) at concentration of 1 μM based on the conjugated 5-FAM-KCRGDC peptide. After 24 h treatment all the wells were fixed with 4% paraformaldehyde and cell nucleus was counterstained with DAPI. Fluorescence signal was recorded using epifluorescence microscope. All the pictures were taken at same time constant without any post modification.

Results and Discussion

To create a functional nanomaterial that is capable of carrying imaging and/or therapeutic agents to a selective tissue site, it is imperative that the targeting ligand be accessible for binding with the receptor target. Two general approaches, the *post-conjugation* method and the *pre-conjugation* method, were, therefore, applied to afford micelle/SCK nanoparticles functionalized with a disulfide-cyclized RGD peptide, KCRGDC. For the *post-conjugation* method, SCK nanoparticles were first prepared from the amphiphilic diblock copolymer precursors (PAA-*b*-PS), according to our established protocol, the cyclic KCRGDC peptide or the amine-terminated PEO_{113}-5-FAM-KCRGDC were then conjugated onto the nanoparticle shell domain through carbodiimide-mediated aqueous amidation (see Experimental Section for details). For the *pre-conjugation* method, the PAA-*b*-PS block copolymers were modified with the KCRGDC peptides *via* amidation chemistry in organic solvent, followed by aqueous assembly into nanostructures and crosslinking across the shell domain of nanoparticles.[27, 28] Coincident with these synthetic efforts were rigorous physicochemical studies to determine the composition and structure of the resulting materials, and biological evaluations to determine the binding affinities between the ligand bound to the nanostructure and receptors either coated on a plate or presented on cells. The synthetic work and physicochemical studies were the focus of my work, whereas the biological studies were performed by experts through collaborations.

Post-conjugation of KCRGDC peptide onto micelles and SCKs.

As depicted in Scheme 2-1, the KCRGDC peptide was attached onto pre-established

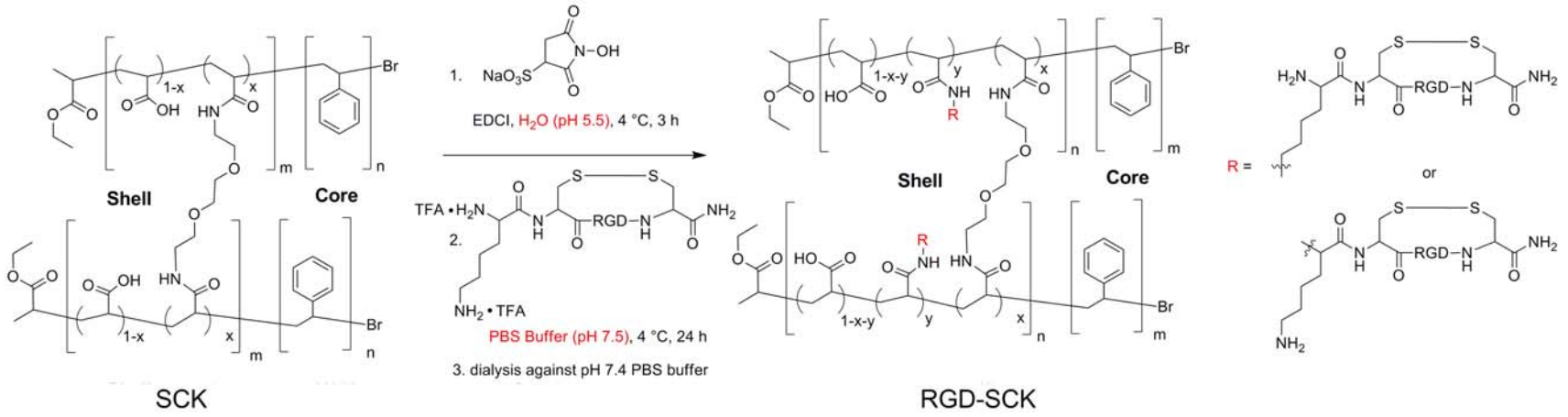

Scheme 2-1. Illustration of post-labeling KCRGDC peptide to micelle/SCK.

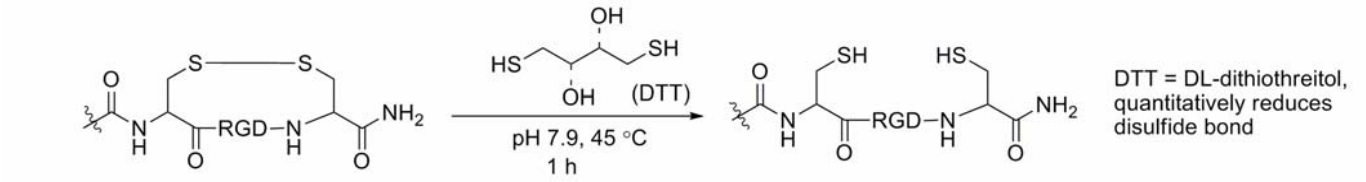

Scheme 2-2. Illustration of the reduction of disulfide bond to thiols.

micelles and SCKs from PAA_{61}-*b*-PS_{34} block copolymer precursor. The synthetic process was based upon modified carbodiimide-mediated aqueous amidation. The first step, activation of carboxylic acid residue, involved the pH value adjustments of reaction media (see Experimental Section for details)[29, 30] to avoid unexpected side reactions, such as the hydrolysis and rearrangement of the activated intermediates. The KCRGDC solution was then added to the reaction mixtures and the final pH values of the reaction mixtures were again adjusted to ~ 7.5, which was reported to be the optimum pH value for aqueous amidation reactions facilitated by sulfo-NHS.[31] Different amounts of peptide (nominal 4, 40, and 400 peptides per micelle/SCK, respectively) were conjugated to the nanoparticles by controlling the coupling stoichiometry between the acrylic acid residues per nanoparticle and the KCRGDC peptide, and the equivalence of EDCI, sulfo-NHS and KCRGDC was controlled to be 1:2:1.

Quantification of the KCRGDC peptides attached onto the micelle/SCK nanoparticles were determined by the Ellman's assay, a conventional technique used for the quantification of thiol (-SH) groups in biological studies.[32] To convert the disulfide bond in the cyclic KCRGDC peptide to thiols, dithiothreitol (DTT) was used (Scheme 2-2) as the reducing agent. The KCRGDC-functionalized nanoparticles with the disulfide bond reduced to thiols were then analyzed for thiol quantity by Ellman's assay as described in the experimental section.

Table 2-1 summarizes the actual average numbers of KCRGDC peptides attached on each nanoparticle, determined by Ellman's assay. The best peptide coupling efficiency was found to be ~ 15% and the lowest coupling efficiency was ~ 3%. As a note, for the two samples with nominal 4 peptides per nanoparticle, quantification of the peptide by Ellman's assay could not provide reliable results due to the very low

concentration of the formed thiol groups. The low coupling efficiency could be attributed to the steric hindrance between the cyclic KCRGDC peptide and the activated ester throughout the shell domain of the nanostructures. As we have already noticed in previous study,[28] the spacer length between the reacting amine group and the cyclic moiety greatly affected the coupling efficiency. Meanwhile, the electronic property of the peptide hydrate might also influence the reaction efficiency.

Table 2-1. IC_{50} values of KCRGDC-micelle/SCKs prepared by post-conjugation method.

Samples	$N_{aggr.}$	Peptide per NP[a]	Peptide per NP[b]	IC_{50} (nM)[d]	
				$\alpha_v\beta_3$	$\alpha_v\beta_5$
KCRGDC				10.5	921
Micelle	125	0	0	> 10,000	> 10,000
20% Crosslinked SCK	125	0	0	> 10,000	> 10,000
50% Crosslinked SCK	125	0	0	> 10,000	> 10,000
KCRGDC-Micelle	125	4	*n.a.*[c]	> 10,000	1.5
	125	40	< 1	> 1,000	0.3
	125	400	65	1,080	26.1
KCRGDC-SCKs 20% Crosslinked	125	4	*n.a.*	> 5,000	> 10,000
	125	40	< 1	> 1,000	> 10,000
	125	400	58	> 1,000	> 5,000
KCRGDC-SCKs 50% Crosslinked	125	4	*n.a.*	> 1,000	> 10,000
	125	40	< 1	380	> 5,000
	125	400	42	37.4	> 10,000

a nominal numbers of peptide per nanoparticle (NP) from stoichiometry; *b* numbers of peptide per nanoparticle measured from Ellman's assay; *c* not available, due to the very low UV signals obtained; *d* IC_{50} values for micelle/SCKs were measured to be the concentrations of the nanoparticles in units of nM.

The *in vitro* $\alpha_v\beta_3$ binding affinity (IC_{50} value) of the peptide-functionalized nanoparticles was then conducted by following the plate-assay protocol for peptides.[33] The binging specificity was determined by comparing the affinity (IC_{50} values) between $\alpha_v\beta_3$ and $\alpha_v\beta_5$. The results of these assays were also outlined in Table 2-1.

For all of the surveyed post-KCRGDC-modified micelles and 20% crosslinked SCKs, poor binding affinities to $\alpha_v\beta_3$ (IC_{50} > 1 μM, *i.e.* over 100-folds of decrease, relative to the control peptide) were observed. Compared to micelles and 20% crosslinked SCKs, enhanced binding affinity, together with the selectivity, to $\alpha_v\beta_3$ were achieved for the 50% crosslinked SCKs. Meanwhile, as the number of peptides per SCK increased from less than 1 to *ca.* 52, the IC_{50} value towards $\alpha_v\beta_3$ decreased from 380 nM to 37.8 nM, *i.e.*, a 10-fold of improvement. It was hypothesized that, for the SCKs with the higher crosslinking extents, the chances for the peptide to react with activated carboxylates beneath the shell domain would decrease due to the framework-like property of the shell domain. Therefore, most of the peptides attached to the nanoparticle were located on the outer surface or periphery of the SCKs and were more accessible for the integrin binding. An interesting phenomenon was observed that the KCRGDC-micelle samples showed very good binding to $\alpha_v\beta_5$, although the peptide itself has poor binding to $\alpha_v\beta_5$. The reason behind this observation was not clear at this stage.

***Post-conjugation* of NH_2-PEO_{113}-5-FAM-KCRGDC onto PEGylated SCKs prepared from mPEG2000$_{5.5}$-*g*-DOTAlysine$_{2.0}$-*g*-$PAA_{58.5}$-*b*-PS_{54}.**

As mentioned in the previous section, the targeting peptide binding affinity could be enhanced by the means of accommodating the peptides away from the nanoparticle moieties. To further explore the "lengthening" effect and provide more accurate quantification of conjugated peptides per nanoparticle without using the tedious

Ellman's assay, NH_2-PEO_{113}-5-FAM-KCRGDC, a KCRGDC derivative was synthesized according to Scheme 2-3 and coupled to PEGylated SCKs as depicted in Figure 2-1 (also see Experimental Section for details). The 5-FAM was introduced as a chromophore for more convenient UV-vis quantification of the peptides covalently attached onto nanoparticles.

With the ultimate goal for developing targeting nanoparticles as potential *in vivo* imaging contrast agents, we used the PEGylated SCK nanoparticles, which have already been demonstrated with sufficient blood circulation time (half-life up to 16 h), to evaluate the targeting efficiency after decorating with the peptide ligands. PEGylated SCKs with 20% and 50% crosslinking extents were prepared from mPEG2000$_{5.5}$-*g*-DOTAlysine$_{2.0}$-*g*-PAA$_{58.5}$-*b*-PS$_{54}$ block copolymer precursors.[27] The DOTA molecules acted as the chelator for radionuclide ^{64}Cu, a promising PET imaging tracer.

The synthetic sequence of NH_2-PEO_{113}-5-FAM-KCRGDC initialized with the installation of carboxylic acid group to the mono-Boc protected diamino-PEO_{113} (compound 1), followed by functional group transformation to the activated ester (compound 3). Compound 3 was then reacted with 5-FAM-KCRGDC (structure shown in Scheme 2-3) *via* amidation chemistry to attach the peptide onto the PEG chain end (compound 4). The Boc protecting group was then removed to afford NH_2-PEO_{113}-5-FAM-KCRGDC as the final product (compound 5). The molar extinction coefficient of the 5-FAM-KCRGDC in 5 mM PBS (pH ~ 7.4 with 5 mM of NaCl) at 492 nm was determined to be 63,000 $M^{-1}cm^{-1}$ and was also used as the molar extinction coefficient for the NH_2-PEO_{113}-5-FAM-KCRGDC. The coupling efficiency of the peptide to the PEG chain was thus determined to be 60%, based upon UV-vis measurement.

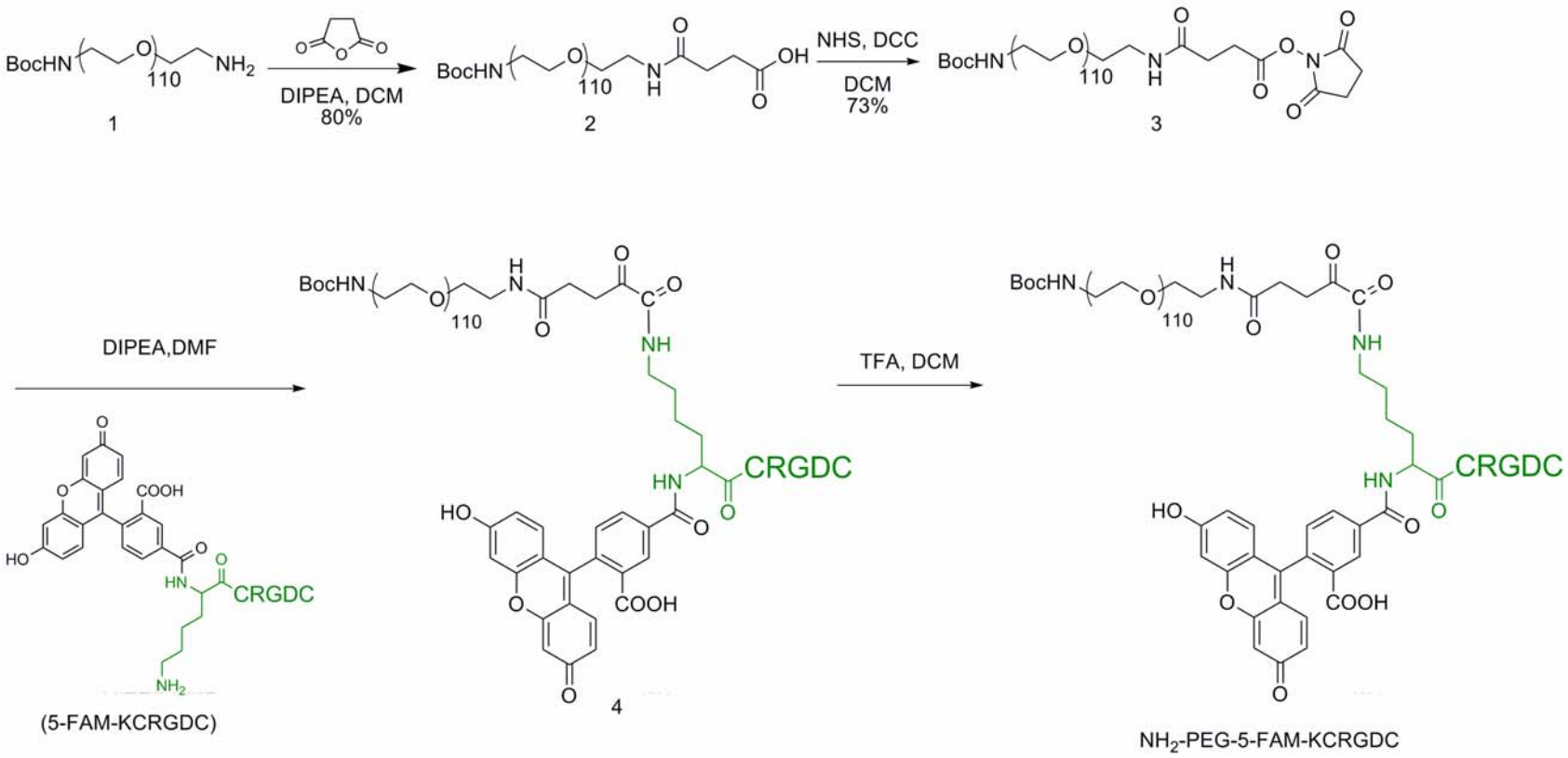

Scheme 2-3. Schematic illustration of the synthesis of NH_2-PEG_{113}-5-FAM-KCRGDC.

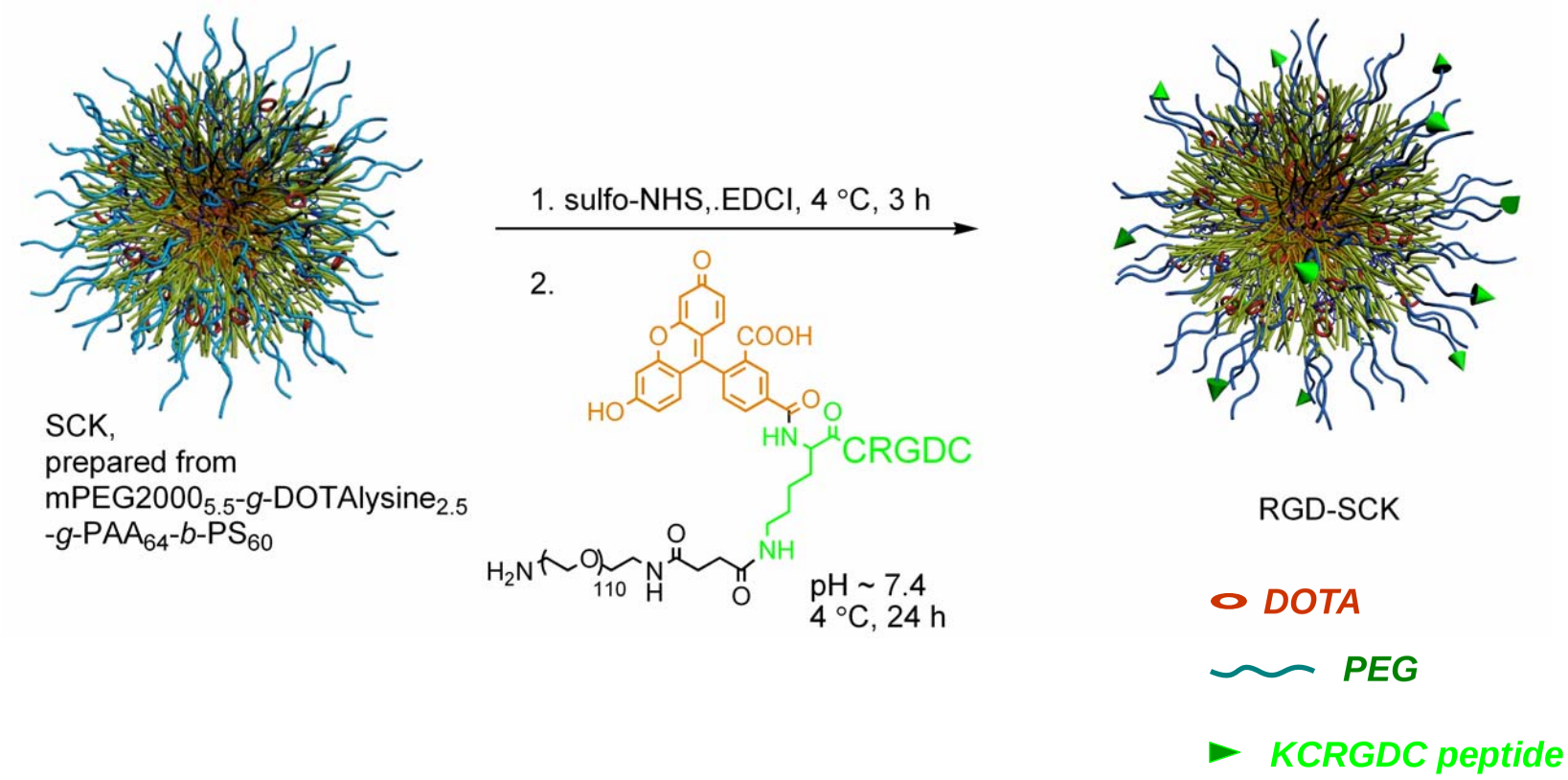

Figure 2-1. Illustration of post-conjugation of NH_2-PEO_{113}-5-FAM-KCRGDC onto SCKs prepared from mPEG2000$_{5.5}$-*g*-DOTAlysine$_{2.5}$-*g*-PAA$_{58}$-*b*-PS$_{54}$.

For the conjugation of NH_2-PEO_{113}-5-FAM-KCRGDC onto the PEGylated nanoparticles, similar procedures to the one mentioned above were followed (Figure 2-1, see Experimental Section for details). After extensive dialysis against 5 mM PBS (pH ~ 7.4 with 5 mM of NaCl) to remove small molecule byproducts and the unattached NH_2-PEO_{113}-5-FAM-KCRGDC, the amounts of the KCRGDC attached onto the nanoparticles were then determined by measuring the UV-vis absorption of these nanoparticles at 492 nm.

The coupling efficiency was found to be extremely low as shown in Table 2-2 (0.6% and 0.4% for 20% and 50% crosslinked PEGylated SCKs, respectively). The fact that the SCKs were surrounded by a layer of hydrated PEO could be attributed as the source for the low coupling efficiencies. The PEO layer not only hindered the big molecule, NH_2-PEO_{113}-5-FAM-KCRGDC, to get access to the activated carboxylic acid groups in the shell of the nanoparticles, but also affected the activation step due to the reduced permeability of the SCK shell domain. Comparing to KCRGDC, whose IC_{50} value to $\alpha_v\beta_3$.was 10.5 nM, both 5-FAM-KCRGDC and PEO_{113}-5-FAM-KCRGDC showed slightly decreased binding affinities to $\alpha_v\beta_3$, which was 23.0 and 21.3 nM, respectively. Due to the inadequate number of peptides per SCK nanoparticle (*ca.* 6 and 4 for 20% and 50% crosslinked PEGylated SCKs, respectively, Table 2-2), no appreciable binding to $\alpha_v\beta_3$ was observed for both the KCRGDC functionalized 20% and 50% crosslinked PEGylated SCKs (IC_{50} up to 10,000 nM, Table 2-2). In fact, the previous results obtained from the "native" SCK experiments (*vide supra*) have already indicated that a minimum amount of 40 KCRGDCs per nanostructure was required to achieve comparable binding affinity.

Table 2-2. IC_{50} values of PEGylated SCKs, post-conjugated with NH_2-PEO_{113}-5-FAM-KCRGDC.

Samples	$N_{aggr.}$	Peptide per NP[a]	Peptide per NP[b]	IC_{50} (nM)[c] $\alpha_v\beta_3$	IC_{50} (nM)[c] $\alpha_v\beta_5$
5-FAM-KCRGDC				23.0	> 1,000
PEO_{113}-5-FAM-KCRGDC				21.3	> 1,000
20% Crosslinked PEO_{113}-5-FAM-KCRGDC-SCK	200	1000	6.3	> 1,000	> 10,000
50% Crosslinked PEO_{113}-FAM-KCRGDC-SCK	200	1000	4.2	> 5,000	> 10,000

a targeted number of peptide per nanoparticle based on stoichiometry; *b* number of peptide per nanoparticle as determined by UV-*vis* (ε_{492nm} = 63,000 $M^{-1}cm^{-1}$); *c* IC_{50} values for micelle/SCKs were measured to be the concentrations of the nanoparticles in units of nM.

The observed trend, *i.e.*, the improvement of $\alpha_v\beta_3$ binding affinity for the KCRGDC-functionalized nanostructure with the increased amount of peptide per nanoparticle, clearly indicated the direction for advancing $\alpha_v\beta_3$ targeting. However, the post-conjugation methodology limited the progress due to the following two concerns: 1) the low reaction efficiency caused unnecessary waste of the peptides and increased the purification difficulty since over 80% of the reacting peptides were keeping "free" inside the reaction mixture; and 2) the problem associated with the quantification of conjugated peptides. These dilemmas made the post-modification approach less attractive and therefore, the alternative and facile pre-conjugation strategy was applied for the next studies (*vide infra*).

Construction of targeting SCKs through pre-conjugation methodology.

During our earlier works for construction of DOTA-SCKs with remarkable radiolabeling efficiency and PEGylated SCKs with tunable biodistributions,[27] a pre-grafting strategy has been developed and demonstrated as a facile and practical approach for attaching large amount of functionalities to nano-materials. This strategy was extended to this study including the following modified protocols: Firstly,

the NH_2-PEO_{113}-5-FAM-KCRGDC molecules were conjugated onto the mPEG2000-*g*-DOTAlysine-*g*-PAA-*b*-PS block copolymer precursors with different length ratios of PAA *vs.* PS in organic solvents (DMF in this study) through carbodiimide-mediated amidation chemistry facilitated by HOBt (Scheme 2-4); Secondly, the concentrations of block copolymer precursors in reaction mixtures were adjusted to *ca.* 1 mg/mL by adding appropriate amounts of DMF. Equal volume of nanopure water (> 18.0 MΩ cm) to that of the DMF was then directly added to the reaction mixture over 6 h to induce the micellization process and "frozen" the formed micelle structures; Finally, SCKs were prepared by crosslinking of the carboxylic acid groups throughout the micelle shell domain with 2,2′-(ethylenedioxy)-bis(ethylamine) *via* amidation chemistry. Initially, the micelles and SCKs were purified through extensive dialysis as described before. However, the fast protein liquid chromatography (FPLC) analyses of these samples indicated the existence of unconjugated NH_2-PEO_{113}-5-FAM-KCRGDC as shown in Figure 2-2. Therefore, the nanoparticles were further purified through Sephadex® size exclusion column chromatography (SEC) for the total removal of free peptides.

Different Sephadex® resins were surveyed, including G25 medium (bead size 50-150 μm, fractionation range 100-5000 Da), G50 medium (bead size 50-150 μm, fractionation range 500-10000 Da), G75 medium (bead size 50-150 μm, fractionation range 1000-50000 Da), and G75 superfine (bead size 20-50 μm, fractionation range 1000-50000 Da). Although the molecular weight of NH_2-PEO_{113}-5-FAM-KCRGDC was ~ 6,300 Da, its complete removal was only achieved by columns packed with superfine G75 resins. The columns were monitored with UV-vis by measuring the absorbance of each collected fraction (*ca.* 4

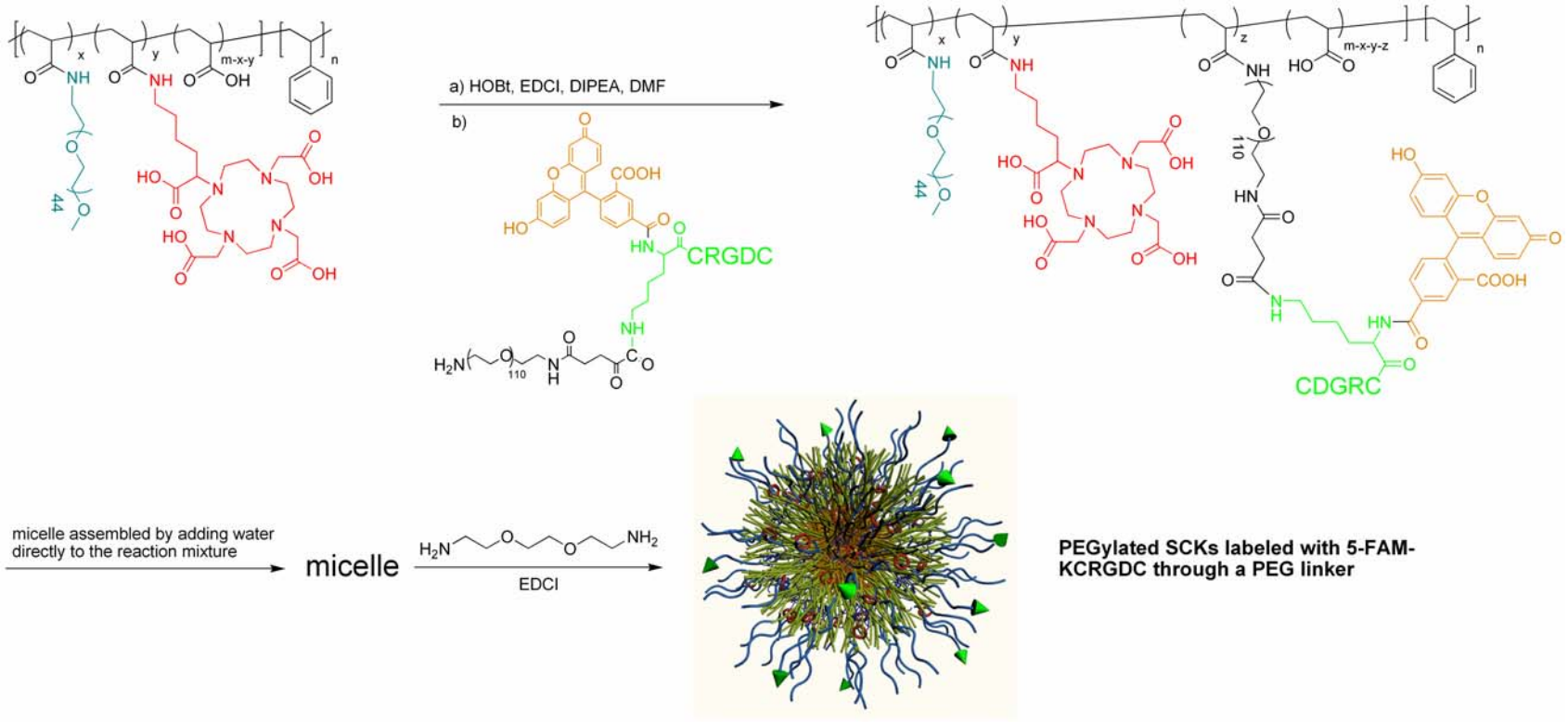

Scheme 2-4. Graphic representation of the synthesis PEGylated SCKs labeled with KCRGDC peptide by pre-labeling NH_2-PEO_{113}-5-FAM-KCRGDC onto the SCK precursor, mPEG2000-*g*-DOTAlysine-*g*-PAA-*b*-PS.

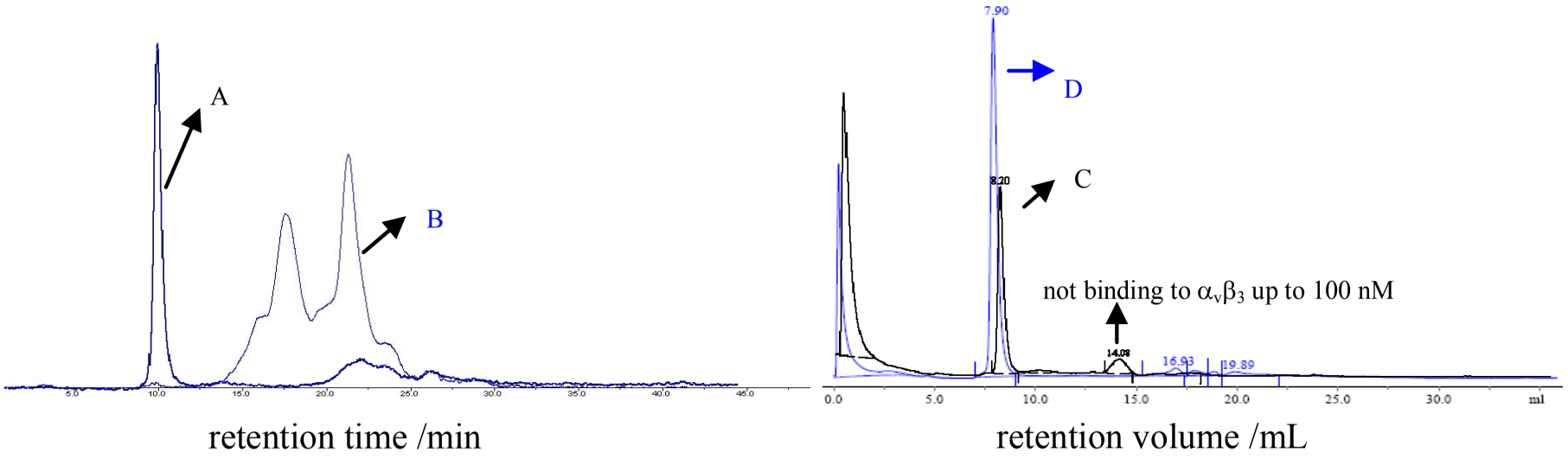

Figure 2-2. Fast protein liquid chromatography (FPLC, performed by Dr. Yongjian Liu) traces of A: control sample of RGD-NP prepared from Pre-conjugation method and purified by dialysis in 5 mM PBS (pH ~ 7.4) for 4 d; B: NH_2-PEO_{113}-5-FAM-KCRGDC; C: control sample of RGD-NP prepared from Pre-conjugation method and purified by dialysis in 150 mM PBS (pH ~ 7.4) for 30 d; D: sample 2 in table 2-3.

mL) at 492 nm. Figure 2-3 showed that three distributions were separated by the column, with the first one (left) as the nanoparticle fraction, the second one (middle) as the NH_2-PEO_{113}-5-FAM-KCRGDC, and the third one (right) possibly as the 5-FAM-KCRGDC precursor (contamination during the synthetic process of NH_2-PEO_{113}-5-FAM-KCRGDC). The purity of the nanoparticle fraction was further confirmed by FPLC (Figure 2-3). The nanoparticle fractions were then combined and concentrated by Centricon (MWCO 10000 Da) to make the final polymer concentrations around 0.25 mg/mL. After quantification of the peptide amount attached, these samples (samples 2-5 in Table 2-3) were then measured for IC_{50} values to $\alpha_v\beta_3$.

As characterized by transmission electron microscopy (TEM), these nanoscale objects exhibited globular shape (Figure 2-4) and relatively narrow size distributions. Detailed characterization data and the IC_{50} values are summarized in Table 2-3. Compared to the *post-conjugation* method, the *pre-conjugation* method provided increased amount of peptide incorporated into the nanoparticles, as a result of the improved coupling efficiency for amidation reactions conducted in DMF rather than water (Table 2-3).

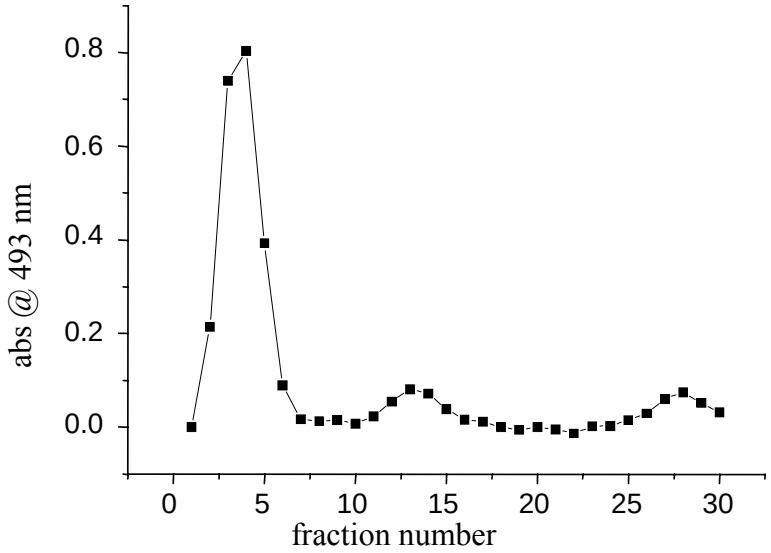

Figure 2-3. Monitoring Sephadex® G75 superfine column fractions by measuring UV absorbance at 492 nm.

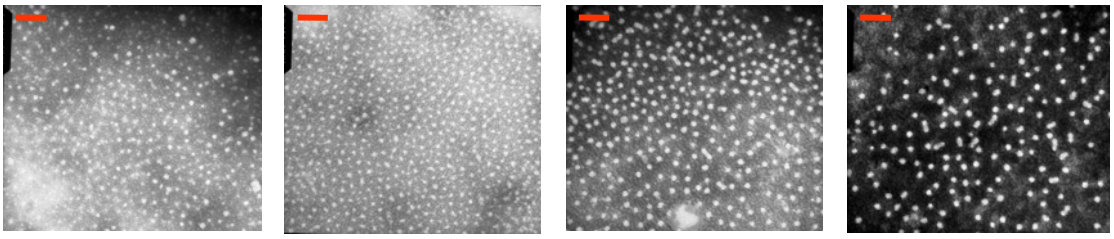

A B C D

Figure 2-4. Transmission electron microscopy (TEM) images of PEGylated micelle/SCK nanoparticles, prepared from pre-labeling the NH_2-PEG5000-5-FAM-KCRGDC onto the amphiphilic PAA-*b*-PS block copolymers. A, micelle from mPEG2000$_{2.4}$-*g*-DOTAlysiney$_{2.0}$-*g*-PEO$_{113}$-5-FAM-KCRGDC$_{0.6}$-*g*-PAA$_{59}$-*b*-PS$_{54}$; B, 50% crosslinked SCK from mPEG2000$_{2.4}$-*g*-DOTAlysiney$_{2.0}$-*g*-PEO$_{113}$-5-FAM-KCRGDC$_{0.6}$-*g*-PAA$_{59}$-*b*-PS$_{54}$; C, micelle from DOTAlysiney$_{2.5}$-*g*-PEO$_{113}$-5-FAM-KCRGDC$_{0.5}$-*g*-PAA$_{65}$-*b*-PS$_{70}$; D, 50% crosslinked SCK from DOTAlysiney$_{2.5}$-*g*-PEO$_{113}$-5-FAM-KCRGDC$_{0.5}$-*g*-PAA$_{65}$-*b*-PS$_{70}$. Scale bar 100 nm.

Table 2-3. Characterization data and IC_{50} values of micelle/SCK nanoparticles conjugated with RGD peptide prepared by pre-conjugating the NH_2-PEO_{113}-5-FAM-KCRGDC onto the amphiphilic PAA_m-*b*-PS_n block copolymers (x, y and z are the average numbers of PEG2000, DOTAlysine and NH_2-PEO_{113}-5-FAM-KCRGDC on each polymer chain).

Sample	description	Polymer Precursor					D_{TEM}	$N_{aggr.}$	Peptide	IC_{50} (nM)[a]	
		x	y	z	m	n	nm		per NP^2	$\alpha_v\beta_3$	$\alpha_v\beta_5$
1	PEO_{113}-5-FAM-KCRGDC									21.3	> 1,000
2	PEO_{113}-5-FAM-KCRGDC-NP (micelle)	5.5	2.0	1.6	64	54	12 ± 2	100	158	>170	n.d
3	PEO_{113}-5-FAM-KCRGDC-SCK-NP (50% Crosslinked SCK)	5.5	2.0	1.6	64	54	12 ± 2	100	160	>141	n.d
4	PEO_{113}-5-FAM-KCRGDC-NP (micelle)	0	0	0.9	66	71	12 ± 2	118	104	>148	n.d
5	PEO_{113}-5-FAM-KCRGDC-SCK-NP (50% Crosslinked SCK)	0	0	0.9	66	71	12 ± 2	118	101	>130	n.d

a IC_{50} values for micelle/SCKs were measured to be the concentrations of the nanoparticles in units of nM

Samples 2-5 in Table 2-3 were prepared through the pre-conjugation method from NH_2-PEO_{113}-5-FAM-KCRGDC functionalized PAA_{66}-*b*-PS_{71} and mPEG2000$_{5.5}$-*g*-DOTAlysine$_{2.0}$-*g*-$PAA_{58.5}$-*b*-PS_{54} block copolymer precursors. Despite of the fact that the nanoparticles were functionalized with more than 100 peptides per particle on average, the binding affinities for $\alpha_v\beta_3$ remained lower, compared with the NH_2-PEO_{113}-5-FAM-KCRGDC control (Table 2-3). No appreciable binding were observed even for nanoparticles with concentration up to 100 nM, which meant that more than five ligand-modified nanoparticles (with totally more than 500 peptides attached) were required to provide similar binding capacity as one NH_2-PEO_{113}-5-FAM-KCRGDC small molecule. The lower binding affinity of these nanoparticles suggested that the majority of the attached peptides might be located underneath the particle surface and were not available for binding to integrin receptors.

***Post-conjugation* of KCRGDC to PEGylated micelles and SCKs bearing periphery carboxylic acids to achieve better accessibility of the peptides for integrin binding.**

Based upon all of the above results, a new method was then developed, to afford nanoparticles with KCRGDC peptide attached to the outer surface (Scheme 2-4). In this method, the PEGylated nanoparticles were still constructed from micellization of PEO-*g*-PAA-*b*-PS amphiphilic block copolymers, however, the PEO grafts carried carboxylic acid chain termini instead of unreactive methoxy groups as in the previous studies. The core-shell morphology of the micelles enabled some of the acid chain ends to be located on the periphery of the micelles (*vide infra*). The peptide, 5-FAM-KCRGDC was then conjugated to the micelles by methods described above in aqueous conditions. Crosslinking the shell domain with di-amino crosslinkers

afforded the corresponding SCKs.

From the amphiphilic block copolymer, PAA_{66}-*b*-PS_{71},[34] DOTAlysine(tetra *t*-butyl ester) and NH_2-PEG3000-OC_3H_6-COOH were attached sequentially through amidation chemistry, as described above, to afford the product, HOOC-$PEG3000_4$-*g*-DOTAlysine(tetra *t*-butyl ester)$_3$-*g*-PAA_{59}-*b*-PS_{71}. The average numbers of DOTA and PEG3000 on each polymer chain were determined by ^{1}H NMR spectroscopy. Protected forms of the DOTA derivatives were used to avoid the consumption of carboxylic acid residues on the DOTA moiety during the amidation process, which has already been demonstrated to be critical for retaining efficient ^{64}Cu chelation.[35] The existence of *t*-butyl esters also facilitated the ^{1}H NMR quantification of the number of DOTAs per polymer chain, due to their unique characteristic resonance signals. The copolymers were then subjected to acidolysis by trifluoroacetic acid to remove the *t*-butyl ester protecting groups to afford HOOC-$PEG3000_4$-*g*-DOTAlysine$_3$-*g*-PAA_{59}-*b*-PS_{71}. Micelles were then assembled through the conventional phase-segregation driven protocol and purified through regular dialysis against nanopure water to remove the organic solvent. The aqueous micelle solution was then subjected to shell crosslinking reaction with 2,2'-(ethylenedioxy)bis(ethylamine) to afford the SCKs with nominal 50% crosslinking extent. Both the micelle and the SCKs were purified by running Sephadex® G75 superfine columns to remove unattached PEG chains.

These PEGylated nanostructures were characterized through the combination of dynamic light scattering (DLS) and TEM. Given the number-averaged hydrodynamic diameter of 32 nm (measured by DLS, see Experimental Section for details) and the averaged diameter of 26 nm for the PS core domain (obtained from TEM image analysis), the averaged shell thickness was ~ 3 nm. For the PEG3000

molecule, the radius of gyration was calculated to be *ca.* 2.3 nm,[36] therefore, it was reasonable to speculate that a considerable amount of the COOH-terminated PEO chain ends would be exposed around the periphery of PEGylated nanospheres. After installation of 5-FAM-KCRGDC functionalities according to the established aqueous amidation methodology and purification through Sephadex ® G75 superfine columns column chromatography, the purity of these samples was confirmed by FPLC (performed by Dr. Yongjian Liu). The final polymer concentrations of both targeting micelle and 50% crosslinked SCKs were adjusted to around 0.20 mg/mL through Centricon (MWCO 10000 Da) and their IC_{50} values to $\alpha_v\beta_3$ were measured (Table 2-4). Greatly enhanced bindings to $\alpha_v\beta_3$ were found both the micelle and SCKs, whose IC_{50} values were determined to be 1.38 nM and 0.49 nM, respectively. The excellent IC_{50} values for these nanostructures indicated that by this synthetic approach, peptides attached on the nanoparticles were most likely on the outer surface of the nanoparticles and thus allowed efficient binding with integrins.

Table 2-4. Characterization data and IC_{50} values of 5-FAM-KCRGDC-labeled nanoparticles by Post-labeling KCRGDC onto micelles with PEG-COOH on the surface.

samples	description	D_{TEM} nm	$N_{aggr.}$	Peptide per NP^2	IC_{50} (nM)[a] $\alpha_v\beta_3$
6	Micelle-5-FAM-KCRGD	26 ± 3	825	170	1.38
7	SCK-5-FAM-KCRGD (50% crosslnked)	26 ± 3	825	170	0.49

[a] IC_{50} values for micelle/SCKs were measured to be the concentrations of the nanoparticles in units of nM.

Internalization of KCRGDC-conjugated nanoparticles in U87MG glioma cells (performed by Dr. Zhiqiang Xu).

Besides measuring the IC_{50} values in a plate assay, *in vitro* cell internalization

studies with U87MG glioma cell line for these nanoparticles were also performed. All six KCRGDC peptide conjugated samples (samples 2-7) showed binding to the glioma cells (Figure 2-5). Cold competition (10 μM unlabeled KCRGDC combined with 1 μM of sample 7 (in peptide concentration)) was found to significantly attenuate both the binding and internalization of sample 7 to the glioma cells (from comparison of Figure 2-5 with Figure 2-6).

As a control, a Fluorescein-5-thiosemicarbazide (FITC) conjugated polymer, mPEG2000$_{2.4}$-*g*-DOTAlysine$_{2.0}$-*g*-FITC$_{0.2}$-*g*-PAA$_{59.4}$-*b*-PS$_{54}$, was prepared from FITC and mPEG2000$_{2.4}$-*g*-DOTAlysine$_{2.0}$-*g*-PAA$_{59.6}$-*b*-PS$_{54}$, *via* amidation chemistry described above. Micelle prepared from this polymer showed no appreciable binding to U87MG glioma cells (Figure 2-7), indicating that the binding of KCRGDC-conjugated nanoparticles to the cells was a result from the conjugated KCRGC peptide.

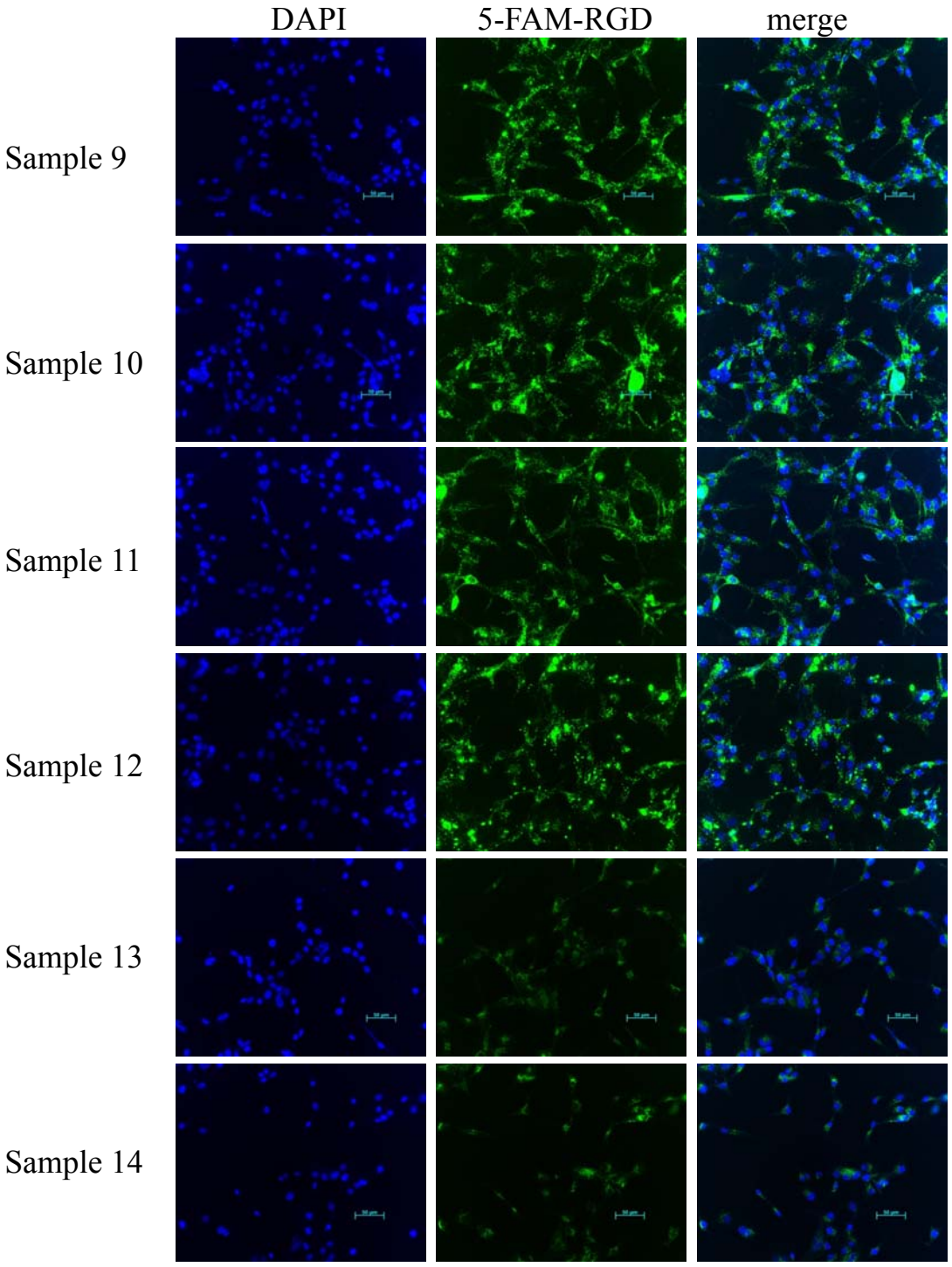

Figure 2-5. Human U87MG glioma cells treated with 1 μM RGD-labeled NPs for 24 h at 37 °C. Scale bar: 50 μm.

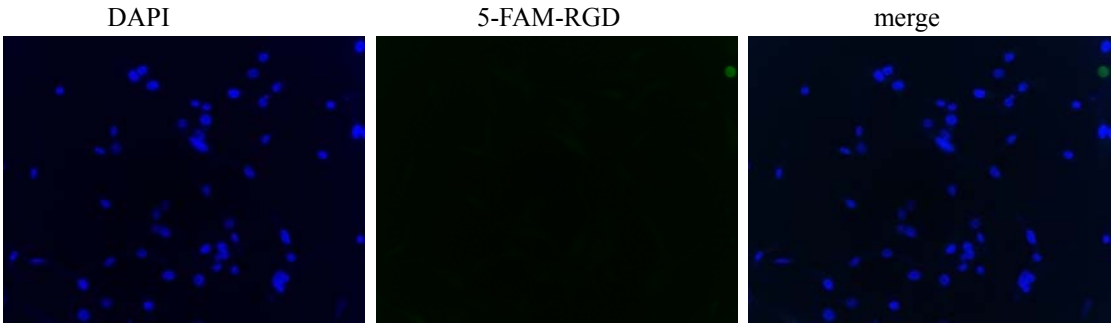

Figure 2-6. Cold competition study conducted by treating U87MG cells with 1 μM RGD-labeled NP (sample 14) and a ten fold excess of KCRGDC (10 μM) for 24 h.

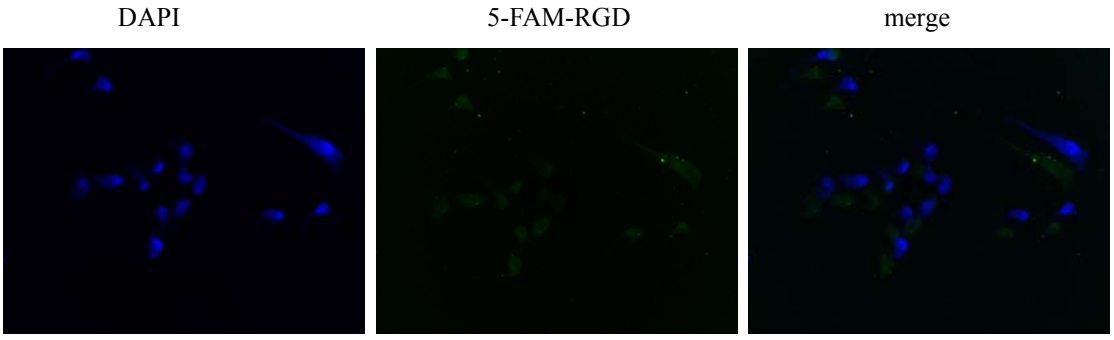

Figure 2-7. Control study conducted by treating U87MG cells with 1 μM unconjugated, FITC-labeled micelle for 24 h.

Conclusions

Methods to develop shell crosslinked nanoparticles bearing cyclic KCRGDC peptide as the nanoscale antagonist to $\alpha_v\beta_3$ integrin were described in this study. The best synthetic approach for attaching large amounts of peptides onto nanoparticles has been established by "hybridizing" the pre-grafting and post-modification strategies, *i.e.*, construction of nano-scale platforms bearing large and tunable quantities of periphery functionalities through the "pre-graft" methodology and then post-modification of these "outer" functionalities with the biologically-active targeting peptides. Optimization of this synthetic methodology and the resulting nanomaterials required a multidisciplinary collaborative approach. The advantages of this synthetic pathway were highlighted by the ~ 10-fold improved binding affinity, obtained from the *in vitro* plate-based assays. The RGD-labeled

nanoparticles showed strong specific binding to U87MG glioma cells. With the good targeting capabilities, sufficient blood retention of these PEGylated SCKs,[27] as well as with efficient radionuclide labeling for PET imaging,[35] these nanoparticles possess good potential to be developed into nanoscale diagnostic and therapeutic agent delivery vehicles.

Acknowledgements

Z. L. thanks Ms. Ashley L. Fiamengo (Ph. D. candidate in Prof. Carolyn J. Anderson's laboratory at Washington University School of Medicine) for measuring the IC_{50} values, Dr. Zhiqiang Xu in Prof. Jeffery R. Leonard's laboratory at Washington University School of Medicine for performing cell internalization studies, Drs. Yongjian Liu in Prof. Michael J. Welch's laboratory at Washington University School of Medicine for the help with FPLC analysis, Mr. Mike. G. Veith for TEM imaging, and the Department of Otolaryngology at Washington University in Saint Louis for use of TEM facilities. Drs Jinqi Xu, Guorong Sun and Andreas Nyström have kindly provided the PAA-*b*-PS block copolymers and their derivatives used for this work. This material is based upon work supported by the National Heart Lung and Blood Institute of the National Institutes of Health as a Program of Excellence in Nanotechnology (HL080729).

References

1. Brooks, P. C.; Clark, R. A.; Cheresh, D. A., Requirement of vascular integrin αvβ3 for angiogenesis. *Science* **1994,** *264* (5158), 569-571.

2. Wilder, R. L., Integrin $\alpha_v\beta_3$ as a target for treatment of rheumatoid arthritis and related rheumatic diseases. *Ann. Rheum. Dis.* **2002,** *61* (90002), 96-99.

3. Creamer, D.; Sullivan, D.; Bicknell, R.; Barker, J., Angiogenesis in psoriasis. *Angiogenesis* **2002,** *5* (4), 231-236.

4. Bishop, G. G.; McPherson, J. A.; Sanders, J. M.; Hesselbacher, S. E.; Feldman, M. J.; McNamara, C. A.; Gimple, L. W.; Powers, E. R.; Mousa, S. A.; Sarembock, I. J., Selective αvβ3-Receptor Blockade Reduces Macrophage Infiltration and Restenosis After Balloon Angioplasty in the Atherosclerotic Rabbit. *Circulation* **2001,** *103* (14), 1906-1911.

5. Chavakis, E.; Riecke, B.; Lin, J.; Linn, T.; Bretzel, R. G.; Preissner, K. T.; Brownlee, M.; Hammes, H. P., Kinetics of integrin expression in the mouse model of proliferative retinopathy and success of secondary intervention with cyclic RGD peptides. *Diabetologia* **2002,** *45* (2), 262-267.

6. Jens Gille, R. A. S., Integrins: Role in Cell Adhesion and Communication. *Ann. N. Y. Acad. Sci.* **1996,** *797* (Microbial Pathogenesis and Immune Response II), 93-106.

7. Seftor, R. E.; Seftor, E. A.; Gehlsen, K. R.; Stetler-Stevenson, W. G.; Brown, P. D.; Ruoslahti, E.; Hendrix, M. J., Role of the $\alpha_v\beta_3$ integrin in human melanoma cell invasion. *Proc. Natl. Acad. Sci. U.S.A.* **1992,** *89* (5), 1557-1561.

8. Montgomery, A. M.; Reisfeld, R. A.; Cheresh, D. A., Integrin $\alpha_v\beta_3$ rescues melanoma cells from apoptosis in three-dimensional dermal collagen. *Proc. Natl. Acad. Sci. U.S.A.* **1994,** *91* (19), 8856-8860.

9. Ruoslahti, E.; Pierschbacher, M. D., New perspectives in cell adhesion: RGD and integrins. *Science* **1987,** *238* (4826), 491-497.

10. Plow, E. F.; Haas, T. A.; Zhang, L.; Loftus, J.; Smith, J. W., Ligand Binding to Integrins. *J. Biol. Chem.* **2000,** *275* (29), 21785-21788.

11. Pasqualini, R.; Koivunen, E.; Ruoslahti, E., αv Integrins as receptors for tumor targeting by circulating ligands. *Nat. Biotech.* **1997,** *15* (6), 542-546.

12. Arap, W.; Pasqualini, R.; Ruoslahti, E., Cancer Treatment by Targeted Drug Delivery to Tumor Vasculature in a Mouse Model. *Science* **1998,** *279* (5349), 377-380.

13. Ellerby, H. M.; Arap, W.; Ellerby, L. M.; Kain, R.; Andrusiak, R.; Rio, G. D.; Krajewski, S.; Lombardo, C. R.; Rao, R.; Ruoslahti, E.; Bredesen, D. E.; Pasqualini, R., Anti-cancer activity of targeted pro-apoptotic peptides. *Nat. Med.* **1999,** *5* (9), 1032-1038.

14. Cai, W.; Niu, G.; Chen, X., Imaging of Integrins as Biomarkers for Tumor Angiogenesis. *Curr. Pharm. Design* **2008,** *14*, 2943-2973.

15. Lim, E. H.; Danthi, N.; Bednarski, M.; Li, K. C. P., A review: Integrin $\alpha_v\beta_3$-targeted molecular imaging and therapy in angiogenesis. *Nanomedicine* **2005,** *1* (2), 110-114.

16. Miller, W. H.; Keenan, R. M.; Willette, R. N.; Lark, M. W., Identification and in vivo efficacy of small-molecule antagonists of integrin $\alpha_v\beta_3$ (the vitronectin receptor). *Drug Discovery Today* **2000,** *5* (9), 397-408.

17. King C.P. Li, M. D. B., Vascular-targeted molecular imaging using functionalized polymerized vesicles. *J. Magn. Reson. Imaging.* **2002,** *16* (4), 388-393.

18. Boturyn, D.; Coll, J.-L.; Garanger, E.; Favrot, M.-C.; Dumy, P., Template Assembled Cyclopeptides as Multimeric System for Integrin Targeting and

Endocytosis. *J. Am. Chem. Soc.* **2004,** *126* (18), 5730-5739.

19. Dubey, P. K.; Mishra, V.; Jain, S.; Mahor, S.; Vyas, S. P., Liposomes Modified with Cyclic RGD Peptide for Tumor Targeting. *J. Drug Target.* **2004,** *12* (5), 7-264.

20. Marko, K. L., M.; Mezo, G.; Mihala, N.; Kutnyanszky, E.; Kiss, E.; Hudecz, F.; Madarasz, E. , A Novel Synthetic Peptide Polymer with Cyclic RGD Motifs Supports Serum-Free Attachment of Anchorage-Dependent Cells. *Bioconjugate Chem.* **2008,** *19* (9), 1757-1766.

21. Ishikawa, A.; Zhou, Y.-M.; Kambe, N.; Nakayama, Y., Enhancement of Star Vector-Based Gene Delivery to Endothelial Cells by Addition of RGD-Peptide. *Bioconjugate Chem.* **2008,** *19* (2), 558-561.

22. Chen, R.; Curran, S. J.; Curran, J. M.; Hunt, J. A., The use of poly(l-lactide) and RGD modified microspheres as cell carriers in a flow intermittency bioreactor for tissue engineering cartilage. *Biomaterials* **2006,** *27* (25), 4453-4460.

23. Montet, X.; Funovics, M.; Montet-Abou, K.; Weissleder, R.; Josephson, L., Multivalent Effects of RGD Peptides Obtained by Nanoparticle Display. *J. Med. Chem.* **2006,** *49* (20), 6087-6093.

24. Kang, H.; Alam, M. R.; Dixit, V.; Fisher, M.; Juliano, R. L., Cellular Delivery and Biological Activity of Antisense Oligonucleotides Conjugated to a Targeted Protein Carrier. *Bioconjugate Chem.* **2008,** *19* (11), 2182-2188.

25. J. L. Turner , D. P., R. Plummer, Z. Chen, A. K. Whittaker, K. L. Wooley, Synthesis of Gadolinium-Labeled Shell-Crosslinked Nanoparticles for Magnetic Resonance Imaging Applications. *Adv. Funct. Mater.* **2005,** *15* (8), 1248-1254.

26. Becker, M. L.; Liu, J.; Wooley, K. L., Functionalized Micellar Assemblies Prepared via Block Copolymers Synthesized by Living Free Radical Polymerization upon Peptide-Loaded Resins. *Biomacromolecules* **2005,** *6* (1), 220-228.

27. Sun, G.; Hagooly, A.; Xu, J.; Nystrom, A. M.; Li, Z.; Rossin, R.; Moore, D. A.; Wooley, K. L.; Welch, M. J., Facile, Efficient Approach to Accomplish Tunable Chemistries and Variable Biodistributions for Shell Cross-Linked Nanoparticles. *Biomacromolecules* **2008,** *9* (7), 1997-2006.

28. Xu, J.; Sun, G.; Rossin, R.; Hagooly, A.; Li, Z.; Fukukawa, K.-I.; Messmore, B. W.; Moore, D. A.; Welch, M. J.; Hawker, C. J.; Wooley, K. L., Labeling of Polymer Nanostructures for Medical Imaging: Importance of Cross-Linking Extent, Spacer Length, and Charge Density. *Macromolecules* **2007,** *40* (9), 2971-2973.

29. Lewis, M. R.; Kao, J. Y.; Anderson, A.-L. J.; Shively, J. E.; Raubitschek, A., An Improved Method for Conjugating Monoclonal Antibodies with N-Hydroxysulfosuccinimidyl DOTA. *Bioconjugate Chem.* **2001,** *12* (2), 320-324.

30. Gilles, M. A.; Hudson, A. Q.; Borders, C. L., Stability of water-soluble carbodiimides in aqueous solution. *Anal. Biochem.* **1990,** *184* (2), 244-248.

31. Staros, J. V.; Wright, R. W.; Swingle, D. M., Enhancement by N-hydroxysulfosuccinimide of water-soluble carbodiimide-mediated coupling reactions. *Anal. Biochem.* **1986,** *156* (1), 220-222.

32. Sedlak, J.; Lindsay, R. H., Estimation of total, protein-bound, and nonprotein sulfhydryl groups in tissue with Ellman's reagent. *Anal. Biochem.* **1968,** *25*, 192-205.

33. Haubner, R.; Wester, H.-J.; Reuning, U.; Senekowitsch-Schmidtke, R.; Diefenbach, B.; Kessler, H.; Stocklin, G.; Schwaiger, M., Radiolabeled $\alpha_v\beta_3$ Integrin Antagonists: A New Class of Tracers for Tumor Targeting. *J. Nucl. Med.* **1999,** *40* (6), 1061-1071.

34. Nystrom, A. M.; Wooley, K. L., Thiol-functionalized shell crosslinked knedel-like (SCK) nanoparticles: a versatile entry for their conjugation with biomacromolecules. *Tetrahedron* **2008,** *64* (36), 8543-8552.

35. Sun, G.; Xu, J.; Hagooly, A.; Rossin, R.; Li, Z.; Moore, D. A.; Hawker, C. J.; Welch, M. J.; Wooley, K. L., Strategies for Optimized Radiolabeling of Nanoparticles for *in vivo* PET Imaging. *Adv. Mater.* **2007,** *19* (20), 3157-3162.

36. Devanand, K.; Selser, J. C., Asymptotic behavior and long-range interactions in aqueous solutions of poly(ethylene oxide). *Macromolecules* **2002,** *24* (22), 5943-5947.

37. Sprague, J. E.; Kitaura, H.; Zou, W.; Ye, Y.; Achilefu, S.; Weilbaecher, K. N.; Teitelbaum, S. L.; Anderson, C. J., Noninvasive Imaging of Osteoclasts in Parathyroid Hormone-Induced Osteolysis Using a ^{64}Cu-Labeled RGD Peptide. *J. Nucl. Med.* **2007,** *48* (2), 311-318.

Chapter 3

Nanostructures from Amphiphilic Hyperbranched Fluoropolymers (HBFP) for Imaging and Therapeutic Delivery in the Diagnosis and Treatment of Pediatric Brain Cancers

Abstract

In this chapter, nanoscale micelles from a novel amphiphilic hyperbranched fluoropolymer were studied as drug delivery agent assemblies. The polymer was constructed by a published procedure that involved atom transfer radical polymerization (ATRP) from consecutive copolymerizations of 4-chloromethylstyrene with dodecyl acrylate and then 1,1,1-trifluoroethyl methacrylate with *tert*-butyl acrylate, followed by acidolysis to afford the hydrophilic acrylic acid residues. Cascade blue was functionalized onto these micelle structures as a fluorescence reporter. F3, a 31 amino acid sequence (KDEPQRRSARLSAKPAPPKPEPKPKKAPAKK) which binds specifically to nucleolin was conjugated onto the micelles as the targeting agent. Doxorubicin (Dox), a drug widely used in chemotherapy treatments for many types of cancer, was used as the therapeutic agent. The Dox-loaded and F3-conjugated nanoparticles were tested for *in vivo* effects using a murine intracranial U87MG glioma xenograft tumor model. Specific binding to the tumor-associated angiogenic endothelial cells was observed for F3-peptide conjugated nanoparticles. Compared to untargeted nanoparticles (scramble-peptide conjugated nanoparticles) F3-peptide conjugated

targeting nanoparticles (NP) were concentrated more in the angiogenic tumor blood vessels. Also, Dox carried by these nanoparticles can cause apoptotic effects on the targeted tumor cells, which is expected to lead to targeted therapeutic benefits.

Introduction

The central nervous system (CNS) is the most common site of primary solid tumors in children.[1-4] Glioblastoma multiforme (GBM) is a highly malignant tumor in CNS.[5, 6] Patients diagnosed with GBM usually live less than one year after surgery despite intensive chemotherapy and radiation.[7] One of the biggest challenges for treating these patients is lack of effective therapeutics that could efficiently pass blood brain barrier (BBB) and specifically target to the tumor site.[8-11] Recent studies using nanoparticles as the carrier to deliver both diagnostics and therapeutics have shown promising results among non-CNS malignant tumors.[12-15] However, there have been very few studies using nanoparticles as therapeutic delivery vehicle for the treatment of GBM. Compared to traditional drug carriers, nanoparticle has several advantages such as their extremely small sizes (5-10 nm); possibility of conjugating multifunctional groups onto their surface; and increased retention time and better bio-distribution with PEG-modified nanoparticle.[16-19]

Nucleolin is a phosphoprotein that normally resides in the nucleolus and also plays very important roles in rDNA transcription, ribosome assembly and ribosome biogenesis.[20-24] Certain cancers such as breast cancer show significant up regulation and surface expression of nucleolin protein.[25] As a binding partner for Nucleolin, HMN2 (high mobility protein group 2) has been shown strong interaction with nucleolin in the nucleus.[26] A small peptide (F3 peptide), previously characterized based on sequence homology to HMN2 demonstrated significant binding and internalization both into cancer cell and angiogenic blood vessels.[27-29] Previously we have shown that doxorubicin-loaded nanoparticles from hyperbranched fluoropolymers demonstrated significant

cytotoxic effects on U87MG glioma cell line *in vitro*.[30] To further explore possibility of utilizing this system *in vivo* and specifically targeting glioma tumor cells, in the present study we designed a strategy of conjugating F3 peptide to our nanoparticle and tested *in vivo* effects of this targeting nanoparticle loaded with doxorubicin using U87MG glioma xenograft tumor model. Our preliminary results showed that F3-peptide conjugated targeting nanoparticle not only specifically bound to the tumor-associated angiogenic endothelial cells, doxorubicin carried by these nanoparticles also caused apoptotic effects on the targeted tumor cells. Compared to untargeted nanoparticles (scramble-peptide conjugated nanoparticles), F3-conjugated targeting nanoparticle were concentrated more in the angiogenic tumor blood vessels. Improved biodistribution was achieved by functionalization these nanoparticles with a 750 Da poly(ethylene glycol). This system will not only provide a novel approach to efficiently deliver therapeutics to the targeted tumor site it also potentially attenuate systemic side effects by free Doxorubicin.

Experimental

Materials. All chemicals were purchased from Sigma-Aldrich Chemical Company, unless otherwise noted. Poly(ethylene oxide) amine (PEO_{15}-NH_2, M_n = 750 Da) was purchased from Interzyne (Tampa, FL) and used without further purification. Nanopure water (18 MΩ·cm) was acquired by means of a Milli-Q water filtration system (Millipore Corp.; Bedford, MA). The peptides: F3, FITC-F3, and scrambled F3 (KDEARALPSQRSRKPAPPKPEPKPKKAPAKK), were customized from Chengdu Kaijie Biopharmaceuticals Co. Ltd., Chengdu, China, and was used as received. Supor 25 mm 0.1 μm Spectra/Por Membrane tubes (molecular weight cutoff (MWCO) 6-8000

Da), purchased from Spectrum Medical Industries Inc., were used for dialysis. Superfine Sephadex ® G75 resin (bead diameter: 20-50 μm; fractionation range: 1000-50000 Da (Dextrans)) was purchased from GE Healthcare and was used to purify aqueous nanoparticle samples. Centricon tubes (Amicon Ultra 4, 30 kDa MWCO) were purchased from Millipore Corp., MA.

The hyperbranched amphiphilic fluoropolymer was synthesized by Dr. Wenjun Du as previously reported (polymer 4b).[31]

5 mM PBS (phosphate buffered saline, with 5 mM of phosphates and 5 mM of NaCl) was prepared by mixing NaH_2PO_4 (0.76 g), Na_2HPO_4 (1.93 g) and NaCl (1.17 g) into 4 liters of nanopure water and has a pH ~7.4. 150 mM PBS (phosphate buffered saline, with 150 mM of phosphates and 150 mM of NaCl) was prepared by mixing NaH_2PO_4 (22.7 g), Na_2HPO_4 (59.0 g) and NaCl (35.1 g) into 4 liters of nanopure water and was used as the solvent for running Sephadex® columns (pH ~7.4).

Instrumental. ^{1}H NMR spectra were recorded at 300 on a Varian Unity-plus 300 spectrometer, with the solvent proton signal as the standard.

Dynamic light scattering (DLS) measurements were acquired using a Brookhaven Instruments (Worcestershire, U.K.) system, including a model BI-200SM goniometer, a model BI-9000AT digital correlator, a model EMI-9865 photomultiplier, and a model 95-2 Ar ion laser (Lexel, Corp.; Farmindale, NY) operated at 514.5 nm. Measurements were made at 25 ± 1 °C. Prior to analysis, solutions were filtered through a 0.22 μm Gelman Nylon Acrodisc® 13 membrane filter to remove dust particles. Scattered light was collected at a fixed angle of 90°. The digital correlator was operated with 522 ratio spaced channels, and initial delay of 5 μs, a final delay of 100 ms, and a duration of 10

minutes. A photomultiplier aperture of 400 μm was used, and the incident laser intensity was adjusted to obtain a photon counting of between, 200 and 300 kcps. The calculations of the particle size distributions and distribution averages were performed with the ISDA software package (Brookhaven Instruments Co.), which employed single-exponential fitting, cumulants analysis, non-negatively constrained least-squares (NNLS) and CONTIN particle size distribution analysis routines. The data are presented as the average values from at least four measurements.

Transmission electron microscopy (TEM) measurements were conducted on a Hitachi H600 microscope. Micrographs were collected at 100,000× magnification and calibrated using a 41 nm polyacrylamide bead from NIST. Carbon-coated copper grids were treated with oxygen plasma prior to deposition of the micellar samples. The samples were stained with 1% phosphotungstic acid (PTA) for 1 minute, and then the solution was wicked away and the samples were allowed to dry under ambient conditions. The number-average particle diameters (D_{av}) and standard deviations were generated from the analysis of a minimum of 100 particles from at least three different micrographs.

Fast protein liquid chromatography (FPLC) was performed by Dr. Yongjian Liu in Prof. Michael J. Welch's laboratory at Washington University School of Medicine on an AKTA (GE) system, including a P-920 pump, Columns of Superose 12 10/300 GL, and a UV detector with 254 nm wavelength. The eluent was 20 mM HEPES with 150 mM NaCl and flow rate was 0.8 mL/min. The results were analyzed by UNICORN 3.10.11.

UV-vis spectra were acquired on a Varian Cary 1E UV-vis system (Varian, Inc., Palo Alto, CA) using polystyrene cuvettes.

Preparation of Cascade Blue and F3 Conjugated Micelles. To two solutions of polymer **1**[31] (30 mg 0.33 μmol) in DMF (10 mL) in 20 mL vials were added HBTU (18.5 mg, 49 μmol) and HOBt (6.6 mg, 49 μmol). The solutions were allowed to stir under argon for 1 h. DIPEA (4 mg, 40 μmol) and Cascade Blue (1.54 mg, 2.5 μmol) were added subsequently to each solution. The reaction mixtures were stirred under argon overnight. F3 peptide (9.9 mg, 2.5 μmol) and FITC-F3 peptide (10.1 mg, 2.5 μmol) were added separately and the two reaction mixtures were stirred under argon for 48 h. DMF (15 mL) was added to each vial to afford a 1.0 mg/mL solution (in polymer concentration) and the solutions were dialyzed (MWCO 6000-8000 Da) against nanopure water for 48 h to afford the micelle solution. The micelle solutions were collected and were purified with Sephadex® G75 superfine column with 150 mM PBS (pH ~7.4) as the solvent, to remove unattached F3 peptide and cascade blue. The purified micelle was washed with 5 mM PBS (pH ~7.4) and concentrated by using Centricon tubes (MWCO 30000 a) and monitored by FPLC.

Quantification of Cascade Blue (CB) was determined by UV-vis (400 nm, ε = 28000 $M^{-1}cm^{-1}$, from manufacturer's manual). The conjugation of FITC-F3 was determined by UV absorbance from the FITC conjugated to F3 peptide (488 nm, ε = 39000 $M^{-1}cm^{-1}$ determined by a calibration curve in 5 mM PBS, pH ~ 7.4). Quantification of F3 peptides was deduced from the coupling efficiency of FITC-F3 to the polymer by assuming that the two peptides had approximately the same coupling efficiency.

Preparation of Cascade Blue and F3 (or scrambled F3) Conjugated, PEGylated Micelles. To two solutions of polymer **1**[31] (52 mg 0.57 μmol) in DMF (10 mL) were added HBTU (34.0 mg, 89 μmol) and HOBT (13.2 mg, 97 μmol). The solutions were

allowed to stir under argon for 1 h. DIPEA (10 mg, 100 μmol), NH_2-PEO_{13}-OMe (8.8 mg, 12 μmol) and cascade blue (2.5 mg, 4.1 μmol) were added. The reaction mixtures were stirred under argon overnight. F3 (16.5 mg, 4.14 μmol) and scrambled F3 peptide (sequence: KDEARALPSQRSRKPAPPKPEPKPKKAPAKK) (16.4 mg, 4.10 μmol) were added and the reaction mixtures were stirred under argon for 48 h. DMF (42 mL) was added to afford a 1.0 mg/mL solution (in polymer concentration) and the solution was dialyzed (MWCO 6000-8 000 Da) against nanopure water for 48 h. The micelle solutions were collected and purified with Sephadex® G75 column with 150 mM PBS (pH ~7.4) as the solvent, to remove unattached F3 peptide, Cascade Blue and PEG chains. The purified micelle solutions were washed with 5 mM PBS (pH ~7.4) and concentrated by using Centricon tubes (MWCO 30000 Da) and monitored by FPLC. A portion of the micelles was freeze-dried to powder to analyze the conjugation efficiency of PEGylation. ^{NMR}Mn = 106 kDa. ^{1}H NMR (300 MHz, DMSO-d_6): δ 0.8-2.3 (br, m, *C**H₂*** and *C**H*** of backbone), 4.3-4.7 (s, br, *C**H₂***CF3, Ph*C**H₂***), 6.4-7.5 (m, br, *Ar**H***), 8.2-8.4 (br, *Ar**H*** of cascade blue), 8.6 (s, br, *ArH* of CB), 8.9-9.1 (m, br, *Ar**H*** of CB), 12.0-12.5 (s, br, COO***H***) ppm.

The conjugation of cascade blue (CB) was determined by UV-vis (400 nm, ε = 28000 $M^{-1}cm^{-1}$ from manufacturer's manual). The conjugation of F3 and scrambled F3 was calculated by assuming the same coupling efficiency achieved in the above experiments. (488 nm, ε = 39000 $M^{-1}cm^{-1}$ in 5 mM PBS, pH ~ 7.4).

General Procedures for Dox Loading. A solution of Dox (2.7 mg mL^{-1} in CH_2Cl_2 and 3 equivalent of triethylamine) was added to a micelle solution (4 mL,). The weight percentage for the Dox loaded to the polymer was 30%. The solution was protected from

light and stirred with the container uncapped for 16 h. The removal of unincorporated Dox was achieved using Centricon tubes (MWCO 30000 Da) and centrifuged at 3000 rpm × 5 min. After three cycles of washing and centrifuging, the filtrate was collected and analyzed by UV-vis (488 nm) to confirm the successful removal of the free Dox. The Dox-loaded micelle solutions were then reconstituted to a final volume of 4 mL. The amount of incorporated Dox was determined by UV-vis (480 nm, ε = 12500 $M^{-1}cm^{-1}$ determined by a calibration curve in DMF/PBS 4:1) in a 4:1 v/v mixture of DMF and Dox-micelle solution.

***In vivo* studies on brain tumor mice with Dox-loaded micelles (performed by Dr. Zhiqiang Xu in Prof. Jeffrey R. Leonard at Washington University School of Medicine).** To mice with tumor established in the brain, micelles loaded with Dox were treated by retroorbital injection (twice per week, 0.5mg/kg DOX equivalent for high loading and 0.25mg/kg DOX equivalent for low loading, 5 mg/kg for free DOX) for 4 weeks. At the end of treatment mice were anesthetized and perfused with 4% paraformaldehyde by intracardiac injection. Brain, heart, liver, kidney etc were then harvested and fixed with 4% paraformaldehyde before sent off for paraffin embedding and section. For the immunohistochemistry staining, unstained slides were first processed for antigen retrieval using citrate buffer (pH=6.8). Nucleus was counterstained with Hematoxin.

Results and Discussion

Amphiphilic hyperbranched polymers, constructed with a hyperbranched hydrophobic core and amphiphilic copolymer arms consisting of trifluoroethyl

methacrylate and acrylic acid residuals,[31] were functionalized with cascade blue (CB) ethylene diamine and F3 peptide to afford the CB and F3 functionalized polymer (Scheme 3-1). The coupling of CB and F3 peptide was achieved through amidation chemistry between the amino groups on the CB ethylene diamine or F3 peptide and the acrylic acid residues on the arms of the hyperbranched polymer, facilitated by HOBt and HBTU with DMF as the solvent. After the conjugation, an appropriate amount of DMF was added to the reaction mixture to afford solutions with *ca.* 1 mg/mL. The solutions were dialysed against nanopure water to remove DMF and other small molecule impurities and at the same time to form the micelles in water. The micelles were further purified by running Sephadex® G75 columns, mainly to remove F3 peptides physically-associated to the micelles which were not removed by dialysis. FPLC analysis performed by Dr. Yongjian Liu showed improvement in sample purity after the column (Figure 3-1). The relative intensity of the peak at *ca.* 17.5 min from F3 peptide was greatly reduced.

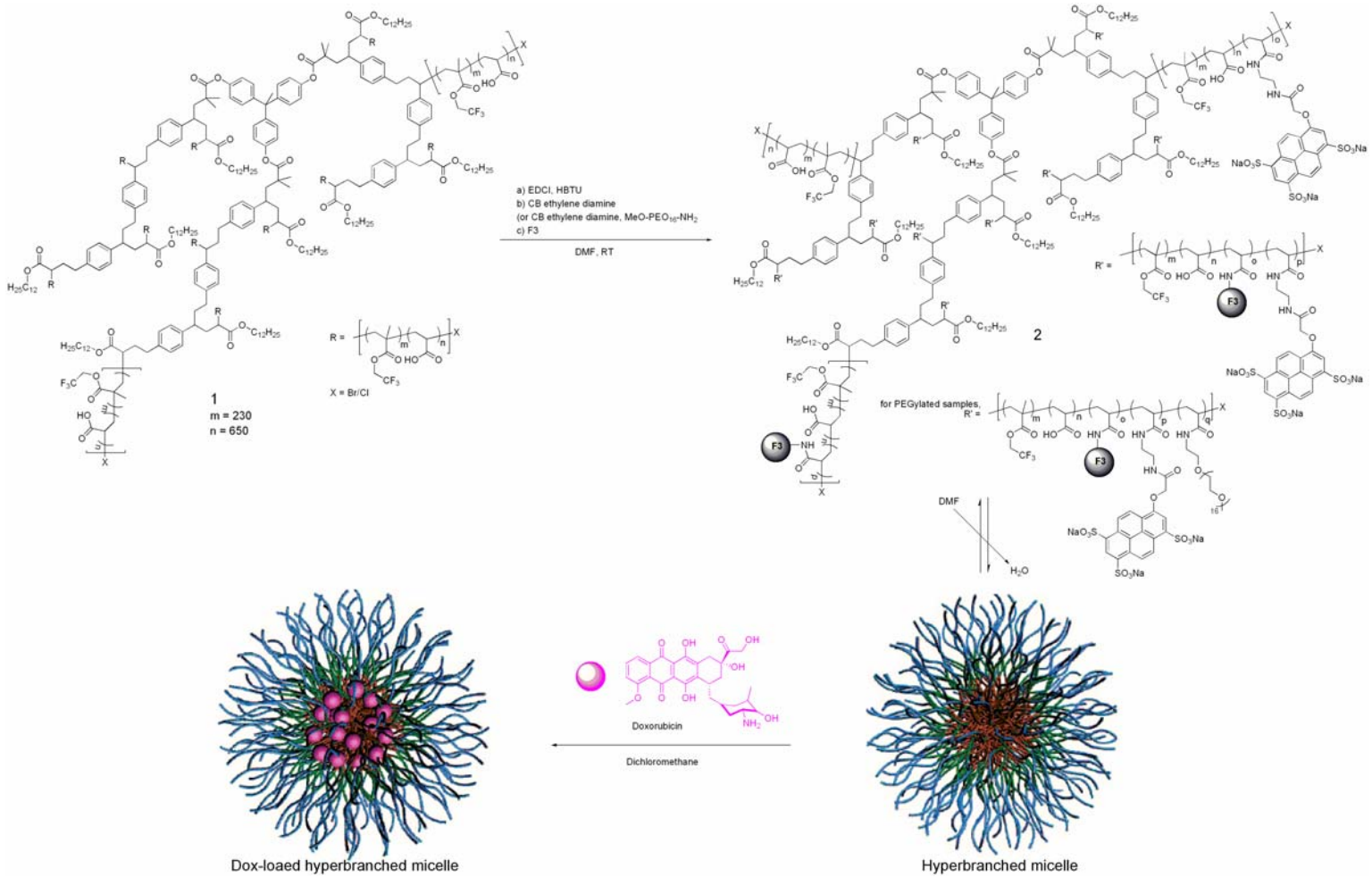

Scheme 3-1. Illustration of the conjugation of cascade blue (CB) ethylene diamine, polyethylene glycol, F3 (or scrambed F3) peptide onto the hyperbranched amphiphilic polymer 1, and following micellization and Dox-loading. (The red coils represent the hydrophobic core and the blue coils represent the amphiphilic arms.)

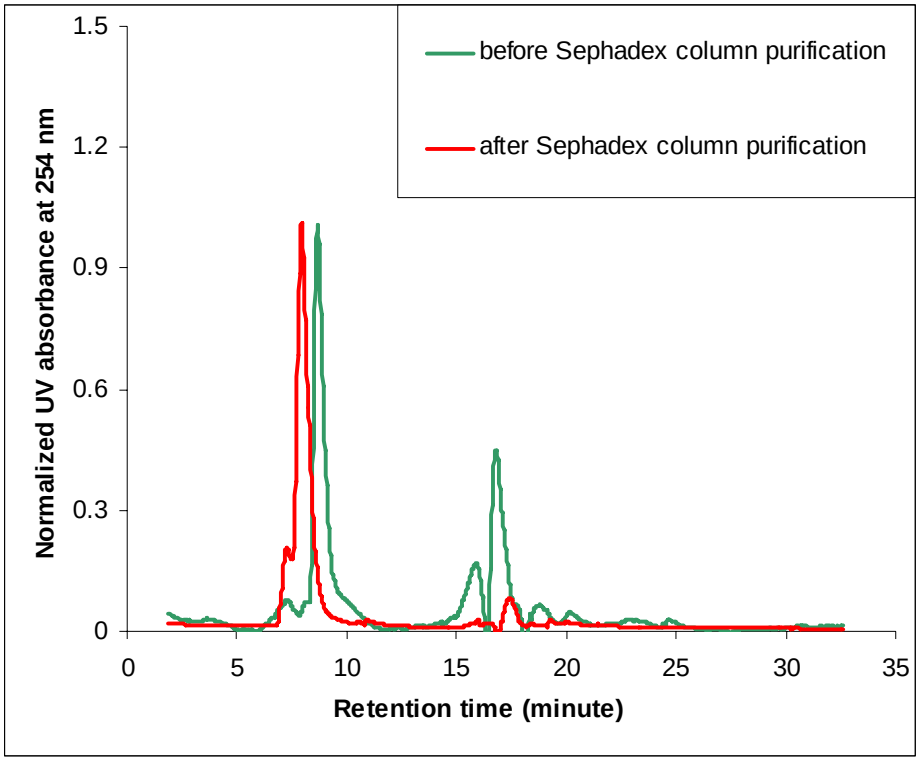

Figure 3-1. Representative FPLC traces of micelles conjugated with F3 peptide before and after purification with Sephadex® G75 columns.

CB was introduced as an optical tracer to localize the micelles while performing both *in vitro* cell internalization studies and *in vivo* tumor targeting studies. The conjugation efficiency of CB was determined by UV-vis (400 nm, ε = 28000 $M^{-1}cm^{-1}$ from manufacturer's manual). .The coupling efficiency of CB to the polymer was calculated to be around 70%. Bradford assay to quantify the F3 targeting peptide with Coomassie Blue had been performed but no obvious color change was observed, possibly because the molecular weight of the peptide was too small (~ 3900 Da).[32] To obtain the coupling yield of the peptide, a control experiment with similar conditions but using FITC-labeled F3 peptide was carried out. The coupling efficiency of the FITC-F3 was then determined by measuring the UV absorption of the final micelle at 488 nm with a molar extinction coefficient 39000 $M^{-1}cm^{-1}$. The coupling efficiency of F3 peptide (and later scrambled

F3 peptide) was assumed to be the same to that of the FITC-F3, which was around 50%. As a control, micelles prepared from the hyperbranched amphiphilic polymer functionalized only with CB was also prepared and characterized from the same methods. For micelles conjugated both with CB and F3, 6.9 CB molecules and 3.0 F3 molecules were attached to one polymer in average. For micelles conjugated only with CB, ca. 5.8 CB molecules were attached to one polymer. Characterization data to these micelles are shown in Table 3-1.

These micelles were then loaded with Dox using a similar procedure published previously.[33] Dichloromethane was used as the organic solvent for Dox and also to swell the core of the micelle, facilitating the loading of the therapeutic. The amount of Dox loaded in micelles was determined by UV-vis measurements. The loading capacities for micelles 1 and 3 were 16 and 15 wt% based on the polymer mass, respectively (Table 3-1).

Table 3-1. Summary of Characterization Data and Doxorubicin Loading for Micelles from F3- and/or CB- conjugated hyperbranched amphiphilic polymer.

Sample	D_{TEM} nm	$D_h(n)$[a] nm	[polymer] mg/mL	F3/ polymer[b]	CB/ polymer[b]	Dox μg/mL[b]	Loading capacity (wt%)
1	7 ± 1	29 ± 4	0.609		5.8	99	16
2	7 ± 1	28 ± 2	0.571		5.8		
3	7 ± 1	29 ± 2	0.636	3.0	6.9	96	15
4	7 ± 1	29 ± 2	0.710	3.0	6.9		

a by DLS. *b* by UV-vis.

To test if the F3 targeting peptide could enhance DOX delivery, DOX-loaded and/or F3-conjugated micelles (sample 1 and 3) were incubated with the U87MG cells and were studied by fluorescence imaging of the Dox (λ_{max}: 480 nm) (These experiments were

performed by Dr. Zhiqiang Xu.). As can be seen in Figure 3-2, an increased amount of DOX was incorporated into the nucleus for the targeted micelles (sample 3), while for the untargeted micelles (sample 1), most of the Dox was located surrounding the nucleus, suggesting an enhanced nuclear uptake of DOX in glioma cells induced by the incorporation of the F3 peptide. At this time, it is not clear how F3 enhanced DOX delivery. It's hypothesized that with F3 targeting peptide, the nanoparticles could bind U87MG cell more efficiently and more strongly, leading to increased cell uptake, and as a result, more DOX was delivered.

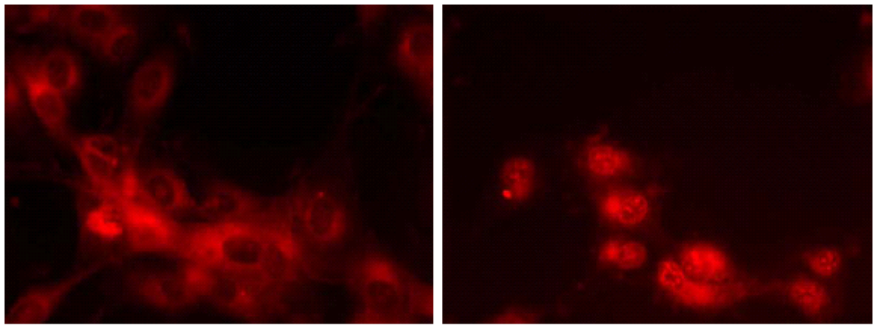

Figure 3-2. Fluorescence images of DOX-loaded micelle without F3 (sample 1, left) and with F3 (sample 3, right) targeting peptide.

A challenge in current brain cancer research is the difficulty for the therapeutics to cross the blood brain barrier (BBB) to reach the tumor tissues and cells. [8-11] Both TEM and DLS measurements have shown that these micelles had small sizes (D_{TEM} = 7 ± 1 nm, $D_h(DLS)_{num}$ ~29 nm). TEM images are shown in Figure 3-3 (poor quality due to difficulties in staining the samples).

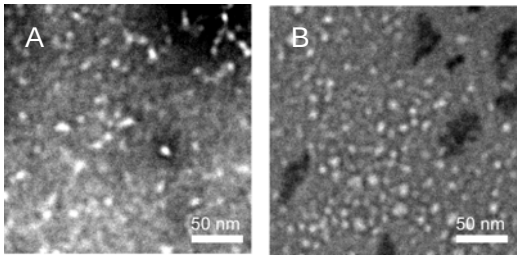

Figure 3-3. Transmission electron microscopy (TEM) images of micelle nanoparticles conjugated with CB and F3 peptide. A, sample 4, non-PEGylated; B, sample 5, PEGylated.

To test if the targeted nanoparticles could pass the BBB in glioma-bearing mice, F3 and CB conjugated micelles (sample 4) were administered into mice with U87MG tumor established by tail vein injection, and the untargeted micelle (sample 2) was used as the control. With a specific polyclonal antibody against cascade blue, significantly larger amounts of staining within the tumor cells in the brain were detected (Figure 3-4, right), as compared with the control (Figure 3-4, left), indicating that F3 conjugated nanoparticles can indeed pass the BBB to reach the tumor cells and the presence of F3 can facilitate the tumor targeting process. In figure 3-3, the purple color indicates the

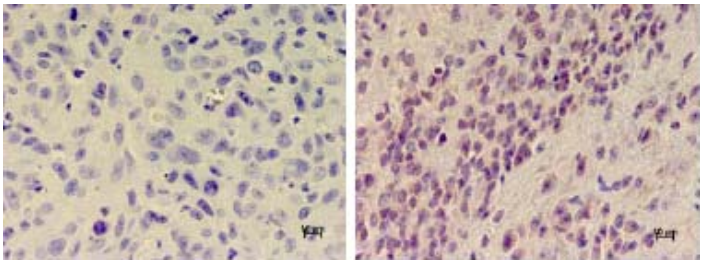

Figure 3-4. Immunohistochemistry (IHC) stains of brain tumor from U87MG xenograft mice treated with untargeted micelle (sample 2, left) and targeted micelle (sample 4, right). (IHC staining using specific antibody against cascade blue, ABC method.) Scale bar: 10 μm.

presence of CB-functionalized micelle in the tumor cells. These experiments were performed by Dr. Zhiqiang Xu.

Dox-loaded micelles (samples 1 and 3) were administered by retroorbital injection, into mice implanted intracranially with tumors. Brain, heart, liver, spleen and kidney tissues were harvested after the treatment. Compared to untargeted micelles, targeted micelles were more concentrated within tumor-associated blood vessels (Figure 3-5, black arrow) while tumor cells adjacent to these blood vessels also showed significant amounts of micelles within their cytoplasm and nuclei (Figure 3-5, red arrow). Some of these tumor cells showed fragmented DNA indicating apoptotic response (Figure 3-5, thick red arrow). In contrast, untargeted micelles were distributed evenly among tumor cells and blood vessels, suggesting that this was mediated through non-specific leaky blood brain barrier (BBB). Although targeted micelles showed promising binding to the tumor cells, it was found that significant amounts of the micelles were localized in the liver and spleen, suggesting that the biodistribution needs to be improved. These experiments were performed by Dr. Zhiqiang Xu.

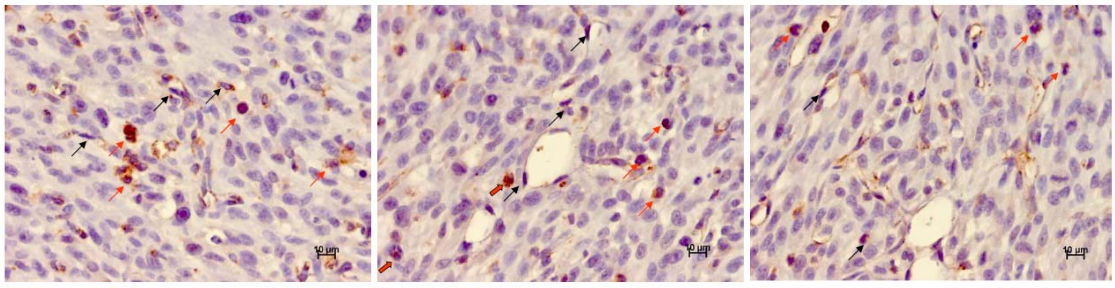

CB-DOX-NP CB-F3-DOX-NP CB-F3-DOX-NP

Figure 3-5. Immunohistochemistry (IHC) stains of brain tumor from U87MG xenograft mice treated with untargeted micelles (sample 1, left) and targeted micelles (sample 3, middle and right). (IHC staining using specific antibody against cascade blue, ABC method) Scale bar: 10 μm.

Since the introduction of poly(ethylene glycol) was reported to enhance the biodistribution,[34] PEGylated micelles were then synthesized (Scheme 3-1). For our study, NH_2-PEO_{16}-OMe (MW = 750 Da) was selected with the concern that short PEO might have little hindering effects on the peptide binding. Micelles with ca. 20 MeO-PEO_{16} grafts per polymer were prepared, and conjugated with CB and F3 peptide (sample 5 in Table 3-2). As a control, CB-conjugated and PEGylated micelles functionalized with a scrambled F3 peptide (sequence: KDEARALPSQRSRKPAPPKPEPKPKKAPAKK) were also prepared (sample 6 in Table 3-2). The PEG contents of the two samples were *ca.* 14 wt%.

Table 3-2. Summary of Characterization Data and Doxorubicin Loading for Micelles from F3-CB-PEG750-Polymer.

Sample	D_{TEM} nm	$D_h(n)$[a] nm	[polymer] mg/mL	PEG per polymer[b]	F3 per polymer[c]	CB per polymer[c]	Dox μg/mL[c]	Loading capacity (wt%)
5	8 ± 1	28 ± 2	0.339	20	3.1	3.8	58	17
6	7 ± 1	30 ± 2	0.250	20	3.1[d]	3.8	38	15

a by DLS. *b* by ^{1}H NMR. *c* by UV-*vis*. *d* scrambled F3 (KDEARALPSQRSRKPAPPKPEPKPKKAPAKK).

These two PEGylated samples were also administered to brain tumor bearing mice. As can be seen from figure 3-6, F3 conjugated targeting NPs were more concentrated in the angiogenic tumor blood vessels in the brain than scrambled F3 conjugated micelles, suggesting the targeting is a result of the specific binding of the F3 peptide to the tumor cells. Compared to non-PEGylated NPs, slightly better biodistribution was obtained. Increasing the PEG content might be able to further enhance the biodistribution.[34]

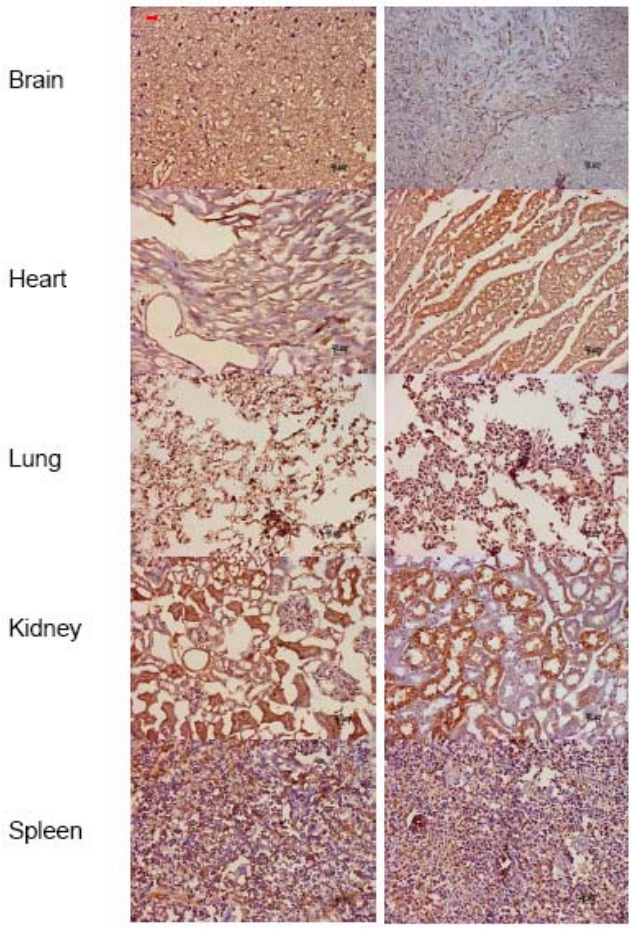

Figure 3-6. Immunohistochemistry (IHC) stains of brain tumor, xenografts of heart, lung, kidney and spleen, from U87MG mice treated with PEGylated NPs (untargeted, left, sample 6; targeted, right, sample 5). (IHC staining using specific antibody against cascade blue, ABC method) Scale bar: 20 μm.

Conclusions

In summary, micelle nanostructures have been assembled from a novel amphiphilic hyperbranched block copolymer and studied as a DOX delivery system to pass the blood brain barrier for treatment of brain tumors. It was found that F3 peptide conjugated nanoparticles not only specifically bind to the tumor-associated angiogenic endothelial cells, doxorubicin carried by these nanoparticles also caused apoptotic effects on the targeted tumor cells. PEGylation was found to enhance the biodistribution of these materials This system showed potential to provide a novel approach to efficiently deliver therapeutics to targeted tumor sites, and also to potentially attenuate systemic side effects caused by free doxorubicin. This nanoparticle system could be a good candidate for drug delivery applications.[31]

References

1. Shaker Abdullah, I. Q. E. B. "Advances in the Management of Pediatric Central Nervous System Tumors" *Ann. N.Y. Acad. Sci.* **2008,** *1138* (Recent Advances in Clinical Oncology), 22-31.

2. Hargrave, D. R.; Zacharoulis, S. "Pediatric CNS tumors: current treatment and future directions" *Expert Rev. Neurother.* **2007,** *7* (8), 1029-1042.

3. Buckner, J. C.; Brown, P. D.; O'Neill, B. P.; Meyer, F. B.; Wetmore, C. J.; Uhm, J. H. "Central Nervous System Tumors" *Mayo Clin. Proc.* **2007,** *82* (10), 1271-1286.

4. Wilne, S.; Collier, J.; Kennedy, C.; Koller, K.; Grundy, R.; Walker, D. "Presentation of childhood CNS tumours: a systematic review and meta-analysis" *Lancet Oncol.* **2007,** *8* (8), 685-695.

5. Zhu, H.; Acquaviva, J.; Ramachandran, P.; Boskovitz, A.; Woolfenden, S.; Pfannl, R.; Bronson, R. T.; Chen, J. W.; Weissleder, R.; Housman, D. E.; Charest, A. "Oncogenic EGFR signaling cooperates with loss of tumor suppressor gene functions in gliomagenesis" *Proc. Natl. Acad. Sci. U.S.A.* **2009,** *106* (8), 2712-2716.

6. Kostianovsky, A. M.; Maier, L. M.; Anderson, R. C.; Bruce, J. N.; Anderson, D. E. "Astrocytic Regulation of Human Monocytic/Microglial Activation" *J. Immunol.* **2008,** *181* (8), 5425-5432.

7. Leighton, C.; Fisher, B.; Bauman, G.; Depiero, S.; Stitt, L.; MacDonald, D.; Cairncross, G. "Supratentorial low-grade glioma in adults: an analysis of prognostic factors and timing of radiation" *J. Clin. Oncol.* **1997,** *15* (4), 1294-1301.

8. Riemer, C.; Burwinkel, M.; Schwarz, A.; Gultner, S.; Mok, S. W. F.; Heise, I.; Holtkamp, N.; Baier, M. "Evaluation of drugs for treatment of prion infections of the central nervous system" *J. Gen. Virol.* **2008,** *89* (2), 594-597.

9. Kocisko, D. A.; Morrey, J. D.; Race, R. E.; Chen, J.; Caughey, B. "Evaluation of new cell culture inhibitors of protease-resistant prion protein against scrapie infection in mice" *J. Gen. Virol.* **2004,** *85* (8), 2479-2483.

10. Larramendy-Gozalo, C.; Barret, A.; Daudigeos, E.; Mathieu, E.; Antonangeli, L.; Riffet, C.; Petit, E.; Papy-Garcia, D.; Barritault, D.; Brown, P.; Deslys, J.-P. "Comparison of CR36, a new heparan mimetic, and pentosan polysulfate in the treatment of prion diseases" *J. Gen. Virol.* **2007,** *88* (3), 1062-1067.

11. Trevitt, C. R.; Collinge, J. "A systematic review of prion therapeutics in experimental models" *Brain* **2006,** *129* (9), 2241-2265.

12. Messerschmidt, S. K. E.; Musyanovych, A.; Altvater, M.; Scheurich, P.; Pfizenmaier, K.; Landfester, K.; Kontermann, R. E. "Targeted lipid-coated nanoparticles: Delivery of tumor necrosis factor-functionalized particles to tumor cells" *J. Controlled Release* **2009,** *137* (1), 69-77.

13. Batrakova, E. V.; Kabanov, A. V. "Pluronic block copolymers: Evolution of drug delivery concept from inert nanocarriers to biological response modifiers" *J. Controlled Release* **2008,** *130* (2), 98-106.

14. Mitra, A.; Nan, A.; Line, B. R.; Ghandehari, H. "Nanocarriers for Nuclear Imaging and Radiotherapy of Cancer" *Curr. Pharm. Des.* **2006,** *12* (36), 4729-4749.

15. Paradossi, G.; Cavalieri, F.; Chiessi, E. "Soft Condensed Matter in Pharmaceutical Design" *Curr. Pharm. Des.* **2006,** *12* (11), 1403-1419.

16. Kohler, N.; Sun, C.; Wang, J.; Zhang, M. "Methotrexate-Modified Superparamagnetic Nanoparticles and Their Intracellular Uptake into Human Cancer Cells" *Langmuir* **2005,** *21* (19), 8858-8864.

17. Sun, G.; Hagooly, A.; Xu, J.; Nystrom, A. M.; Li, Z.; Rossin, R.; Moore, D. A.; Wooley, K. L.; Welch, M. J. "Facile, Efficient Approach to Accomplish Tunable Chemistries and Variable Biodistributions for Shell Cross-Linked Nanoparticles" *Biomacromolecules* **2008,** *9* (7), 1997-2006.

18. Okuda, T.; Kawakami, S.; Maeie, T.; Niidome, T.; Yamashita, F.; Hashida, M. "Biodistribution characteristics of amino acid dendrimers and their PEGylated derivatives after intravenous administration" *J. Controlled Release* **2006,** *114* (1), 69-77.

19. Kaul, G.; Amiji, M. "Biodistribution and Targeting Potential of Poly(ethylene glycol)-modified Gelatin Nanoparticles in Subcutaneous Murine Tumor Model" *J. Drug Targeting* **2004,** *12* (9/10), 585-591.

20. Turner, A. J.; Knox, A. A.; Prieto, J.-L.; McStay, B.; Watkins, N. J. "A Novel Small-Subunit Processome Assembly Intermediate That Contains the U3 snoRNP, Nucleolin, RRP5, and DBP4" *Mol. Cell. Biol.* **2009,** *29* (11), 3007-3017.

21. Yang, L.; Reece, J. M.; Cho, J.; Bortner, C. D.; Shears, S. B. "The Nucleolus Exhibits an Osmotically Regulated Gatekeeping Activity That Controls the Spatial Dynamics and Functions of Nucleolin" *J. Biol. Chem.* **2008,** *283* (17), 11823-11831.

22. Cui, Z.; DiMario, P. J. "RNAi Knockdown of Nopp140 Induces Minute-like Phenotypes in Drosophila" *Mol. Biol. Cell* **2007,** *18* (6), 2179-2191.

23. Ugrinova, I.; Monier, K.; Ivaldi, C.; Thiry, M.; Storck, S.; Mongelard, F.; Bouvet, P. "Inactivation of nucleolin leads to nucleolar disruption, cell cycle arrest and defects in centrosome duplication" *BMC Molecular Biology* **2007,** *8* (1), 66.

24. Coute, Y.; Kindbeiter, K.; Belin, S.; Dieckmann, R.; Duret, L.; Bezin, L.; Sanchez, J.-C.; Diaz, J.-J. "ISG20L2, a Novel Vertebrate Nucleolar Exoribonuclease Involved in Ribosome Biogenesis" *Mol. Cell Proteomics* **2008,** *7* (3), 546-559.

25. Destouches, D.; El Khoury, D.; Hamma-Kourbali, Y.; Krust, B.; Albanese, P.; Katsoris, P.; Guichard, G.; Briand, J. P.; Courty, J.; Hovanessian, A. G. "Suppression of Tumor Growth and Angiogenesis by a Specific Antagonist of the Cell-Surface Expressed Nucleolin" *PLoS ONE* **2008,** *3* (6), e2518.

26. Anisimov, S. V.; Tarasov, K. V.; Riordon, D.; Wobus, A. M.; Boheler, K. R. "SAGE identification of differentiation responsive genes in P19 embryonic cells induced to form cardiomyocytes in vitro" *Mech. Dev.* **2002,** *117* (1-2), 25-74.

27. Porkka, K.; Laakkonen, P.; Hoffman, J. A.; Bernasconi, M.; Ruoslahti, E. "A fragment of the HMGN2 protein homes to the nuclei of tumor cells and tumor endothelial cells in vivo" *Proc. Natl. Acad. Sci. U.S.A.* **2002,** *99* (11), 7444-7449.

28. Reddy, G. R.; Bhojani, M. S.; McConville, P.; Moody, J.; Moffat, B. A.; Hall, D. E.; Kim, G.; Koo, Y.-E. L.; Woolliscroft, M. J.; Sugai, J. V.; Johnson, T. D.; Philbert, M. A.; Kopelman, R.; Rehemtulla, A.; Ross, B. D. "Vascular Targeted Nanoparticles for Imaging and Treatment of Brain Tumors" *Clin. Cancer Res.* **2006,** *12* (22), 6677-6686.

29. Christian, S.; Pilch, J.; Akerman, M. E.; Porkka, K.; Laakkonen, P.; Ruoslahti, E. "Nucleolin expressed at the cell surface is a marker of endothelial cells in angiogenic blood vessels" *J. Cell Biol.* **2003,** *163* (4), 871-878.

30. Du, W.; Xu, Z.; Nystrom, A. M.; Zhang, K.; Leonard, J. R.; Wooley, K. L. "19F- and Fluorescently Labeled Micelles as Nanoscopic Assemblies for Chemotherapeutic Delivery" *Bioconjugate Chem.* **2008,** *19* (12), 2492-2498.

31. Du, W.; Nystrom, A. M.; Zhang, L.; Powell, K. T.; Li, Y.; Cheng, C.; Wickline, S. A.; Wooley, K. L. "Amphiphilic Hyperbranched Fluoropolymers as Nanoscopic 19F Magnetic Resonance Imaging Agent Assemblies" *Biomacromolecules* **2008,** *9* (10), 2826-2833.

32. Antharavally, B. S.; Mallia, K. A.; Rangaraj, P.; Haney, P.; Bell, P. A. "Quantitation of proteins using a dye-metal-based colorimetric protein assay" *Anal. Biochem.* **2009,** *385* (2), 342-345.

33. Gillies, E. R.; Frechet, J. M. J. "pH-Responsive Copolymer Assemblies for Controlled Release of Doxorubicin" *Bioconjugate Chem.* **2005,** *16* (2), 361-368.

34. Sun, G.; Xu, J.; Hagooly, A.; Rossin, R.; Li, Z.; Moore, D. A.; Hawker, C. J.; Welch, M. J.; Wooley, K. L. "Strategies for Optimized Radiolabeling of Nanoparticles for *in vivo* PET Imaging" *Adv. Mater.* **2007,** *19* (20), 3157-3162.

Chapter 4

Labeling of Shell Crosslinked Nanoparticles (SCKS) for MRI

Zicheng Li, Debasish Banerjee, Jie Zheng, Guorong Sun, Jinqi Xu, Joel R. Garbow, Pamela K. Woodard, Dennis A. Moore, Joseph J. H. Ackerman and Karen L. Wooley

Abstract

DOTAlysine-functionalized micelles and shell crosslinked nanoparticles (SCKs) were synthesized and labeled with gadolinium(III) for their development as nanoscale magnetic resonance imaging (MRI) contrast agents. The chelating agent, DOTAlysine, was introduced onto the polymeric materials by either micelle/SCK post-modification or pre-conjugation onto the amphiphilic block copolymer precursors of the micelle/SCKs. The amphiphilic diblock copolymers PAA-*b*-PS (poly(acrylic acid)-*b*-polystyrene), with different block ratios, different block lengths, and with or without DOTA functionalization, were self-assembled into micelles and crosslinked intra-micellarly throughout their corona *via* amidation chemistry, upon reaction with 2,2'-(ethylenedioxy)bis-ethylamine, to afford SCKs with different extents of crosslinking.

After the conjugation of Gd-DOTAlysine complex onto micelle/SCK nanoparticles, improved relaxivities were observed, compared to commercial contrast agents such as Magnevist (Gd-DTPA) and DOTAREM (Gd-DOTA). The nanoparticles contributed to increase the rotational correlation lifetime of the Gd-DOTA. Additionally, the highly hydrated nature of the poly(acrylic acid) shell layer in which the Gd-DOTAlysine was located allowed for rapid water exchange to achieve enhanced relaxation properties. The resulting materials exhibited large ionic relaxivities (40 $mM^{-1}s^{-1}$, at 40 °C under

0.5 T). In addition to the enhanced relaxivities, the properties of these nanoparticles, such as non-toxicity to mammalian cells and capability for polyvalent targeting, make them good candidates for utilization as nanoscale magnetic resonance imaging contrast agents within biological systems.

INTRODUCTION

Magnetic resonance imaging (MRI) is one of the widely used modalities for noninvasive medical diagnosis, which provides real-time high-resolution images of body tissues. MRI measures the NMR signals of nuclei, mainly protons of water. The differences in signal intensity can create contrast in the images, thereby enabling differentiation of the types of tissues and detection of disease states.[1]

MRI has been advanced with the development of contrast agents (CAs) that provide more specific and clearer images and enlargements of detectable organs and systems, leading to a wide scope of applications of MRI not only for diagnostic radiology but also for therapeutic medicine.[2] Current MRI contrast agents are in the form of either paramagnetic metal complexes or magnetic metal nanoparticles.[3] In T1-weighted imaging, more intense signals are usually observed in regions with faster water proton longitudinal relaxation rates. With the addition of paramagnetic metal complexes, such as gadolinium (Gd^{III}) or manganese (Mn^{II}) complexes, the longitudinal (T_1) relaxation of water protons can be accelerated and brighten contrast in regions where the complexes localization is exerted.[4, 5] These paramagnetic metal complexes are also referred as positive contrast agents since more intense images are obtained. Nowadays, approximate 30% of MRI investigations use a contrast agent.[6] The majority of T_1

contrast agents currently used are stable complexes of gadolinium(III) (Gd^{III}), which has seven unpaired electrons, making it the most paramagnetic among the stable metal ions.[7-9] The slow relaxation of the Gd^{III} electron spin is also an additional favorable factor.[7] These complexes are usually ternary complexes of Gd^{III} (such as Magnevist, the predominant contrast agent in commercial use today, which is comprised of a Gd^{III} within the chelating ligand diethylenetriaminepentaacetic (DPTA)), in which the Gd^{III} cation is complexed with a multidentate ligand (heptadentate or octodentate) and coordinated with water molecules.[5, 10-13] The ligand is required for safety purposes, to ensure that the highly toxic Gd^{III} sequestered *in vivo* and that the complex can be excreted intact, while the coordinated water molecules are required for contrast. The Gd^{III} ion relaxes the coordinated water molecules, which are in fast exchange with bulk water, resulting in a shortened T_1 value for the bulk (and MRI observable) water. The ability of the contrast agent to enhance the longitudinal relaxation rate ($1/T_1$) of the solvent (mostly water) is referred as the longitudinal relaxivity R; see Equation (1) in which $\Delta(1/T_1)$ is the change in relaxation rate of the solvent after addition of contrast agent with metal concentration [M] in unit of mM.[4]

$$R = \frac{\Delta(1/T_1)}{[M]} \qquad (1)$$

At equal concentrations, a metal complex with enhanced relaxivity will appear brighter in an image compared to a complex of lower relaxivity; alternately a complex with higher relaxivity can provide the same contrast as a low relaxivity complex, but at a lower dose.

Relaxivity can be factored into two terms that accounts for the relaxation effect due to the coordinated inner-sphere water molecules (R^{IS}) and an outer-sphere term (R^{OS}), which

encompasses contributions of relaxation to the second and outer-sphere water molecules. The relaxivity contributions from the directly coordinated inner-sphere water molecules usually weigh much more than that from the outer-sphere water molecules. The inner-sphere relaxivity is given by Equation (3), which is derived from the description of two-site exchange.[4, 14]

$$R = R^{IS} + R^{OS} \tag{2}$$

$$R^{IS} = \frac{q}{[H_2O]} \frac{1}{T_{1M} + \tau_m} \tag{3}$$

Here q is the number of coordinated water molecules, the water concentration of water is in mM, T_{1m} is the rotational correlation lifetime of the coordinated waters (s) and τ_m is the lifetime of the coordinated water molecules (inverse of the water-exchange rate, $k_{ex} = 1/\tau_m$). Optimal relaxivity of the Gd^{III} complex is mainly dependent upon the two key features: the water-exchange rate ($1/\tau_m$) and the rotational correlation lifetime T_{1m}.[15, 16] Faster water exchange rate and longer rotational correlation life lead to enhanced relaxivities. The water-exchange rate is currently under intense scrutiny in deployment and development of novel chelators, to which the Gd^{III} is coordinated, and remarkable improvements have been observed compared to DTPA.[17-21] While the rotational correlation lifetime has been found to increase through conjugation of the Gd^{III} complexes to slowly tumbling macromolecular objects, including inorganic materials,[22, 23] dendrimers,[15, 24, 25] polymers,[26, 27] self-assembling materials,[10, 28, 29] etc. Due to the potential to display a large number of complexes in a confined volume and to simultaneously incorporate targeting/delivering functions, macromolecules and nanoparticles have been studied intensively as the scaffold for contrast agents.[4, 5, 30, 31]

In this study, a derivative of DOTA, DOTAlysine, was used as the chelator for Gd^{III} to form Gd-DOTA complex. Shell crosslinked nanoparticles (SCKs) were used as the nano-scale scaffold for the Gd-DOTA complex. SCKs are self-assembled core-shell nanomaterials, originating from the crosslinking the shell domain of micelles assembled from amphiphilic block copolymers (poly(acrylic acid)-*b*-polystyrene (PAA-*b*-PS) in this work). The SCKs obtained have a robust structure due to the covalent crosslinking reaction, and have controllable sizes ranging from 10 to 100 nm.[10, 32-34] Gd-labeled SCKs also serve well for blood pool imaging, as a result of long circulation times, in contrast to their small molecular counterparts in which rapid clearance rates from the blood and passage into tissues prohibit blood pool imaging.[34, 35] Additionally, the shell layer of the SCKs can be functionalized with targeting ligands such as folic acid,[36] or peptides containing RGD motif as the $\alpha_v\beta_3$ integrin receptor antagonist,[37] and cell penetrating peptide such as HIV-TAT PTD and PNA.[38, 39] Nanoscale MRI contrast agents prepared from Gd-DOTA-functionalized SCK/micelles showed enhanced relaxivities over small molecule Gd^{III} complexes. In addition to the enhanced relaxivities, the properties of these nanoparticles, such as capability for polyvalent targeting, non-toxicity to mammalian cells and re-direction of biodistribution, make them good candidates for potential utilizations in biological systems.

Results and Discussion

To investigate and optimize the conditions and methodologies for labeling of the water-swollen shells of shell crosslinked knedel-like (SCK) nanoparticles, two synthetic approaches were carried out to afford micelles and SCKs functionalized with Gd-DOTAlysine complex (Scheme 4-1). **Strategy I** was the straightforward post-labeling of Gd^{III} onto nanoparticles pre-installed with DOTAs. It included the preparation of DOTAlysine-grafted amphiphilic block copolymers, DOTAlysine-*g*-PAA-*b*-PS, followed by their self-assembly into micelles and shell crosslinking into SCKs. The micelles and SCKs labeled with the DOTAlysine chelator were then loaded with Gd^{III} to afford Gd-DOTAlysine labeled nanoparticles. **Strategy II** was the pre-labeling of Gd^{III} onto nanoparticles. It involved the preparation of Gd-DOTAlysine functionalized amphiphilic block copolymers, Gd-DOTAlysine-*g*-PAA-*b*-PS, followed by micelles and SCKs formation. The amphiphilic block copolymer used in this work, PAA_{60}-*b*-PS_{35} was prepared through sequential atom transfer radical polymerization (ATRP) of *t*-butyl acrylate and styrene to afford poly(*tert*-butyl acrylate)-*b*-polystyrene (P*t*BA-b-PS), followed by acidolysis with trifluoroacetic acid in dichloromethane to remove the *t*-butyl ester protecting groups.[34] Synthesis of the chelator to Gadolinium, DOTAlysine, was reported previously.[34]

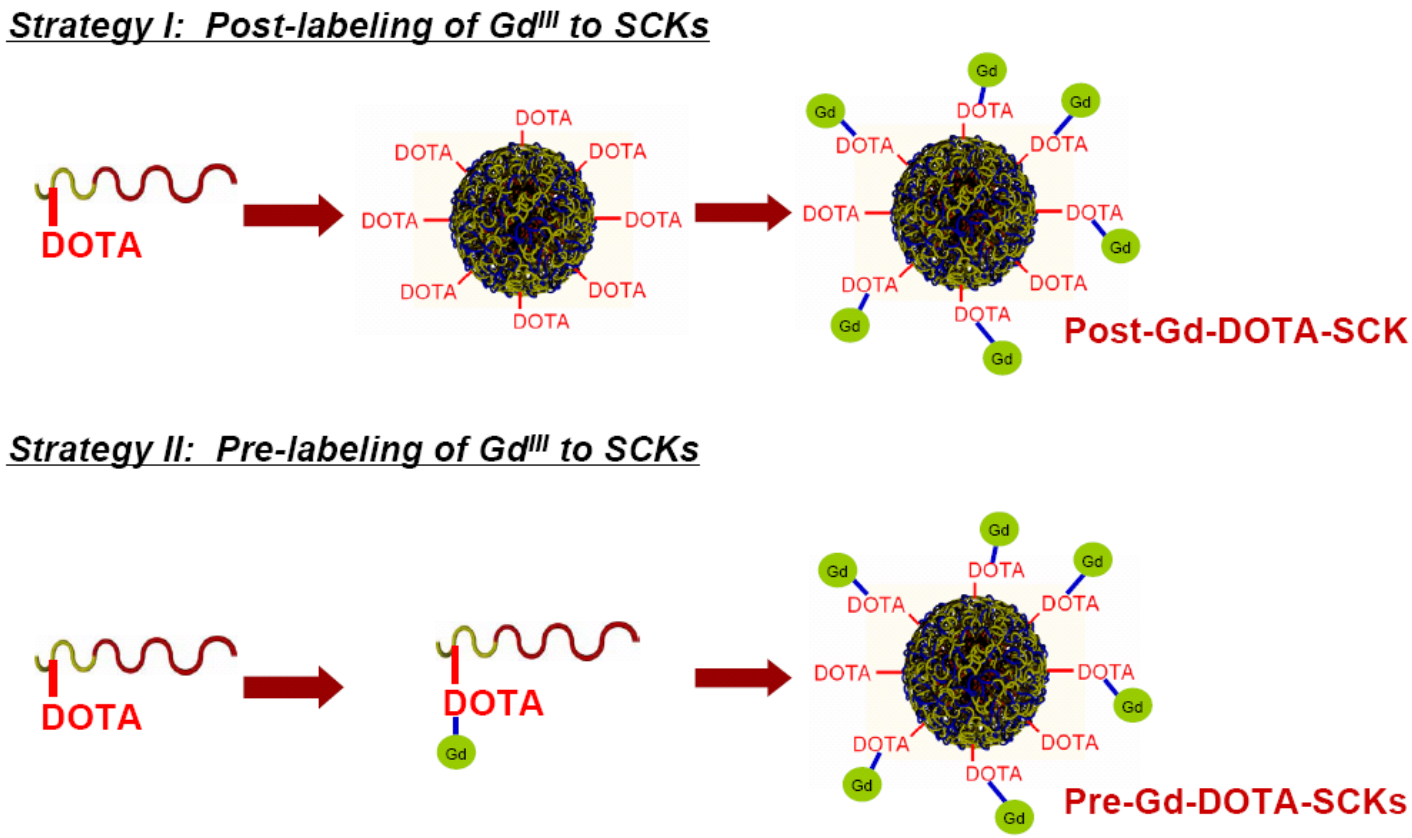

Scheme 4-1. Graphic representation of the strategies to prepare Gd-DOTAlysine labeled micelle/SCKs. **Strategy I:** Post-labeling of Gd^{III} onto nanoparticles, including the preparation of DOTAlysine-*g*-PAA-*b*-PS, followed by self-assembly into micelles and shell crosslinking into SCKs. The micelles and SCKs labeled with the DOTAlysine chelator were then loaded with Gd^{III} to afford Gd-DOTAlysine labeled nanoparticles. **Strategy II:** Pre-labeling of Gd^{III} onto nanoparticles. It involves preparation of Gd-DOTAlysine labeled block copolymers, Gd-DOTAlysine-*g*-PAA-*b*-PS, from which micelles and SCKs were prepared.

DOTAlysine was attached to PAA_{60}-*b*-PS_{35}, *via* amidation chemistry between the amino groups on the lysine and the carboxyl groups along the PAA block. The reaction was conducted in anhydrous DMF. EDCI and HOBt were added to activate the carboxylic acid groups on the PAA block. DOTAlysine and DIPEA were then added as a DMF solution. The purification was then performed by dialysis against nanopure water to remove small molecular impurities. The obtained aqueous polymer solution was lyophilized to afford DOTAlysine-grafted PAA_{60}-*b*-PS_{35}. Two polymers with average numbers of 4.0 and 7.0 DOTAlysine molecules per polymer chain (obtained from ^{1}H NMR spectroscopy analysis), $DOTAlysine_4$-*g*-PAA_{56}-*b*-PS_{35} and $DOTAlysine_7$-*g*-PAA_{53}-*b*-PS_{35}, were synthesized.

Micellizations of the above two block copolymer precursors and crosslinking reactions were carried out through "conventional" protocols to assemble nanostructures. Nanopure water, a selective solvent for the DOTAlysine-*g*-PAA block segment, was added gradually to the copolymer solution in DMF (a common solvent for both the hydrophilic and hydrophobic blocks, ~ 1.0 mg/mL) until 50 wt% of water content was reached. Finally, the organic solvent was removed through extensive dialysis again water to afford micelles in aqueous media. These micelles were stabilized by covalently crosslinking the shell PAA domain with 2,2'-(ethylenedioxy)-bis(ethylamine) mediated by EDCI to afford the SCKs. Small molecule impurities were again removed by dialysis. SCKs with nominal 20% and 50% crosslinking extents were prepared from both micelles. The final polymer concentrations for these nanoparticles were *ca.* 0.25 mg/mL.

Characterizations of the micelles and SCKs by transmission electron microscopy (TEM) revealed globular shapes of these nanostructures with number-averaged TEM diameters (D_{av}) of 13 ± 1 nm and 12 ± 1 nm, assembled from

DOTAlysine$_7$-*g*-PAA$_{53}$-*b*-PS$_{35}$, and DOTAlysine$_4$-*g*-PAA$_{56}$-*b*-PS$_{35}$, respectively. Figure 4-1 shows the TEM images for the micelle and 50% crosslinked SCKs prepared from DOTAlysine$_{7.0}$-*g*-PAA$_{53}$-*b*-PS$_{35}$. No discernable D_{av} differences were observed between micelles and SCKs. The number-averaged hydrodynamic diameters ($D_{h,n}$) for these nanoparticles were determined by dynamic light scattering (DLS) and were measured as 21 ± 3 nm. The aggregation number, which is defined as the average number of polymer chains in one nanoparticle, was calculated from the D_{av} of the nanoparticles based upon the fact that only the PS core domains were visualizable by TEM (after negatively staining) according to the following equation:

$$N_{aggr} = \frac{\rho \cdot \frac{4}{3}\pi\left(\frac{D_{av}}{2}\right)^3}{M_n} \cdot N_A \qquad (4)$$

where N_{aggr} is the aggregation number, ρ is the density of PS block (1.05 g/cm^3), D_{av} is the average TEM diameter of the nanoparticles, M_n is the molecular weight of the PS block and N_A is Avogadro's constant (6.022×10^{23} mol^{-1}).

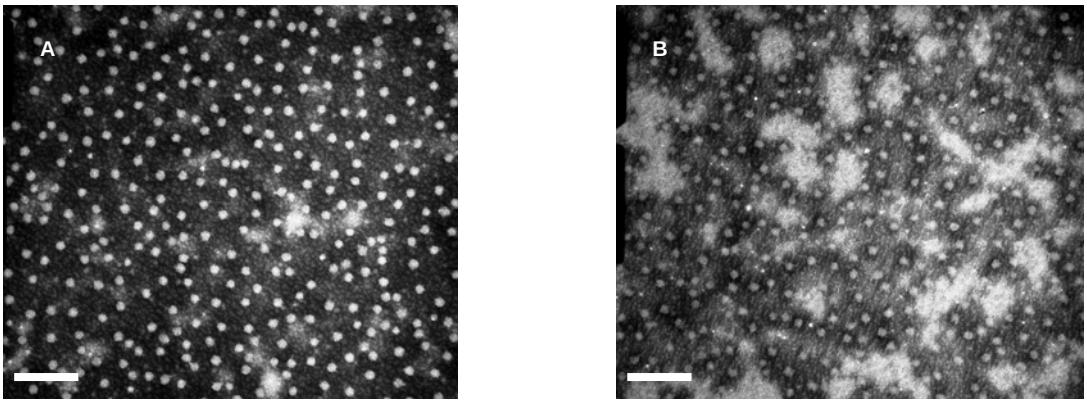

Figure 4-1. Transmission electron micrographs of A) micelle prepared from DOTAlysine$_7$-*g*-PAA$_{53}$-*b*-PS$_{35}$ and B) 50% crosslinked SCKs from DOTAlysine$_7$-*g*-PAA$_{53}$-*b*-PS$_{35}$, each as a dry sample upon a carbon-coated copper grid and negatively stained with 1 wt% of phosphotungstic acid (PTA). Scale bar denotes 100 nm.

To form the nanoscale MRI contrast agents, the micelles and SCKs prepared from DOTAlysine$_7$-*g*-PAA$_{53}$-*b*-PS$_{35}$ were incubated with $GdCl_3$ aqueous solution (N(DOTA) : N(Gd^{III}) = 1 : 2) at 60 °C for 6 h. Exhaustive dialysis of the reaction mixtures into presoaked dialysis tubings (MWCO 6,000-8,000 Da) against nanopure water (pre-treated with Chelax® 100 to remove any heavy metal present) was carried out to remove free Gd^{III} ions to afford Gd-DOTAlsyine-micelles and SCKs as the nanoscale magnetic resonance contrast agents (Post-Gd-DOTA-Micelle/SCKs). TEM and DLS characterizations of these nanoparticles showed almost no particle size variations from the corresponding precursors. Concentrations of Gd^{III} were then determined by inductively coupled plasma-mass spectrometry (ICP-MS), using standard In^{III} and Tb^{III} solutions as the internal standards. According to Gd^{III} measured concentrations, the Gd^{III} coupling efficiency to DOTAlysine was between 75% and 85%, *i.e.*, 75%-85% of the DOTAlysine molecules were complexed with Gd^{III}.

The governing water relaxation linear relationship was described as equation 4.

$$R_1 = R \times [Gd^{III}] + R_1^0 \quad (5)$$

where R is relaxivity ($mM^{-1}s^{-1}$), R_1 and R_1^0 are the water relaxation rate constants (s^{-1}) with and without the relaxation agent, respectively, and [Gd^{III}] is the concentration of relaxation agent in mM.

Proper amounts of D_2O were then added to the nanoparticles functionalized with Gd-DOTAlysine to prepare the nanoparticle relaxation agents in a H_2O:D_2O mixture (90/10 v/v). The presence of D_2O allows the use of a field/frequency lock as generally required on high field analytical NMR spectrometers and it will not interfere with relaxation determinations at low field where a field/frequency lock is not generally required. For each micelle/SCK functionalized with Gd-DOTAlysine, a

series of dilutions with different Gd^{III} concentrations in H_2O:D_2O (90/10 v/v) were prepared. Water relaxation constants (R_1) to these dilutions were measured by the inversion recovery pulse sequence at multiple agent concentrations. The measured R_1 constants were plotted *vs.* [Gd^{III}] and the data were fit to a straight line as per above equation (example shown in Figure 4-2). The slope yields R with units of $mM^{-1}s^{-1}$. As a note, the data were expressed as R per mM Gd^{III}, not R per mM nanoparticle, *i.e.*, the ionic relaxivity. Each rate constant R_1 was measured in triplicate. The water relaxation constants were measured by Dr. Debasish Banerjee.

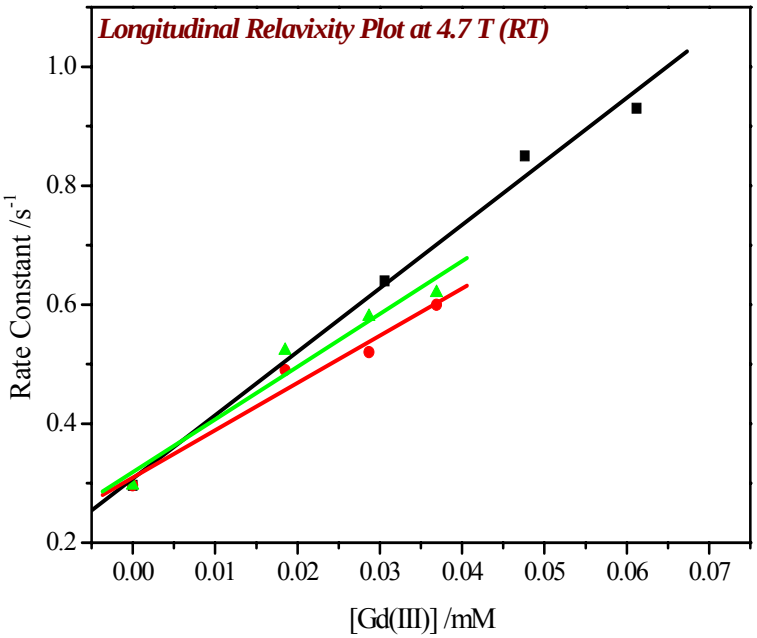

Figure 4-2 Representative plot of rate constant *vs.* [Gd]

The T_1 relaxivities (R) of the 20% and 50% crosslinked SCKs from DOTAlysine$_7$-*g*-PAA$_{53}$-*b*-PS$_{35}$ were tested at field strengths of 4.7, 3.0 and 1.5 T, at room temperature (Table 4-1). Compared to Gd-DOTAlysine, whose relaxivity value at room temperature under 1.5 T was determined as 3.9 $mM^{-1}s^{-1}$, the maximum relaxivity, obtained from 20% crosslinked Gd-DOTA-SCK conjugates (prepared from DOTAlysine$_7$-*g*-PAA$_{53}$-*b*-PS$_{35}$ and loaded with *ca.* 530 Gd^{III} per SCK), was 60 $mM^{-1}s^{-1}$ per Gd^{III}, in the same field strength at room temperature, *ca.* 15-fold higher

than that of Gd-DOTAlysine. As mentioned previously, and demonstrated here, the incorporation of lanthanide complexes into a macromolecular structure has been shown to improve relaxivity due to the slow tumbling rate of the macromolecular structures. Also, as expected, the relaxivities of the SCKs increased as the field strengths decreased, since it is well known that T_1 relaxivity typically decreases with increasing field strength for slow tumbling contrast agents.[40, 41] No appreciable changes in the ionic relaxivity were found between 20% and 50% crosslinked SCKs functionalized with Gd-DOTAlysine. Also, with the larger number of Gd ions on each nanoparticle, these materials showed very large molecular relaxivities, 33,100 $mM^{-1}s^{-1}$ and 46,700 $mM^{-1}s^{-1}$ under 1.5 T for the 20% and 50% crosslinked SCKs ,respectively.

Table 4-1. Relaxivity values collected under different field strengths for 20% and 50% crosslinked SCK nanoscale contrast agents prepared from DOTAlysine$_7$-*g*-PAA$_{53}$-*b*-PS$_{35}$. *(Post-Gd-DOTA-Micelle/SCKs)*

entry	extent of crosslinking	D_{av}(TEM) nm	$N_{aggr.}$	# Gd per SCK	R_{Gd}[a] ($mM^{-1}s^{-1}$)			R_{SCK}[b] ($mM^{-1}s^{-1}$)		
					4.7 T	*3.0 T*	*1.5 T*	*4.7 T*	*3.0 T*	*1.5 T*
A	20%	13±1	205	529	21.3	34.2	62.7	11200	18100	33100
B	50%	13±1	205	826	20.9	30.9	56.6	17200	25500	46700

a T_1 relaxivity per mM of Gd^{III}. *b* Relaxivity per mM of SCK.

However, it was found that about six months after the preparation of the above SCK nanoscale contrast agents, free Gd^{III} ions were detected by Arsenazo III (2,2'-(1,8-dihydroxy-3,6-disulfonaphthylene-2,7-bisazo)dibenzenearsonic acid) test (Arsenazo III gives unique UV-*vis* absorbance spectrum (λ_{max} ~650 nm) in the presence of free Gd^{III} ions) (Figure 4-3).[10, 11] The peak that appeared at 654 nm indicated the presence of free or loosely bound Gd^{III} ions. Since the shell layer of the SCKs is comprised predominantly of amides, acids, and ether subunits, the SCKs might also bind Gd^{III} ions. However, compared to Gd-DOTAlysine, whose stability constant is in the range of 1×10^{25} M^{-1} at neutral pH values, the binding of Gd^{III} ions to the shell of the SCKs are weak and are readily dissociated from the SCKs.[10, 42,43]

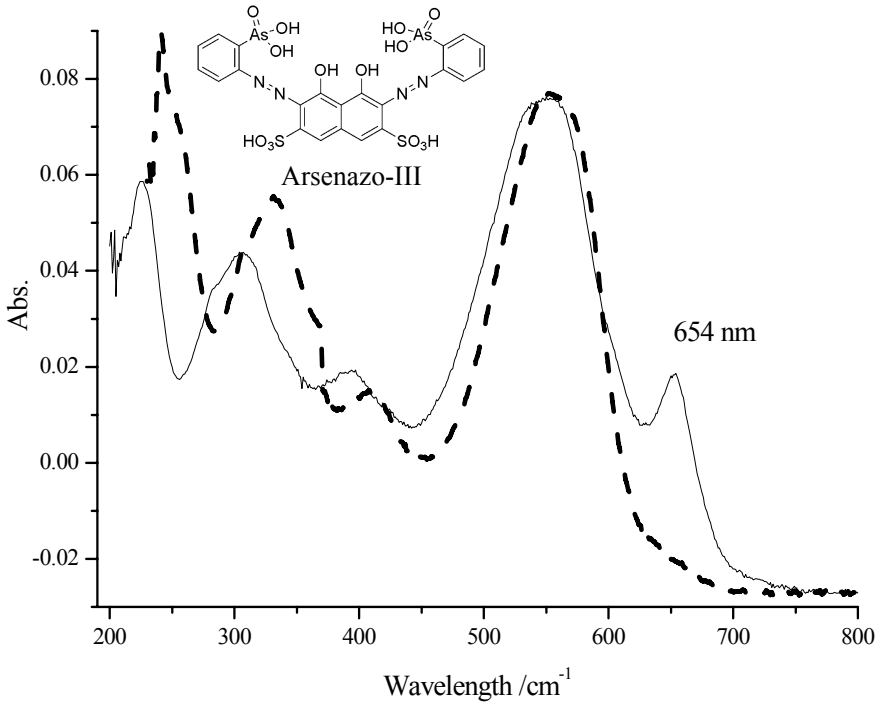

Figure 4-3. UV-*vis* spectra of Arsenazo III test: the dashed spectrum is of the neat Arsenazo III aqueous solution; the solid spectrum is of the reaction mixture of Arsenazo III and 20% crosslinked SCKs from DOTAlysine$_7$-*g*-PAA$_{53}$-*b*-PS$_{35}$. The appearance of the peak at 654 nm showed the presence of free Gd^{III} ions.

The presence of free or weakly bound Gd^{III} ion is a significant problem for in vivo applications of these nanomaterials, for instance in MRI, due to its high toxicicity,[44] To remove free or weakly bound Gd^{III} ion, the reaction mixtures were treated with DTPA (diethylenetriaminepentaacetic acid) to challenge Gd^{III} ions not chelated with DOTAlysine, followed by exhaustive dialysis in presoaked dialysis tubings (MWCO 6,000-8,000 Da) against nanopure water. The Gd-DTPA complex was reported to have a similar stability constant as Gd-DOTA.[42] By this method, micelles, and 20% and 50% crosslinked SCKs loaded with Gd-DOTAlysine were prepared (table 4-2). Arsenazo III tests of the nanoparticle solutions showed "negative" results, demonstrating that no free or weakly bound Gd^{III} ions were present. Table 4-2 showed the T_1 relaxivity values of these three nanoscale MR contrast agents at room temperature under 4.7, 3.0 and 1.5 T. Although these materials were clean from free Gd^{III} ions, the ionic relaxivity values decreased drastically compared to the

above materials that had not undergone DTPA challenge. The maximum ionic relaxivity was only 21.5 $mM^{-1}s^{-1}$ under 1.5 T, while it was 62.7 $mM^{-1}s^{-1}$ for the first set of nanoparticles not treated with DTPA. Also, similar relaxivity values were observed for each sample under the three different field strengths. It was reported that for small, fast tumbling molecules such as Gd-DTPA, T_1 relaxivity showed almost no change while increasing field (3.4, 3.3, 3.1, 3.2 $mM^{-1}s^{-1}$ under 4.7 T, 3.0 T, 1.5 T and 0.5 T, respectively).[45-47] Therefore, we hypothesized that the presence of non-covalently bound Gd-DTPA had caused the similar relaxivities under different fields, since the interaction between the various functionalities in the PAA shell of the nanoparticles and DTPA can make the complete removal of Gd-DTPA *via* dialysis difficult.

Table 4-2. Relaxivity values measured under different field strengths for micelles, 20% and 50% crosslinked SCK nanoscale contrast agents prepared from Post-DOTAlysine$_4$-*g*-PAA$_{56}$-*b*-PS$_{35}$. *DTPA* was used to remove Gd^{III} not chelated to DOTAlysine. *(Post-Gd-DOTA-Micelle/SCKs)*

entry	extent of crosslinking	D_{av}(TEM) nm	$N_{aggr.}$	# Gd per SCK	R_{Gd}[a] ($mM^{-1}s^{-1}$)			R_{SCK}[b] ($mM^{-1}s^{-1}$)		
					4.7 T	*3.0 T*	*1.5 T*	*4.7 T*	*3.0 T*	*1.5 T*
C	0	12±1	162	660	10.7	16.4	21.5	7120	10900	14300
D	20%	12±1	162	310	7.9	9.8	11.0	2400	3000	3140
E	50%	12±1	162	280	8.9	10.8	12.5	2500	3020	3500

a T_1 relaxivity per mM of Gd. *b* Relaxivity per mM of SCK.

To solve these problems encountered (presence of free Gd^{III} ions without DTPA challenge and complications that originated from the DTPA challenge), and to generate "clean" nanoscale contrast agents, **strategy II** was applied. In this strategy, block copolymers covalently labeled with Gd-DOTAlysine complex were first prepared (Gd-DOTAlysine-*g*-PAA-*b*-PS), from which micelles were assembled and SCKs were then constructed. To afford Gd-DOTAlysine-*g*-PAA-*b*-PS, two methods were performed, as shown in scheme 4-2. Method A involved the preparation DOTAlysine-*g*-PAA-*b*-PS through the previous methods (*vide supra*), followed with Gd^{III} loading by incubating the polymer solution with the solution of $GdCl_3$ in DMF at

room temperature; dialysis of the reaction mixture in presoaked dialysis tubing (MWCO 6-8000 Da) against nanopure water was carried out and the polymer was obtained after lyophilization. Method B entailed the preparation of Gd-DOTAlysine complex first, and the complex was then covalently attached onto PAA-*b*-PS *via* carbodiimide-mediated amidation chemistry in DMF. The final functionalized block copolymer precursors were obtained after dialysis purification and lyophilization.

From method A, a series of DOTAlysine-grafted polymers were synthesized with averages of 2.3, 3.0, 3.8, and 8.0 DOTAlysines per polymer chain, respectively, as determined by ^{1}H NMR spectroscopy. By method B, Gd-DOTAlysine$_{1.3}$-*g*-PAA$_{58.7}$-*b*-PS$_{35}$ was prepared and the numbers of Gd-DOTAlysine units per polymer were determined by ICP-MS (the presence the paramagnetic Gd^{III} ions affected ^{1}H NMR quantification). Pre-Gd-DOTA-Micelle/SCKs were then prepared from the corresponding Gd-DOTAlysine-*g*-PAA-*b*-PS precursors, with varying numbers of DOTAs per nanostructure and different extents of crosslinking. Results from the Arsenazo-III test indicated that these materials were clean from free or weakly bound Gd^{III} ions.

Method A

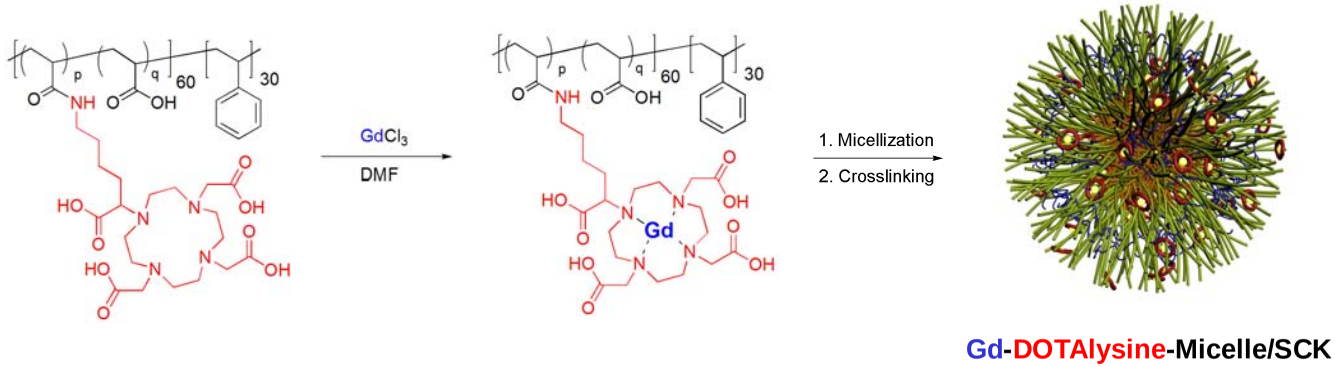

Method B

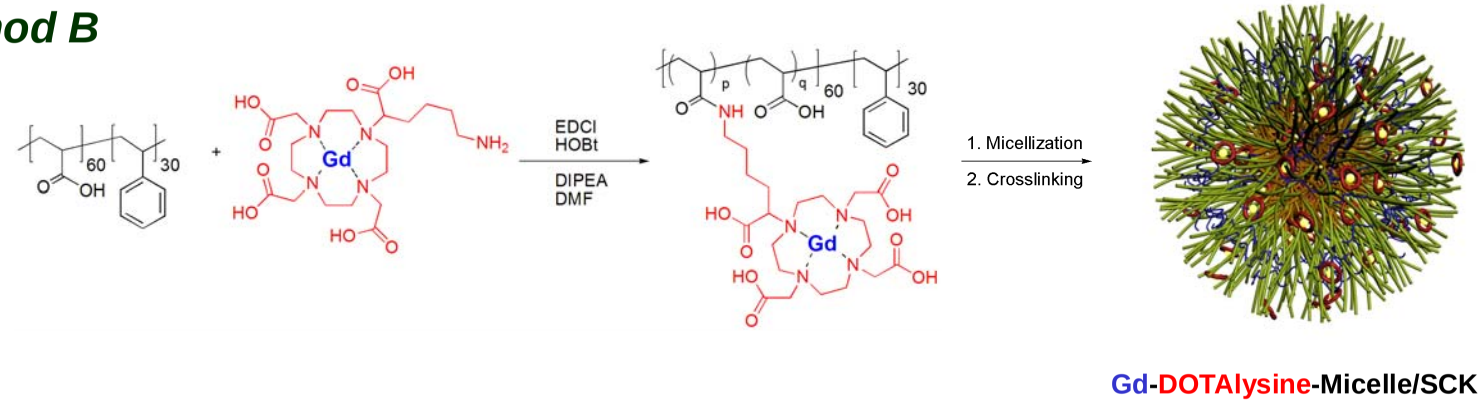

Scheme 4-2. Illustration of methods used to prepare Pre-Gd-DOTA-Micelle/SCKs by **strategy II**.

At different temperatures and under different field strengths, both T_1 and T_2 relaxivity values for these materials were determined by the inversion recovery pulse sequence at multiple agent concentrations (Table 4-3) (Relaxivities under 0.5, 1.5 and 4.7 T were measured by Dr. Debasish Banerjee. Relaxivities under 3.0 T were measured by Dr. Jie Zheng). For the micelle samples, except for sample K, all micelles with approximately 1.0 Gd^{III} per polymer chain, *i.e.*, samples E, F, H and M, showed similar T_1 relaxivities under the same measuring conditions, around 27 $mM^{-1}s^{-1}$ under 0.5 T at 40 ºC, no matter through synthetic method A or B. These results indicated that there was no obvious difference between the two preparation methods regarding to the relaxivity values achieved. Micelle K, whose precursor had more Gd^{III} content, 2.1 Gd^{III} per polymer chain, showed slightly larger T_1 relaxivities than micelles with *ca.* 1.0 Gd per polymer chain. Theoretically, the relaxivities are independent with Gd^{III} concentrations and for our case, it was speculated that parts of the Gd^{III} ions on the nanoparticles might be strictly confined inside certain small spaces and the water molecules were not quite accessible to these Gd^{III} ions. For Gd-based MR contrast agents, two key factors to enhance the T_1 relaxivity are increase of the water exchange rate and increase of the rotational correlation time. Samples prepared from polymers with more numbers of Gd^{III} per chain could have relatively more Gd^{III} that were in an environment with good water accessibility and had faster water exchange rates, thus leading to relatively larger relaxivities.

Again, for each sample, the T_1 relaxivities decreased as the field strength increased. It's also observed that under the same field strength, higher T_1 relaxivities were obtained at lower temperatures. This can be explained by the fact that at lower temperatures, the tumbling rates of the nanoparticles is reduced and leads

to a long rotational correlation lifetime of the Gd-DOTAlysine complex, which further provides enhanced T_1 relaxivity. It was also observed that under the same measuring conditions, T_1 relaxivities for nanoparticles increased as the extent of crosslinking increased (from micelle to 20% crosslinked SCKs to 50% crosslinked SCKs). One possible explanation was that the crosslinking throughout shell domain of the micelles inhibited the movement (mainly rotation) of the Gd-DOTAlysine as well and resulted in an elongated rotational correlation time. The maximum T_1 relaxivity, obtained from 50% crosslinked Pre-Gd-DOTA-SCK conjugates (sample L, prepared from $Gd_{1.6}$-$DOTA_{8.0}$-*g*-PAA_{52}-*b*-PS_{35}), was 39.6 $mM^{-1}s^{-1}$ per Gd, in an applied magnetic field 0.5 T at 40 °C, *ca*. 11-fold higher than that of Gd-DOTAlysine (3.4 $mM^{-1}s^{-1}$). For the T_2 relaxivities, these nanoparticular contrast agents also showed enhanced values compared with Gd-DOTA (in the range from 3.2 to 4.1 $mM^{-1}s^{-1}$ under 0.5-4.7 T).[45] The trend of increasing T_2 relaxivities with increasing extents of crosslinking was also observed, but the influences from temperatures and field strengths on T_2 relaxivities were minor in comparison with the effects on T_1 relaxivities.

Table 4-3. Relaxivity values at different temperatures and various field strengths for Pre-Gd-DOTA-Micelle/SCK nanoscale MR contrast agents.

sample	# DOTA per polymer chain	#Gd per chain	Preparation method	Extent of crosslinking	Relaxivities ($mM^{-1}s^{-1}$)[a]										D_{TEM} (nm)
					0.5 T	1.5 T				3.0 T				4.7 T	
					40 ℃	*22 ℃*		*37 ℃*		*22 ℃*		*37 ℃*		*40 ℃*	
					T_1	T_1	T_2	T_1	T_2	T_1	T_2	T_1	T_2	T_1	
F	2.3	1.0	A	0 (micelle)	27.0	25.51	42.51	23.37	48.03	16.49	44.29	14.5	46.14	8.7	11±1
G	3.8	1.4	A	0 (micelle)	26.8	16.34	22.81	14.95	24.44	11.62	22.27	9.63	21.02	10.1	11±1
H	3.0	1.3	A	0 (micelle)	22.2	18.32	24.77	16.37	23.76	16.52	24	16.08	20.23	10.3	18±1
I	3.0	0.91	A	20 %	35.6	28.56	39.48	24.23	41.14	24.04	40.5	18.12	41.9	16.8	18±1
J	3.0	0.84	A	50 %	38.7	29.57	44.36	25.3	42.3	23.9	42.06	12.07	37.88	15.1	18±1
K	8.0	2.1	A	0 (micelle)	35.0	27.24	41.58	22.84	39.59	19.51	40.79	18.27	37.26	13.8	15±1
L	8.0	1.6	A	50 %	39.6	31.71	45.13	26.53	43.04	23.82	44.33	19.13	38.44	15.4	15±1
M	1.3	1.3	B	0 (micelle)	27.1	24.46	36.16	20.59	36.4	16.14	34.1	14.63	31.39	7.4	14±2
N	1.3	1.3	B	20 %	34.7	30.29	43.2	25.71	41.2	21.98	41.17	18.1	37.43	8.1	14±2
O	1.3	1.3	B	50 %	36.7	32.32	42.13	26.61	43.31	22.21	38.35	19.09	36.57	7.1	14±2

a T_1 relaxivity per mM of Gd^{III}.

Experimental Section

Materials

All solvents were purchased from Sigma-Aldrich and were used without further purification unless otherwise noted. Trifluoroacetic acid (TFA; 95%; Aldrich), 2,2′-(ethylenedioxy)-bis(ethylamine) (97%; Aldrich), 1-(3′-dimethylaminopropyl)-3-ethylcarbo-diimide methiodide (EDCI; 98%; Aldrich), palladium on carbon (10 wt% loading; Aldrich), were used as received. DOTAlysine(tetra *t*-butyl ester) was provided by Dr. Dennis A. Moore at Covidien Inc., Saint Louis, MO. Diehthylenetriaminepentaacetic acid (DTPA, >99%) was purchased from Aldrich. Gadolinium chloride ($GdCl_3$; 99.99%) was purchased from Aldrich and used as received. Supor 25 mm 0.1 μm Spectra/Por Membrane tubes (molecular weight cutoff (MWCO) 3,500 or 6-8000 Da), purchased from Spectrum Medical Industries Inc., were used for dialysis. Nanopure water (18 MΩ·cm) was acquired by means of a Milli-Q water filtration system (Millipore Corp.; Bedford, MA). Chelax® 100 resin was purchased from Bio-Rad Laboratories, Inc., CA, and was to remove heavy metal present in all the aqueous solvent used in this work.

5 mM PBS (phosphate buffered saline, with 5 mM of phosphates and 5 mM of NaCl) was prepared by mixing NaH_2PO_4 (0.76 g), Na_2HPO_4 (1.93 g) and NaCl (1.17 g) into 4 liters of nanopure water and has a pH ~7.4.

Instrumental

^{1}H NMR spectra were recorded on a Varian 300 MHz spectrometer interfaced to a UNIX computer using Mercury software. Chemical shifts are referred to the solvent proton resonance. Infrared spectra were acquired on a Perkin-Elmer Spectrum BX FT-IR instrument using KBr pellets.

Absolute molecular weight and molecular weight distribution were determined by Gel Permeation Chromatography (GPC). GPC was performed on a Waters 1515 HPLC system (Water Chromatography Inc., Medford, MA), equipped with a Waters 2414 differential refractometer, a PD2020 dual-angle (15 ° and 90 °) light scattering detector (Precision Detector, Inc.), and a three-column series PL gel 5 μm Mixed columns (Polymer Laboratories Inc.). The system was equilibrated at 35 °C in anhydrous THF, which served as the polymer solvent and eluent (flow rate set to 1.00 mL/min then determined gravimetrically). All instrumental calibrations were conducted using a series of nearly monodispersed polystyrene standards. Data were collected upon an injection of a 200 μL of polymer solution in THF (*ca*. 5.0 mg/mL), and then analyzed using Discovery 32 software (Version, Precision Detectors Inc). Inter-detector delay volume and the light scattering detector calibration constant were determined by calibration using a nearly monodispersed polystyrene standard (Pressure Chemical Co., M_p = 90 kDa, M_w/M_n < 1.04). The differential refractometer was calibrated with standard polystyrene reference material (SRM 706 NIST), of known specific refractive index increment dn/dc (0.184 mL/g). The dn/dc values of the analyzed polymers were then determined from the differential refractometer response.

Differential scanning calorimetry (DSC) measurements were performed with a DSC822^e instrument (Mettler-Toledo, Inc.) in a temperature range of – 100 to 180 °C with a ramp rate of 10 °C/min under nitrogen. Data were acquired and analyzed using STAR^e software (Mettler-Toledo, Inc.). The glass transition temperature, T_g, was determined at the midpoint of the inflection tangent upon the third heating scan.

Samples for transmission electron microscopy (TEM) measurements were diluted with 1 wt% of phosphotungstic acid (PTA) stain solution (v/v, 1:1). Carbon grids

were exposed to oxygen plasma treatment to increase the surface hydrophilicity. Micrographs were collected at 100,000 magnifications. The number average particle diameters (D_{av}) and standard deviations were generated from the analysis of a minimum of 150 particles from at least three different micrographs.

The average heights for the nanoparticles were determined by performing tapping-mode AFM under ambient conditions in air. The AFM instrumentation consisted of a Nanoscope III BioScope system (Digital Instruments, Veeco Metrology Group; Santa Barbara, CA) and standard silicon tips (type, OTESPA-70; L, 160 μm; normal spring constant, 50 N/m; resonance frequency, 246-282 kHz). Samples for AFM imaging analysis were prepared through spin-coating *ca*. 2.0 μL of the nanoparticle solution (typical concentration: 0.2 mg/mL) onto freshly cleaved mica plates (Ruby clear mica, New York Mica Co.) and allowed to dry freely in air. The number-average particle heights (H_{av}) values and standard deviations were generated from the sectional analysis of more than 150 particles from several different regions.

Hydrodynamic diameters (D_h) and size distributions for the SCKs in aqueous solutions were determined by dynamic light scattering (DLS). The DLS instrument consisted of a Brookhaven Instruments Limited (Worcestershire, U.K.) system, including a model BI-200SM goniometer, a model BI-9000AT digital correlator, a model EMI-9865 photomultiplier, and a model 95-2 Ar ion laser (Lexel Corp., Farmindale, NY) operated at 514.5 nm. Measurements were made at 20 °C. Prior to analysis, solutions were filtered through a 0.22 μm Millex GV PVDF membrane filter (Millipore Corp., Medford, MA) and then centrifuged in a model 5414 microfuge (Brinkman Instruments, Inc., Westbury, NY) for 10 minutes to remove dust particles. Scattered light was collected at a fixed angle of 90 °. The digital correlator was operated with 522 ratio spaced channels, and initial delay of 5

μs, a final delay of 100 ms, and a duration of 10 minutes. A photomultiplier aperture of 400 μm was used, and the incident laser intensity was adjusted to obtain a photon counting of between 200 and 300 kcps. Only measurements in which the measured and calculated baselines of the intensity autocorrelation function agreed to within 0.1% were used to calculate particle sizes. The calculations of the particle size distributions and distribution averages were performed with the ISDA software package (Brookhaven Instruments Company), which employed single-exponential fitting, cumulants analysis, non-negatively constrained least-squares (NNLS) and CONTIN particle size distribution analysis routines. All determinations were made in triplicate.

Gadolinium concentrations were determined by inductively coupled plasma-mass spectrometry. Measurements were performed on a 7500ce Agilent, quadrupole mass spectrometer, equipped with an octapole reaction cell for removal of polyatomic interferences, and using 2% HNO_3 as the matrix. Tl^{III} and In^{III} standard solutions purchased from Aldrich were used as the internal standards. All determinations were made in triplicate.

UV-vis spectra were acquired on a Varian Cary 1E UV-*vis* system (Varian, Inc., Palo Alto, CA) using polystyrene cuvettes.

Measurements of relaxation times at 3 T were performed by Prof. Jie Zheng at Washington University School of Medicine. Measurements of relaxation times at 0.5 T, 1.5 T and 4.7 T were performed by Dr. Debasish Banerjee (former Postdoc associate in Prof. Joseph J. H. Ackerman's laboratory at Washington University School of Medicine). All measurements were performed in triplicate.

Experimental

Syntheses of DOTAlysine, PAA_{60}-*b*-PS_{35}, DOTAlysine-grafted PAA_{60}-*b*-PS_{35}, and micelle/SCK preparation from these polymers were described before by Dr. Jinqi Xu (former Postdoc associate in Prof. Karen L. Wooley's laboratory at the Department of Chemistry of Washington University).[34]

General Procedure for DOTAlysine-*g*-PAA-*b*-PS Synthesis: Grafting DOTAlysine onto PAA-*b*-PS by amidation involved the following: To a round-bottom flask equipped with a magnetic stir bar, was added a sample of PAA-*b*-PS block copolymer and anhydrous N,N-dimethylformamide (DMF). The mixture was stirred for 1 h at room temperature to ensure that a clear and homogeneous solution was obtained. To this solution, was added 1-[3′-(dimethylamino)propyl]-3-ethylcarbodiimide methiodide (EDCI) and 1-hydroxybenzotriazole (HOBt) and the reaction mixture was stirred for 1 h at room temperature. Finally, a pre-mixed solution of DOTAlysine (as a TFA salt) and N,N-diisopropylethylamine (DIPEA) in anhydrous DMF was added and the reaction mixture was further stirred for 20 h at room temperature. The reaction mixture was then transferred to pre-soaked dialysis tubing (MWCO ca. 6000 to 8000 Da) and dialyzed against nanopure H_2O (18.0 MΩ·cm, pre-treated with Chelex100) for 4 d to remove the organic solvent and small molecule by-products. The aqueous solution was then lyophilized to afford the product as white solid. The numbers of DOTAlysine molecules per polymer chain were determined by ^{1}H NMR spectroscopy analyses. The DOTAlysine coupling yields were determined to be larger than 85%.

General Procedures for Micelle Formation. To a solution of DOTAlysine-*g*-PAA-*b*-PS diblock copolymer in THF (*ca.* 1.0 mg/mL), an equal volume of nanopure H_2O was added dropwise *via* a syringe pump over 6 h. The reaction mixture was further stirred for *ca*. 16 h at room temperature before

transferring to a presoaked dialysis tubing (MWCO *ca.* 6,000-8,000 Da), and dialyzed against nanopure H_2O for 4 days, to afford a micelle solution with the final polymer concentration of 0.20-0.30 mg/mL.

General Procedures for the Crosslinking of PAA Block to Form SCKs. To a solution of micelle in nanopure H_2O, was added dropwise a solution of 2,2'-(ethylenedioxy)bis(ethylamine) (*ca.* 1.0 mg/mL) in nanopure H_2O over 10 min. The reaction mixture was stirred for *ca*. 2 h at room temperature. To this solution, was added dropwise *via* syringe pump over 30 min, a solution of 1-[3'-(dimethylamino)propyl]-3-ethylcarbodiimide methiodide in nanopure H_2O. The reaction mixture was further stirred 20 h at room temperature before transferring to a presoaked dialysis tubing (MWCO *ca.* 6,000-8,000 Da), and dialyzed against nanopure H_2O for 4 days, to remove all of the impurities and afford the SCK solution. The nominal crosslinking extent (20% and 50%) were based on the stoichiometry of the crosslinker (2,2'-(ethylenedioxy)bis(ethylamine)) to that of the carboxylic acids on the PAA domain. The general stoichiometry employed to achieve 20% nominal crosslinking was 9:2.2:1 for carboxylic acid units : EDCI : crosslinker, and to achieve 50% nominal crosslinking, the stoichiometry was 3.6:2.2:1.

General Procedures for Gd^{III} chelation onto DOTAlysine labeled micelle/SCKs. Equivalent amount of $GdCl_3$ was added to the micelle/SCK solutions, as an aqueous solution. The reaction mixtures were then stirred at 60 °C for 6 h. After cooling to room temperature, the reaction mixtures were transferred into presoaked dialysis tubings (MWCO *ca.* 6,000-8,000 Da) and exhaustive dialysis against nanopure water (pre-treated with chelax) was carried out to remove free Gd^{III}.

Preparation of Gd-DOTAlysine-*g*-PAA$_{60}$-*b*-PS$_{35}$ Block Copolymers. Two methods were carried out to afford PAA-*b*-PS, grafted with Gd-coordinated DOTAlysine:

(1) DOTAlysine was grafted onto the amphiphilic block copolymer PAA$_{60}$-*b*-PS$_{35}$ by conventional amidation chemistry in organic solvent described above, with coupling efficiencies larger than 85%. After purification by dialysis against water and lyophilization, the average numbers of DOTAlysine per polymer chain were determined by ^{1}H NMR. Four different samples were prepared, with the average numbers of DOTAlysine per polymer chain being 2.3, 3.0, 3.8 and 8.0. The polymers, DOTAlysine-*g*-PAA$_{60}$-*b*-PS$_{35}$, were then dissolved in DMF and incubated with $GdCl_3$, which was added as a DMF solution. Dialysis against nanopure water was carried out to remove un-coordinated Gd^{III}, Gd-DOTAlysine-*g*-PAA$_{60}$-*b*-PS$_{35}$ was obtained after lyophilization.

(2) Gd-Coordinated DOTAlysine was prepared first as described as below. To a stirred solution of DOTAlysine (23.0 mg, 33.2 μmol) in 8.0 mL of nanopure water at ambient temperature was added $GdCl_3$ (8.7 mg, 33 μmol). The pH of the mixture was adjusted to around 7.5 with a dilute NaOH solution. The mixture was allowed to stir for 8 h. Aliquots of the reaction mixture were removed and Arsenazo III (2,2'-(1,8-dihydroxy-3,6-disulfonaphthylene-2,7-bisazo)dibenzenearsonic acid), which gives unique UV-vis absorbance spectra (λ_{max} ~650 nm) in the presence of free Gd^{III} was used to monitor the progress of the reaction.[12-13] More DOTAlysine (0.3 equivalent, in 3 batches) was added to the reaction mixture until the Arsenazo-III indicator tested negative. The reaction mixture was then lyophilized to afford Gd-DOTAlysine as a yellow powder.

Gd-DOTAlysine was grafted to the block copolymer PAA_{60}-*b*-PS_{35} by following a procedure similar to that used to graft DOTAlysine. Due to the presence of the paramagnetic Gd^{III}, the average number of Gd-DOTAlysine per polymer chain was determined by ICP-MS. One sample, with averagely 1.3 Gd-DOTAlysine per polymer chain, was prepared.

General Procedures for Micellization of Gd-DOTAlysine-*g*-PAA_{61}-*b*-PS_{34} and Shell Crosslinking into SCKs. To a solution of Gd-DOTAlysine-*g*-PAA_{60}-*b*-PS_{35} in DMSO (*c.a.* 1.0 mg/mL), was added dropwise an equal volume of nanopure water *via* a syringe pump over 6 h. The mixture was further stirred for 12 h, followed by dialysis against nanopure water for 4 d to afford a clear micelle solution.

To a solution of micelle in nanopure water, was added dropwise a solution of 2,2'-(ethylenedioxy)-bis(ethylamine) (*c.a.* 1.0 mg/mL) over 10 min. The reaction mixture was stirred for *ca.* 2 h. A solution of EDCI (1-[3'-(dimethylamino)propyl]-3-ethylcarbodiimide methiodide) in nanopure water was to the reaction mixture via a syringe pump over 30 min. The reaction mixture was further stirred for 20 h, followed by dialysis against nanopure water for 4 d, to remove all of the impurities and afford the SCK solution.

Conclusions

The production of a new type of nanoscale contrast agent for magnetic resonance imaging, Gd-DOTAlysine-Micelle/SCKs, has been described. Methods to afford clean nanoscale contrast agents without the contamination of free Gd^{III} ions have been developed. Compared to the small molecule complex, Gd-DOTAlysine, enhanced T_1 relaxivities were achieved, which was a result from increased rotational correlation

time. It was also found that T_1 relaxivities increased as the extent of crosslinking of the micelles increased. With the good blood pool imaging capabilities, and potential for active targeting (described in previous chapters), as well as the enhanced T_1 relaxivities, Gd-DOTAlysine functionalized SCKs have the potentials to serve as promising candidates for *in vivo* MRI imaging.

Acknowledgements

Z. L. thanks Dr. Debasihsh Banerjee and Dr. Jie Zheng for performing experiments to determine the relaxivities, Prof. Joseph J. H. Ackerman and Dr. Joel R. Garbow for their helpful discussions and suggestions. Z. L. also acknowledges Mr. M. G. Veith for TEM imaging, Dr. Daniel Giammar for assistance with ICP-MS, and the Department of Energy, Environmental & Chemical Engineering at Washington University in Saint Louis for use of ICP-MS facilities. This material is based upon work supported by the National Heart Lung and Blood Institute of the National Institutes of Health as a Program of Excellence in Nanotechnology (HL080729).

References

1. Tatjana, N. P.-V.; Luce Vander, E.; Kristof, K.; Sophie, L.; Carmen, B.; Feng, C.; Rik Van, D.; Yicheng, N.; Robert, N. M.; Koen, B. "Pharmacokinetic and in vivo evaluation of a self-assembled gadolinium(III)-iron(II) contrast agent with high relaxivity" *Contrast Med. Mol. Imaging* **2006**, *1* (6), 267-278.

2. Sabrina, L.; Robert, R.; Tóth, É.; Merbach, A. E. "Gd^{III} Complexes with Fast Water Exchange and High Thermodynamic Stability: Potential Building Blocks for High-Relaxivity MRI Contrast Agents" *Chem. Eur. J.* **2003**, *9* (15), 3555-3566.

3. Hifumi, H.; Yamaoka, S.; Tanimoto, A.; Citterio, D.; Suzuki, K. "Gadolinium-Based Hybrid Nanoparticles as a Positive MR Contrast Agent" *J. Am. Chem. Soc.* **2006**, *128* (47), 15090-15091.

4. Peter, C.; John, C. A., Jr.; Stephen, U. D.; Matthew, T. G.; Normand, J. C.; Sarah, A. M.; Marga, S.; Stephan, G. Z.; Richard, J. L.; Arnold, M. R.; Thomas, J. M.; Randall, B. L. "When are Two Waters Worse Than One? Doubling the Hydration Number of a Gd-DTPA Derivative Decreases Relaxivity" *Chem. Eur. J.* **2005**, *11* (20), 5795.

5. Caravan, P.; Ellison, J. J.; McMurry, T. J.; Lauffer, R. B. "Gadolinium(III) Chelates as MRI Contrast Agents: Structure, Dynamics, and Applications" *Chem. Rev.* **1999**, *99* (9), 2293-2352.

6. Prasuhn, D. E.; Yeh, R. M.; Obenaus, A.; Manchester, M.; Finn, M. G. "Viral MRI contrast agents: coordination of Gd by native virions and attachment of Gd complexes by azide-alkyne cycloaddition" *Chem. Commun.* **2007**, (12), 1269-1271.

7. Tóth, É.; Helm, L.; Merbach, A. "Relaxivity of MRI Contrast Agents" *Top. Curr. Chem.* **2002**, *221* ((Contrast Agents I)), 61-101.

8. David, E. S.; Eyk, A. S.; Matthias, N.; Mikhail, S. N.; Takashi, M.; George, D.; Fred, R.; Luanda, G.; Anthony, R.; Ralph, W.; Lee, J. "Magnetic resonance imaging of cardiomyocyte apoptosis with a novel magneto-optical nanoparticle" *Magn. Reson. Med.* **2005**, *54* (3), 718-724.

9. Silvio, A.; Claudia, C.; Sebastiano, C.; Simonetta Geninatti, C.; Eliana, G.; Fabio, M. "Insights into the use of paramagnetic Gd(III) complexes in MR-molecular imaging investigations" *J. Magn. Reson. Imaging* **2002**, *16* (4), 394-406.

10. J. L. Turner, D. P., R. Plummer, Z. Chen, A. K. Whittaker, K. L. Wooley "Synthesis of Gadolinium-Labeled Shell-Crosslinked Nanoparticles for Magnetic Resonance Imaging Applications" *Adv. Funct. Mater.* **2005**, *15* (8), 1248-1254.

11. Pippin, C. G.; Parker, T. A.; McMurry, T. J.; Brechbiel, M. W. "Spectrophotometric method for the determination of a bifunctional DTPA ligand in DTPA-monoclonal antibody conjugates" *Bioconjugate Chem.* **1992**, *3* (4), 342-345.

12. Magerstädt, M.; Otto, A. G.; Martin, W. B.; David, C.; Lars, B.; Richard, H. K.; Mary, E. G.; Matthias, N. "Gd(DOTA): An alternative to Gd(DTPA) as a T1,2 relaxation agent for NMR imaging or spectroscopy" *Magn. Reson. Med.* **1986**, *3* (5), 808-812.

13. Caravan, P.; Astashkin, A. V.; Raitsimring, A. M. "The Gadolinium(III)-Water Hydrogen Distance in MRI Contrast Agents" *Inorg. Chem.* **2003**, *42* (13), 3972-3974.

14. Lauffer, R. B. "Paramagnetic metal complexes as water proton relaxation agents for NMR imaging: theory and design" *Chem. Rev.* **1987**, *87* (5), 901-927.

15. Rudovsky, J.; Botta, M.; Hermann, P.; Hardcastle, K. I.; Lukes, I.; Aime, S. "PAMAM Dendrimeric Conjugates with a Gd−DOTA Phosphinate Derivative and Their Adducts with Polyaminoacids: The Interplay of Global Motion, Internal Rotation, and Fast Water Exchange" *Bioconjugate Chem.* **2006**, *17* (4), 975-987.

16. Lowe, M. P. "MRI Contrast Agents: The Next Generation" *Aust. J. Chem.* **2002**, *55* (9), 551-556.

17. Aime, S.; Botta, M.; Fasano, M.; Terreno, E. "Prototropic and Water-Exchange Processes in Aqueous Solutions of Gd(III) Chelates" *Acc. Chem. Res.* **1999**, *32* (11), 941-949.

18. Sophie Laurent, L. V. E., Sylvain Houzé, Nathalie Guérit, Robert N. Muller "Synthesis and Characterization of Various Benzyl Diethylenetriaminepentaacetic Acids (dtpa) and Their Paramagnetic Complexes, Potential Contrast Agents for Magnetic Resonance Imaging" *Helv. Chim. Acta* **2000**, *83* (2), 394-406.

19. Sophie Laurent, F. B., Luce Vander Elst, Robert N. Muller "Relaxivity and Transmetallation Stability of New Benzyl-Substituted Derivatives of Gadolinium&bond;DTPA Complexes" *Helv. Chim. Acta* **2004**, *87* (5), 1077-1089.

20. Doble, D. M. J.; Botta, M.; Wang, J.; Aime, S.; Barge, A.; Raymond, K. N. "Optimization of the Relaxivity of MRI Contrast Agents: Effect of Poly(ethylene glycol) Chains on the Water-Exchange Rates of GdIII Complexes" *J. Am. Chem. Soc.* **2001**, *123* (43), 10758-10759.

21. Silvio, A.; Daniela Delli, C.; Enzo, T. "Novel pH-Reporter MRI Contrast Agents" *Angew. Chem. Int. Ed.* **2002**, *41* (22), 4334-4336.

22. Kim, D. K.; Mikhaylova, M.; Wang, F. H.; Kehr, J.; Bjelke, B.; Zhang, Y.; Tsakalakos, T.; Muhammed, M. "Starch-Coated Superparamagnetic Nanoparticles as MR Contrast Agents" *Chem. Mater.* **2003**, *15* (23), 4343-4351.

23. Lin, Y.-S.; Hung, Y.; Su, J.-K.; Lee, R.; Chang, C.; Lin, M.-L.; Mou, C.-Y. "Gadolinium(III)-Incorporated Nanosized Mesoporous Silica as Potential Magnetic Resonance Imaging Contrast Agents" *J. Phys. Chem. B* **2004**, *108* (40), 15608-15611.

24. Langereis, S.; de Lussanet, Q. G.; van Genderen, M. H. P.; Backes, W. H.; Meijer, E. W. "Multivalent Contrast Agents Based on Gadolinium−Diethylenetriaminepentaacetic Acid-Terminated Poly(propylene imine) Dendrimers for Magnetic Resonance Imaging" *Macromolecules* **2004**, *37* (9), 3084-3091.

25. Hisataka, K.; Sang-Kyung, J.; Satomi, K.; Hideo, Y.; Xuzhen, H.; Michael, V. K.; Martin, W. B.; Peter, L. C.; Robert, A. S. "Polyamine dendrimer-based MRI contrast agents for functional kidney imaging to diagnose acute renal failure" *J. Magn. Reson. Imaging* **2004**, *20* (3), 512-518.

26. Ladd, D. L.; Hollister, R.; Peng, X.; Wei, D.; Wu, G.; Delecki, D.; Snow, R. A.; Toner, J. L.; Kellar, K.; Eck, J.; Desai, V. C.; Raymond, G.; Kinter, L. B.; Desser, T. S.; Rubin, D. L. "Polymeric Gadolinium Chelate Magnetic Resonance Imaging Contrast Agents: Design, Synthesis, and Properties" *Bioconjugate Chem.* **1999**, *10* (3), 361-370.

27. Fu, Y.; Raatschen, H.-J.; Nitecki, D. E.; Wendland, M. F.; Novikov, V.; Fournier, L. S.; Cyran, C.; Rogut, V.; Shames, D. M.; Brasch, R. C. "Cascade Polymeric MRI Contrast Media Derived from Poly(ethylene glycol) Cores: Initial Syntheses and Characterizations" *Biomacromolecules* **2007**, *8* (5), 1519-1529.

28. Kristof Kimpe, T. N. P.-V., Sophie Laurent, Corinne Piérart, Luce Vander Elst, Robert N. Muller, Koen Binnemans "Potential MRI Contrast Agents Based on Micellar Incorporation of Amphiphilic Bis(alkylamide) Derivatives of $[(Gd\text{-}DTPA)(H_2O)]^{2-}$" *Eur. J. Inorg. Chem.* **2003**, *2003* (16), 3021-3027.

29. Accardo, A.; Tesauro, D.; Roscigno, P.; Gianolio, E.; Paduano, L.; D'Errico, G.; Pedone, C.; Morelli, G. "Physicochemical Properties of Mixed Micellar Aggregates

Containing CCK Peptides and Gd Complexes Designed as Tumor Specific Contrast Agents in MRI" *J. Am. Chem. Soc.* **2004**, *126* (10), 3097-3107.

30. Caravan, P.; Cloutier, N. J.; Greenfield, M. T.; McDermid, S. A.; Dunham, S. U.; Bulte, J. W. M.; Amedio, J. C.; Looby, R. J.; Supkowski, R. M.; Horrocks, W. D.; McMurry, T. J.; Lauffer, R. B. "The Interaction of MS-325 with Human Serum Albumin and Its Effect on Proton Relaxation Rates" *J. Am. Chem. Soc.* **2002**, *124* (12), 3152-3162.

31. Anderson, E. A.; Isaacman, S.; Peabody, D. S.; Wang, E. Y.; Canary, J. W.; Kirshenbaum, K. "Viral Nanoparticles Donning a Paramagnetic Coat: Conjugation of MRI Contrast Agents to the MS2 Capsid" *Nano Lett.* **2006**, *6* (6), 1160-1164.

32. Becker, M. L.; Liu, J.; Wooley, K. L. "Functionalized Micellar Assemblies Prepared via Block Copolymers Synthesized by Living Free Radical Polymerization upon Peptide-Loaded Resins" *Biomacromolecules* **2005**, *6* (1), 220-228.

33. Qinggao, M.; Karen, L. W. "The preparation of t-butyl acrylate, methyl acrylate, and styrene block copolymers by atom transfer radical polymerization: Precursors to amphiphilic and hydrophilic block copolymers and conversion to complex nanostructured materials" *J. Polym. Sci., Part A: Polym. Chem.* **2000**, *38* (S1), 4805-4820.

34. Xu, J.; Sun, G.; Rossin, R.; Hagooly, A.; Li, Z.; Fukukawa, K.-i.; Messmore, B. W.; Moore, D. A.; Welch, M. J.; Hawker, C. J.; Wooley, K. L. "Labeling of Polymer Nanostructures for Medical Imaging: Importance of Cross-Linking Extent, Spacer Length, and Charge Density" *Macromolecules* **2007**, *40* (9), 2971-2973.

35. Sun, G.; Hagooly, A.; Xu, J.; Nystrom, A. M.; Li, Z.; Rossin, R.; Moore, D. A.; Wooley, K. L.; Welch, M. J. "Facile, Efficient Approach to Accomplish Tunable

Chemistries and Variable Biodistributions for Shell Cross-Linked Nanoparticles" *Biomacromolecules* **2008**, *9* (7), 1997-2006.

36. Pan, D.; Turner, J. L.; Wooley, K. L. "Folic acid-conjugated nanostructured materials designed for cancer cell targeting" *Chem. Commun.* **2003**, (19), 2400-2401.

37. Pan, D.; Turner, J. L.; Wooley, K. L. "Shell Cross-Linked Nanoparticles Designed To Target Angiogenic Blood Vessels via $\alpha_v\beta_3$ Receptor-Ligand Interactions" *Macromolecules* **2004**, *37* (19), 7109-7115.

38. Zhang, K.; Fang, H.; Chen, Z.; Taylor, J.-S. A.; Wooley, K. L. "Shape Effects of Nanoparticles Conjugated with Cell-Penetrating Peptides (HIV Tat PTD) on CHO Cell Uptake" *Bioconjugate Chem.* **2008**, *19* (9), 1880-1887.

39. Fang, H.; Zhang, K.; Shen, G.; Wooley, K. L.; Taylor, J.-S. A. "Cationic Shell-Cross-Linked Knedel-like (cSCK) Nanoparticles for Highly Efficient PNA Delivery" *Mol. Pharmaceutics* **2009**, *6* (2), 615-626.

40. Blockley, N. P.; Jiang, L.; Gardener, A. G.; Ludman, C. N.; Francis, S. T.; Gowland, P. A. "Field strength dependence of R1 and R relaxivities of human whole blood to prohance, vasovist, and deoxyhemoglobin" *Magn. Reson. Med.* **2008**, *60* (6), 1313-1320.

41. Washburn, K. E.; Eccles, C. D.; Callaghan, P. T. "The dependence on magnetic field strength of correlated internal gradient relaxation time distributions in heterogeneous materials" *J. Magn. Reson.* **2008**, *194* (1), 33-40.

42. László Burai, V. H., RóBert Király, éva Tóth, Ern Brücher "Stability constants and 1H relaxation effects of ternary complexes formed between gd-dtpa, gd-dtpa-bma, gd-dota, and gd-edta and citrate, phosphate, and carbonate ions" *Magn. Reson. Med.* **1997**, *38* (1), 146-150.

43. Aime, S.; Botta, M.; Ermondi, G.; Fedeli, F.; Uggeri, F. "Synthesis and NMRD studies of gadolinium(3+) complexes of macrocyclic polyamino polycarboxylic ligands bearing .beta.-benzyloxy-.alpha.-propionic residues" *Inorg. Chem.* **1992**, *31* (6), 1100-1103.

44. Tweedle, M. F. K., Krishan "Magnetic resonance imaging (MRI) contrast agents " *Top. Biol. Inorg. Chem.* **1999**, *2* (Metallopharmaceuticals II), 1-43.

45. Rohrer, M. B., H.; Mintorovitch, J.; Requardt, M.; Weinmann, H. J. "Comparison of Magnetic Properties of MRI Contrast Media Solutions at Different Magnetic Field Strengths" *Invest. Radiol.* **2005**, *40* (11), 715-724.

46. Caravan, P. "Strategies for increasing the sensitivity of gadolinium based MRI contrast agents" *Chem. Soc. Rev.* **2006**, *35* (6), 512-523.

47. Peter, C.; Christian, T. F.; Luca, F.; Ritika, U. "Influence of molecular parameters and increasing magnetic field strength on relaxivity of gadolinium- and manganese-based T_1 contrast agents" *Contrast Media Mol. Imaging* **2009**, *4* (2), 89-100.

Chapter 5

Peptide-mediated Growth of Silver Nanoparticles with Shell Crosslinked Nanoparticles (SCKs) as the Template

Abstract

In this work, silver nanoparticles were synthesized with polymeric shell crosslinked nanoparticles (SCKs) and a metal binding peptide, AG-P35, as the templates. The SCKs possessing an amphiphilic core-shell morphology were prepared from the aqueous self assembly of the amphiphilic block copolymer of acrylic acid and methyl acrylate (PAA_{105}-*b*-PMA_{184}) and subsequent crosslinking of the shell domain through amidation reaction of 2,2'-(ethylenedioxy)bis-ethylamine with the carboxylic acid groups on the micelle. It was found that both the SCKs and the peptide can influence the growth of silver nanoparticles. Silver nanoparticles of various morphologies, such as dendrite, flower-like and plate-like nanoparticles, were obtained by varying the ratios of SCK, AG-P35 and silver nitrate.

Introduction

Inorganic nanocrystals have been attracting considerable interests due to their novel properties which are strongly influence by their size, shape, surface composition, spatial ordering, and interaction with surrounding environments.[1] These materials are considered to be intriguing functional materials with wide potential applications in various fields such as magnetic resonance imaging,[2, 3] catalysis,[4] electrochemistry,[5] biological labeling,[6] optoelectronics,[7] photoluminescence[8] and surface enhanced Raman scattering[9, 10].

Controlling the size of nanocrystals is of particular interest because of the effect these parameters have on the observed properties of the nanocrystals. However, the fact that nanoparticles and assemblies exhibit unique electrical, optical, magnetic, and catalytic properties is not only because of the dramatic increase in the surface area/volume ratio as the particle size is reduced but also because of the emergence of collective and nanoscale properties as a result of the interparticle arrangement or assembly.[11] It is the exploration of such nanostructures that has captured the growing interests of research at the interfaces of chemistry, physics, biology, and materials science. While many nanoparticles exhibit unique electronic properties different from their bulk counterparts, the incorporation of macromolecules into metal or semiconductor nanoparticles produces interesting photoinduced charge transfer and separation.[12] The electrical properties of thin-film assemblies of metal nanoparticles mediated by bifunctional mediators have been exploited for chemiresistor sensing,[13] where the

sorption of volatile organic compounds (VOCs) leads to a change in electron hopping or tunneling properties depending upon particle size, interparticle distance, and medium properties. Various macromolecules and their assemblies, such as viruses and proteins,[14-19] polymers,[20, 21] porous polymer matrices,[22] microemulsions,[23] starch vermicelli[1] and cellulose,[24] have been studied as templates to grow inorganic nanoparticles. Synthetic peptides are also being developed to direct the growth of inorganic nanoparticles[25-27]. These peptides are designed to bind to certain faces of inorganic nanocrystals.

Among all the metal nanoparticles, silver nanoparticles have been intensively studied because of their intriguing optical, electronic, magnetic and mechanical properties.[24, 28, 29] In particular, silver nanoparticles interact with light better than any know chromophore,[30] they also play an important role in antimicrobial activity,[31] catalysis[32] and facilitated olefin transport[33].

In this work, we chose shell crosslinked nanoparticles (SCKs) as the scaffolding and template for silver nanoparticle growth. The peptide, AG-P35 (WSWRSPTPHVVT), reported to be able to direct the growth of silver nanocrystals due to its ability to bind the (1 1 1) face of silver nanocrystals,[27] was selected as the co-template. SCKs are self-assembled core-shell materials, originating from micelles assembled from amphiphilic block copolymers that are stabilized through a crosslinking reaction, to afford a robust structure of controlled size (10-200 nm).[34, 35] This particular work focused on SCKs from poly(acrylic acid)-*b*-poly(methyl acrylate), prepared by the crosslinking of the PAA shell domain of the micelle, with a diamino-terminated di-ethylene glycol crosslinker. Growth of silver nanoparticles with various morphologies, such as

dendrites, flower-like and layer-structured assemblies, was achieved. The nanoparticle growth was found to be strongly dependent upon stoichiometry and incubation time. In this chapter, the influence of the SCK and the peptide AG-P35 upon the growth of silver nanoparticles is discussed. Silver nanoparticles formed with SCK as the template may find potential as a nano-antimicrobial agent. These SCK nanoparticles derived from poly(acrylic acid)-*b*-poly(methyl acrylate) were found to be both non-toxic to mammalian cells and non-immunogenic within mice.[36] Additionally, targeting ligands such as folic acid and $\alpha_v\beta_3$ integrin receptors can be easily functionalized onto the shell layer of the SCK, as described in previous chapter and also in literature.[37]

Results and Discussion

The SCK nanoparticles were prepared from the aqueous assembly of the amphiphilic diblock copolymer, poly(acrylic acid)$_{105}$-*b*-poly(methyl acrylate)$_{184}$ (PAA$_{105}$-*b*-PMA$_{184}$), and crosslinking of the resultant micellar structure throughout the shell layer. The amphiphilic block copolymer was prepared through sequential atom transfer radical polymerization (ATRP) of *t*-butyl acrylate and methyl acrylate to afford P*t*BA-*b*-PMA (this polymer was a gift from a former group member, Dr. Zhiyun Chen), followed by acidolysis by trifluoacetic acid in dichloromethane to remove the *t*-butyl ester protecting groups. Through addition of water to the THF solution of the amphiphilic block copolymer, micelle was formed. Covalent crosslinking of the shell domain carboxylic acid group of the micelle with 2,2'-(ethylenedioxy)-bis(ethylamine) and 1-(3′-dimethylaminopropyl)-3-ethylcarbo-diimide methiodide (EDCI) was performed to

afford the SCKs. In this study, a nominally 50% crosslinked SCK was used. The SCK was characterized by DLS (D_h(num) 45 ± 4 nm) and TEM (33 ± 2 nm) (**Figure 5-1**).

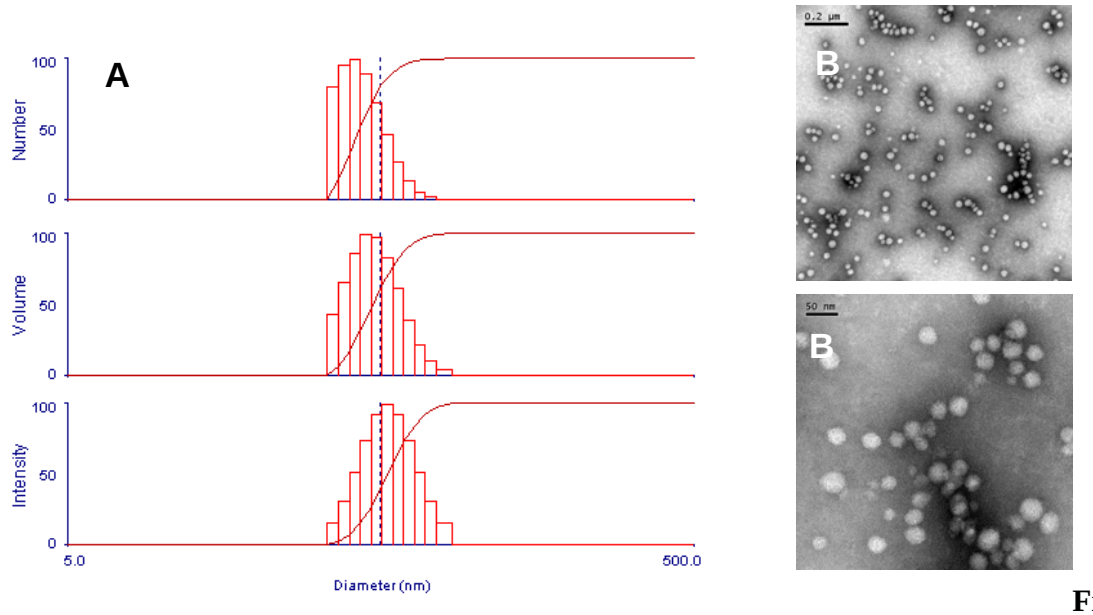

Fig

Figure 5-1. A) Particle size distribution from dynamic light scattering (DLS) of the SCKs. B) Transmission electron microscopy (TEM) images of the SCKs.

In general, for silver nanoparticle growth, an aqueous solution of SCKs was incubated with AG-P35 for 24 h, followed by the addition of $AgNO_3$ (**Scheme 5-1**). Aliquots of the reaction mixture were taken at different time points and the growth of silver nanoparticles was monitored by TEM and SEM. Experiments with varied ratios of polymer/peptide/$AgNO_3$ were performed (**Table 5-1**).

Since the peptide AG-P35 was reported to be able to reduce $AgNO_3$ to Ag, no reducing agents were introduced when AG-P35 was used. For the first experiment, SCK and AG-P35 were incubated under ambient conditions for 24 h, followed by the addition of $AgNO_3$ solution. Dendritic silver nanoparticles were obtained. These dendritic silver nanoparticles were composed of near-spherical silver nanoparticles with TEM diameters around 30 nm, which was similar to that of the SCK nanoparticles. It.

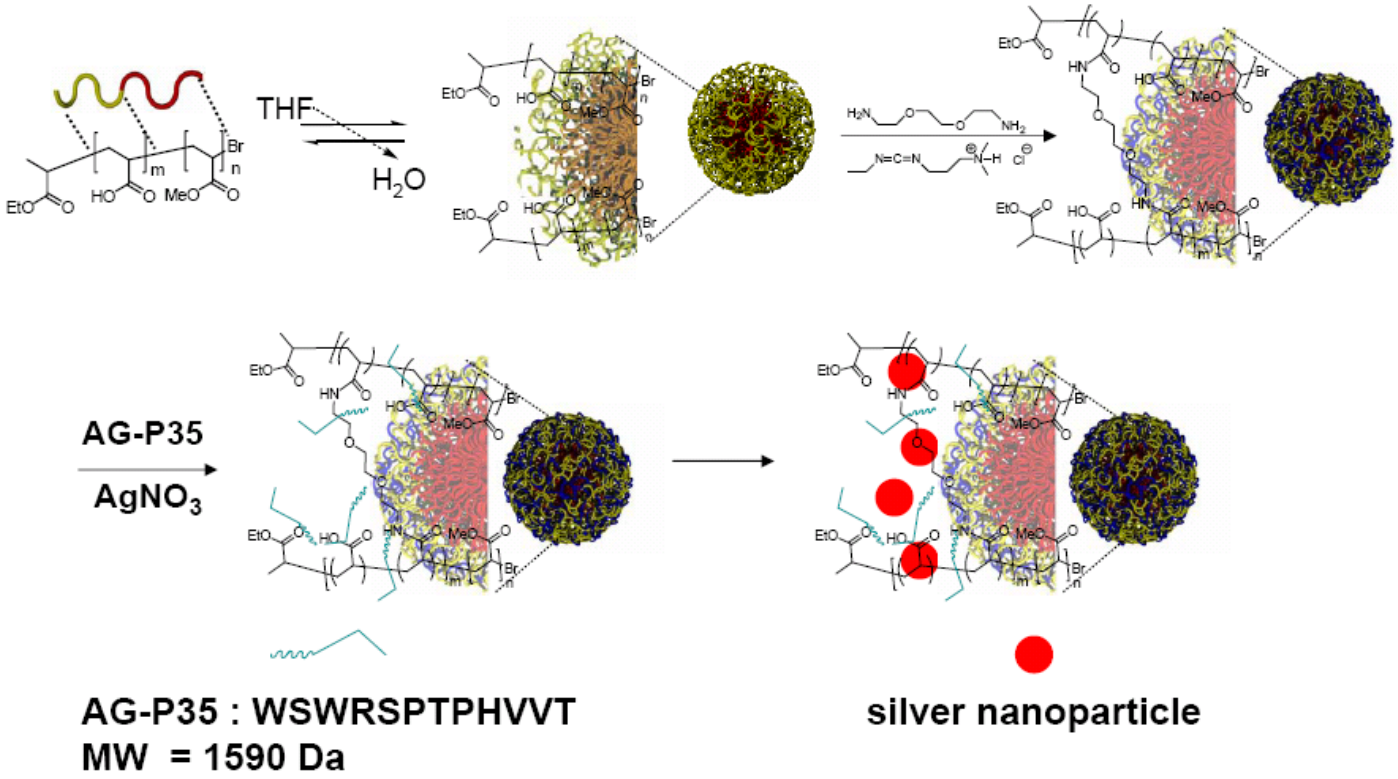

Scheme 5-1. Graphic representation of the synthesis of silver nanoparticles with SCKs and peptide AG-P35 as the templates. From a THF solution of the amphiphilic block copolymer, PAA_{105}-*b*-PMA_{184}, micellar structures were formed through controlled addition of water. SCKs were formed by crosslinking the shell layer with a diamino crosslinker, through amidation. The SCKs were incubated with AG-P35 and silver nitrate to form silver nanoparticles.

Table 5-1. Experimental information to grow silver nanoparticles. Concentrations: [SCK] = 0.240 mg/mL; [AG-P35] = 0.20 mg/mL; [$AgNO_3$] = 30 mM; [NH_2NH_2] = 2.0 M. For exp. 1 and 6, the SCK was incubated with AG-P35 for 24 h prior to $AgNO_3$ addition. For experiments 1 - 5, the final volumes were adjusted to 8 mL by addition of nanopure water. For experiment 6, the final volume was adjusted to 5 mL by addition of nanopure water.

exp.	SCK	AG-P35	$AgNO_3$	NH_2NH_2	[COOH]/ [AG-P35]/$AgNO_3$
1	6.80 mL	0.90 mL	20 μL		5.95/0.2/1
2	6.80 mL		120 μL	3.6 μL	5.95/0/1
3		0.90 mL	20 μL		0/0.2/1
4			1.00 mL	15 μL	
5	6.80 mL		20 μL		5.95/ 0/1
6	0.50 mL	0.20 mL	1.00 mL		0.009/0.0004/1

was also observed that the size of the dendritic silver nanoparticles increased with incubation time (**Figure 5-2**) It's hypothesized that the silver cations are immobilized in the shell domain of the SCK, through non-covalent interactions. Later reduction affords the silver nanoparticles with TEM diameters around 30-40 nm. These silver nanoparticles have strong interactions between each other and tend to form aggregates, resulting in a dendritic assembly of the spherical silver nanoparticles. The extent of aggregation increases with incubation time, which in turn gives increasing sizes.

As the control experiments, $AgNO_3$ was incubated with SCK/NH_2NH_2 (exp. 2), AG-P35 (exp. 3) and NH_2NH_2 (exp. 4), respectively (the NH_2NH_2 here was introduced as the reducing agent for the formation of Ag from $AgNO_3$). For exp. 2 and exp. 4, the reaction mixtures both turned brown upon the addition of hydrazine, indicating the fast reduction of Ag^+ by NH_2NH_2. Irregularly shaped nanoobjects were observed by TEM (**Figure 5-2**). No nanoparticles were observed by TEM for exp. 4.

Due to its instability, $AgNO_3$ can decompose and undergo self-redox reaction to form elemental silver. Experiments to grow silver nanoparticles by incubating $AgNO_3$ with SCK solutions were performed (exp. 5). Aliquots of reaction mixtures were taken at different time points and analyzed by scanning electron microscopy (SEM) and energy dispersive X-Ray (EDX) spectroscopy. As can be seen from the SEM images for exp. 5 (**Figure 5-3**), nanoparticles with flower-like structure were formed almost right upon the mixing of $AgNO_3$ and the SCK solution. In the first 80 min, the sizes of these nanoparticles were around 3 μm, and no obvious size expansion with incubation time was observed, except that the branches of the

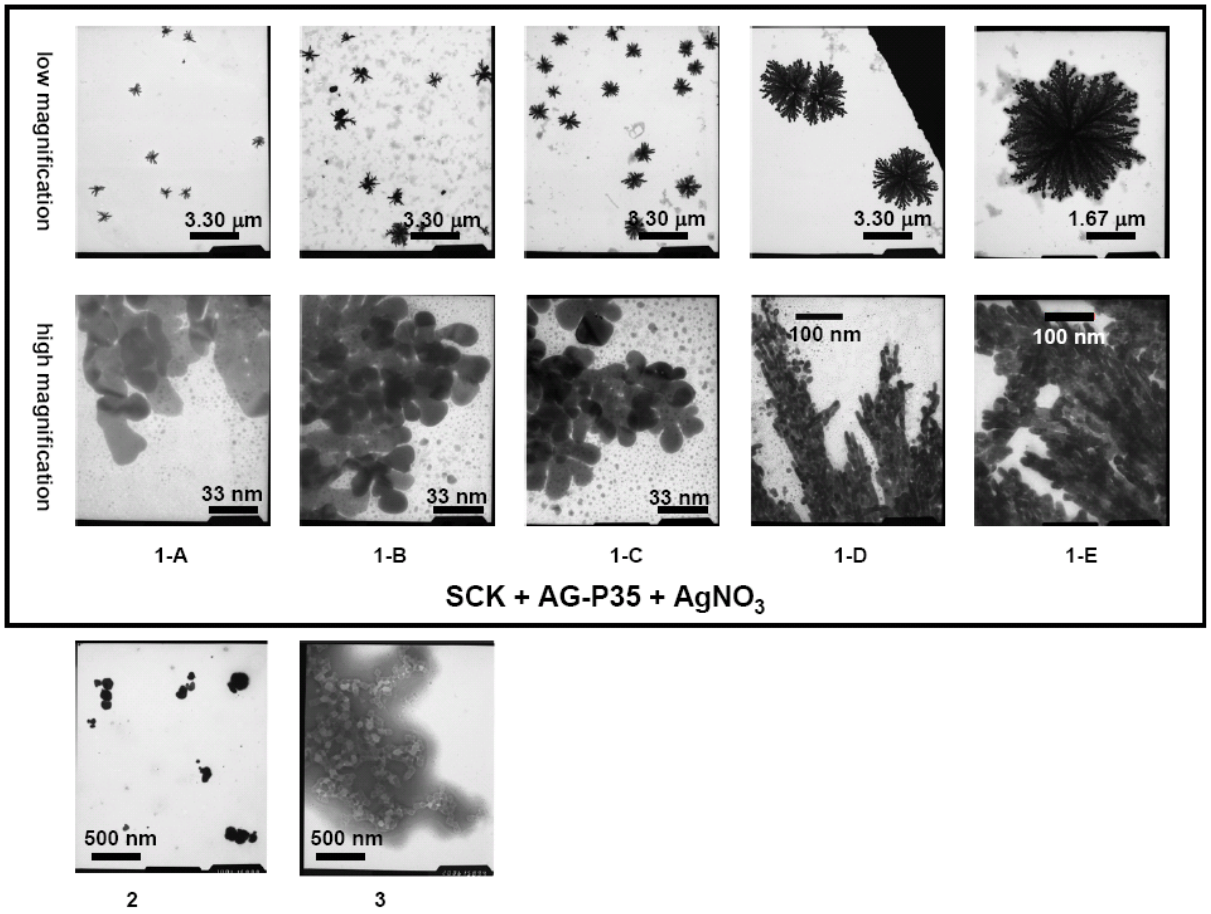

Figure 5-2. Transmission electron microscopy (TEM) images of silver nanoparticles grown in experiments 1-3. Images for 1-A, 1-B, 1-C, 1-D and 1-E were from samples prepared at 0.5 h, 1.5 h, 4.5 h, 11.5 h and 27.5 h after the addition of silver nitrate, respectively.

nanoparticles were getting thicker. Larger nanostructures were obtained at 10 h, around 7 μm. For the control experiment without SCK, flower-like nanostructures were also observed. Unlike the nanostructures obtained in the presence of SCK, the end of each branch was stretching out towards all directions and formed a fan-like end. It's unknown whether the silver nanoparticles formed in the aqueous solution, or on the TEM grids after water was evaporated. Energy dispersion X-ray microscopy (EDX) confirmed that these structures were silver nanoparticles (**Figure 5-4**). This indicated that the SCKs were acting as the template to form more ordered silver nanostructures and that AG-P35 was contributing to the formation of spherical silver nanoparticles.

Dendritic silver nanoparticles were grown when the amounts of silver nitrate, SCK and AG-P35 (COOH/AG-P35/$AgNO_3$ = 5.95/0.2/1) were comparable. The growth of silver nanoparticles with high loading of silver nitrate was also studied (COOH/AG-P35/$AgNO_3$ = 0.009/0.0004/1, exp. 6). When $AgNO_3$ was in highly excess amount, nanocrystals composed of silver nano-plates were formed (**Figure 5-5**). It's observed that at the beginning of the crystallization (2 h incubation), no obvious silver nano-plates were formed. After 10 h incubation, highly ordered layered structures were formed. For the control experiment ($AgNO_3$ with the same concentration without SCK or Ag-P35), layered structures were also observed, but the assembly of the layers were of less order. Silver nitrate at high concentrations tends to form randomly assembled nano-plates. With the incorporation of SCK and AG-P35, non-plate silver nanoparticle was first formed and served as the nucleating core for further silver deposition. Since silver nitrate was in a large excess, highly ordered nano-plates assembly was achieved.

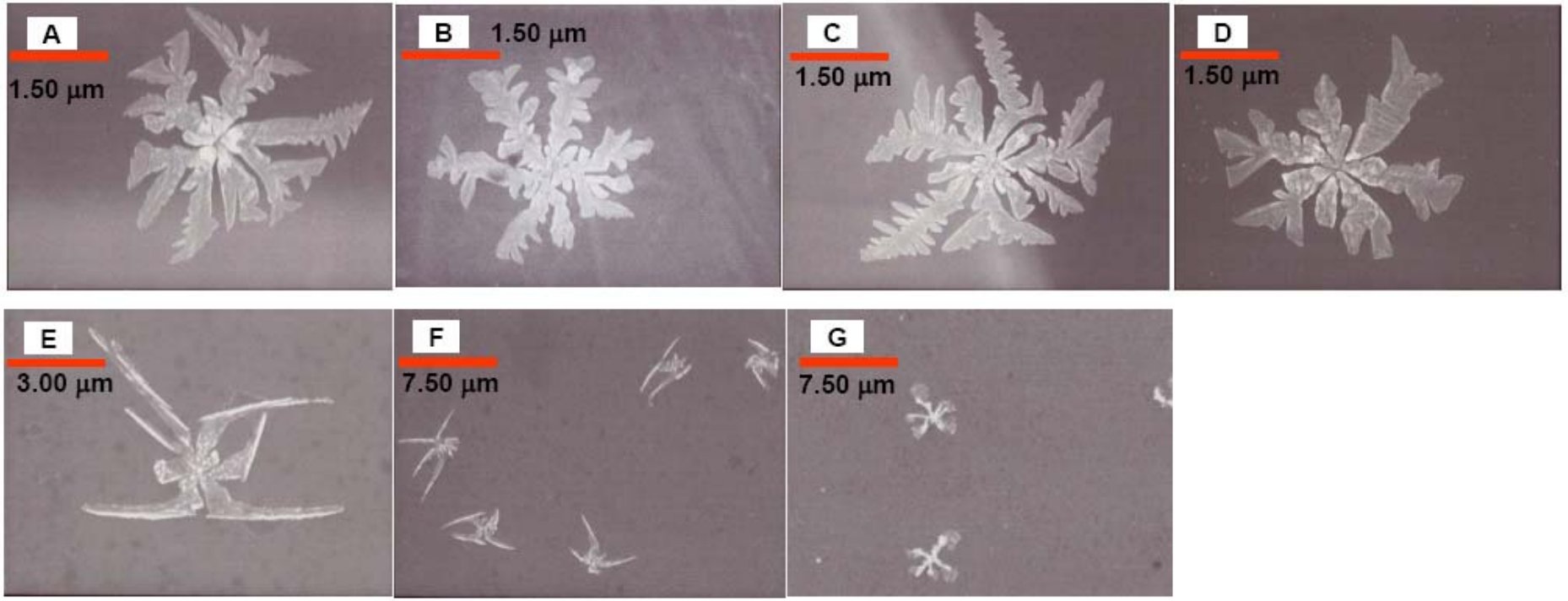

Figure 5-3. Scanning electron microscopy (SEM) images of silver nanoparticles obtained by exp. 5. Images were taken from samples prepared at 11 min (A), 21 min (B), 41 min (C), 81 min (D), 5 h (E) and 10 h (F) after the addition of silver nitrate. Image G was from the control experiment: silver nitrate aqueous solution (with equal silver nitrate concentration to that of exp. 5), image was taken at 10 h.

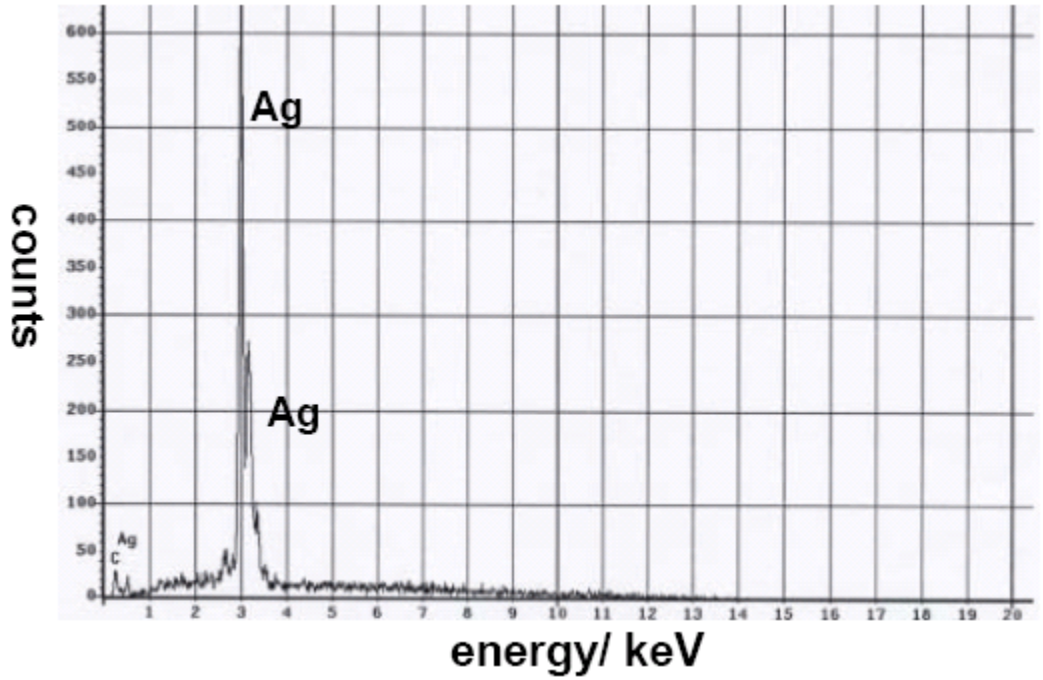

Figure 5-4. Energy dispersion X-ray (EDX) microanalysis of the nanoparticles.

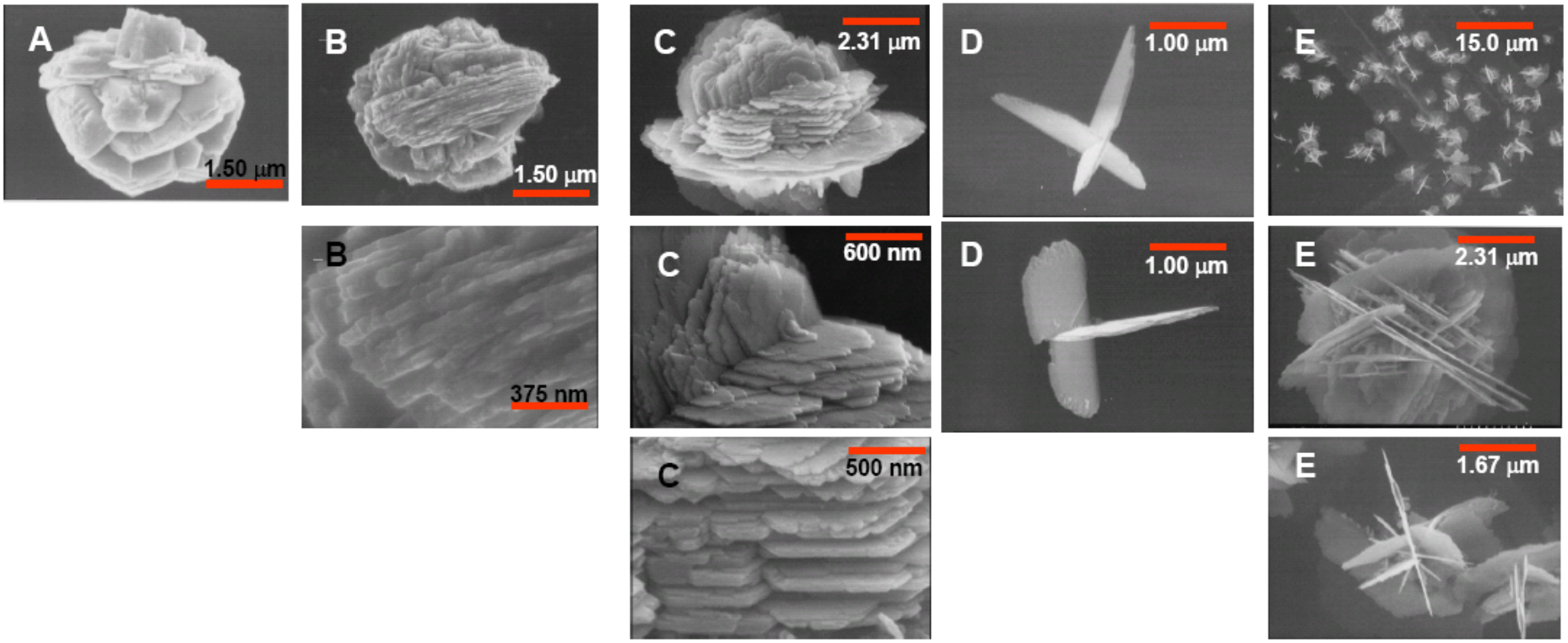

Figure 5-5. Scanning electron microscopy (SEM) images of silver nanoparticles obtained by exp. 6. Images were taken from samples prepared at 2 h (A), 10 h (B), and 60 h (C) after the addition of silver nitrate. Control experiment with equal silver nitrate concentration was performed and SEM images were taken from samples prepared at 2 h (D) and 60 h (E).

Experimental Section

Materials All solvents were purchased from Sigma-Aldrich and were used without further purification unless otherwise noted. Trifluoroacetic acid (TFA; 95%; Aldrich), 2,2′-(ethylenedioxy)-bis(ethylamine) (97%; Aldrich), 1-(3′-dimethylaminopropyl)-3-ethylcarbo-diimide methiodide (EDCI; 98%; Aldrich), were used as received. Supor 25 mm 0.1 μm Spectra/Por Membrane tubes (molecular weight cutoff (MWCO) 3,500 or 6-8000 Da), purchased from Spectrum Medical Industries Inc., were used for dialysis. Nanopure water (18 MΩ·cm) was acquired by means of a Milli-Q water filtration system (Millipore Corp.; Bedford, MA). Silver nitrate ($AgNO_3$, 99.0%) and hydrazine hydrate ($NH_2NH_2{\cdot}H_2O$, 25% in H_2O) were purchased from Aldrich. The peptide, AG-P35 (WSWRSPTPHVVT, 99%), was customized from New England Peptide, LLC., MA. The block copolymer, poly(*tert*-butyl acrylate)$_{105}$-*b*-polymer(methyl acrylate)$_{184}$ (P*t*BA$_{105}$-*b*-PMA$_{184}$), was synthesized by Dr. Zhiyun Chen through sequentially incorporating *tert*-butyl acrylate and methyl acrylate by atom transfer radical polymerization (ATRP) procedures. The P*t*BA segment was later converted into poly(acrylic acid) (PAA) block through acidolysis by TFA.

Instrumental

^{1}H NMR spectra were recorded on a Varian 300 MHz spectrometer interfaced to a UNIX computer using Mercury software. Chemical shifts are referred to the solvent proton resonance. Infrared spectra were acquired on a Perkin-Elmer Spectrum BX FT-IR instrument using KBr pellets.

Differential scanning calorimetry (DSC) measurements were performed with a DSC822^e instrument (Mettler-Toledo, Inc.) in a temperature range of – 100 to 180 °C with a ramp rate of 10 °C/min under nitrogen. Data were acquired and analyzed using STAR^e software (Mettler-Toledo, Inc.). The glass transition temperature, T_g, was determined at the midpoint of the inflection tangent upon the third heating scan.

Hydrodynamic diameters (D_h) and size distributions for the SCKs in aqueous solutions were determined by dynamic light scattering (DLS). The DLS instrument consisted of a Brookhaven Instruments Limited (Worcestershire, U.K.) system, including a model BI-200SM goniometer, a model BI-9000AT digital correlator, a model EMI-9865 photomultiplier, and a model 95-2 Ar ion laser (Lexel Corp., Farmindale, NY) operated at 514.5 nm. Measurements were made at 20 °C. Prior to analysis, solutions were filtered through a 0.22 μm Millex GV PVDF membrane filter (Millipore Corp., Medford, MA) and then centrifuged in a model 5414 microfuge (Brinkman Instruments, Inc., Westbury, NY) for 10 minutes to remove dust particles. Scattered light was collected at a fixed angle of 90 °. The digital correlator was operated with 522 ratio spaced channels, and initial delay of 5 μs, a final delay of 100 ms, and a duration of 10 minutes. A photomultiplier aperture of 400 μm was used, and the incident laser intensity was adjusted to obtain a photon counting of between 200 and 300 kcps. Only measurements in which the measured and calculated baselines of the intensity autocorrelation function agreed to within 0.1% were used to calculate particle sizes. The calculations of the particle size distributions and distribution averages were performed with the ISDA software package (Brookhaven Instruments Company), which employed single-exponential fitting, cumulants analysis, non-negatively constrained

least-squares (NNLS) and CONTIN particle size distribution analysis routines. All determinations were made in triplicate.

Transmission electron microscopy (TEM) was performed in bright-field mode with a JEOL 2000-FX at 150 kV accelerating voltage. Micelle/SCK nanoparticle samples for TEM measurements were diluted with 1 wt% of phosphotungstic acid (PTA) stain solution (v/v, 1:1). No stain was used for silver nanoparticle samples. Carbon grids (Ted Pella, Inc., Redding, CA) were exposed to oxygen plasma treatment to increase the surface hydrophilicity. Micrographs were collected at 100,000 magnifications. The number average particle diameters (D_{av}) and standard deviations were generated from the analysis of a minimum of 150 particles from at least three different micrographs. TEM was performed by Mr. G. Mike Veith.

Scanning electron microscopy (SEM) measurements were performed on a field emission scanning electron microscope (Hitachi s-4500), equipped with a NORAM Instruments energy dispersive X-Ray (EDX) microanalysis system, a back scattering detector, and a mechanical straining stage. Samples for SEM measurements were dropped onto TEM grids (5 μL), and allowed to dry under ambient conditions.

Preparation of poly(acrylic acid)-*b*-poly(methyl acrylate) PAA-*b*-PMA. To a 100 mL round-bottom flask equipped with a stir bar was added the block copolymer P*t*BA$_{105}$-*b*-PMA$_{184}$ (1.20 g, 0.041 mmol (polymer), 4.27 mmol (*t*-butyl ester)) and 25 mL of dichloromethane. To the solution was then added dropwise trifluoacetic acid (TFA) (10 mL, 130 mmol). The reaction mixture was allowed to stir at room temperature overnight. The solvent was removed under reduced pressure and the resultant polymer

was re-dissolved in THF, transferred to presoaked dialysis tubing (MWCO 6-8000 Da) and dialyzed against nanopure water. The resulting aqueous solution was lyophilized to afford a white powder. Yield: 0.90 g (94%). $(T_g)_{PAA}$ = 134 °C. $(T_g)_{PMA}$ = 13 °C. FTIR(cm^{-1}): 3500-2700, 1730, 1601, 1493, 1452, 1392, 1368, 1259, 1164, 846, 757, 704, 542. ^{1}H NMR (DMSO-d_6, 300 MHz, ppm): δ 11.9-12.5 (br, COO***H***), 3.52-3.65 (br, C***H*****$_3$**O), 2.15-2.40 (br, C***H*** of the polymer backbone) 1.30-1.90 (br, C***H*****$_2$** of the polymer backbone). ^{13}C NMR (DMSO-d_6, 75 MHz, ppm): δ 176.0, 174.5, 80.5, 51.6, 34.0-35.0, 15.0.

Preparation of PAA-*b*-PMA micelle. To a 250 round-bottom flask equipped with a stir bar was added the amphiphilic block copolymer (100 mg) and tetrahydrofuran (100 mL) to afford a 1.00 mg/mL solution. After stirring for 2 h, 100 mL of nanopure water was added dropwise *via* a syringe pump over 6 h. The mixture was further stirred for 12 h, followed by dialysis against nanopure water in MWCO 6-8000 Da dialysis tubing for 4 d to afford a clear micelle solution (0.510 mg/mL). D_h(num) = 51 ± 4 nm.

Preparation of PAA-*b*-PMA SCKs. To a solution of micelle in nanopure water (0.269 mmol COOH), was added dropwise a solution of 2,2'-(ethylenedioxy)-bis(ethylamine) (*c.a.* 1.0 mg/mL, 0.0672 mmol) over 10 min. The reaction mixture was stirred for *c.a.* 2 h. A solution of EDCI (1-[3'-(dimethylamino)propyl]-3-ethylcarbodiimide methiodide) in nanopure water (2 mg/mL, 0.134 mmol) was to the reaction mixture *via* a syringe pump over 30 min. The reaction mixture was further stirred for 20 h, followed by dialysis against nanopure water for 4 days in MWCO 6-8000 Da dialysis tubing, to remove all of the impurities and afford the SCK solution (0.240 mg/mL). D_h(num) = 45 ± 4 nm. D_{TEM} = 25 ± 2 nm.

General Procedure for the Preparation of Silver Nanoparticles. $AgNO_3$ solution (aqueous, 30 mM), SCK, and the peptide solution (aqueous, 0.20 mg/mL) were incubated at ambient conditions with varied ratios. Aliquots of the mixture were taken for TEM/SEM measurements.

Conclusions

We have shown here the synthesis of silver nanoparticles by use of shell crosslinked nanoparticles and the surface binding peptide (AG-P35) as the templates. At low silver nitrate concentrations, dendritic silver nanoparticles (1-10 μm) consisting of nearly spherical silver nanoparticles (~ 30 nm) were formed in the presence of SCK and the peptide AG-P35. Without AG-P35, flower-like silver nanoparticles were obtained in the presence of SCKs. Self-assembled silver nano-plates were formed at high silver nitrate concentrations. Silver nanoparticles were also formed from aqueous silver nitrate solution, without the use of either SCK or AG-P35. Whether the silver nanoparticles formed in aqueous solution, or on the TEM grids after water evaporation remains unknown. At higher silver nitrate concentrations, silver nano-assembly consists of nano-plates were formed. The presence of the SCKs and AG-P35 contributed to a higher degree of order compared to the nano-plate structures obtained from $AgNO_3$ only.

Acknowledgments

The author thank Dr. Zhiyun Chen for providing the block copolymer, $PtBA_{105}$-*b*-PMA_{184}, Mr. G. Mike Veith for TEM imaging, Mr. Lawrence Norcio for SEM training and the Department of Energy, Environmental & Chemical Engineering at Washington

University in Saint Louis for use of SEM/EDX facilities. This material is based upon work supported by the National Science Foundation (DMR-0210247).

References

1. Chairam, S.; Poolperm, C.; Somsook, E., Starch vermicelli template-assisted synthesis of size/shape-controlled nanoparticles. *Carbohydr. Polym.* **2009**, *75* (4), 694-704.

2. Berret, J. F.; Sandre, O.; Mauger, A., Size Distribution of Superparamagnetic Particles Determined by Magnetic Sedimentation. *Langmuir* **2007**, *23* (6), 2993-2999.

3. Berret, J.-F.; Schonbeck, N.; Gazeau, F.; El Kharrat, D.; Sandre, O.; Vacher, A.; Airiau, M., Controlled Clustering of Superparamagnetic Nanoparticles Using Block Copolymers: Design of New Contrast Agents for Magnetic Resonance Imaging. *J. Am. Chem. Soc.* **2006**, *128* (5), 1755-1761.

4. Lewis, L. N., Chemical catalysis by colloids and clusters. *Chem. Rev.* **1993**, *93* (8), 2693-2730.

5. Wang, J.; Liu, G.; Engelhard, M. H.; Lin, Y., Sensitive Immunoassay of a Biomarker Tumor Necrosis Factor-α Based on Poly(guanine)-Functionalized Silica Nanoparticle Label. *Anal. Chem.* **2006**, *78* (19), 6974-6979.

6. Nicewarner-Pena, S. R.; Freeman, R. G.; Reiss, B. D.; He, L.; Pena, D. J.; Walton, I. D.; Cromer, R.; Keating, C. D.; Natan, M. J., Submicrometer Metallic Barcodes. *Science* **2001**, *294* (5540), 137-141.

7. Kamat, P. V., Photophysical, Photochemical and Photocatalytic Aspects of Metal Nanoparticles. *J. Phys. Chem. B* **2002**, *106* (32), 7729-7744.

8. Yuwono, A. H.; Zhang, Y.; Wang, J.; Zhang, X. H.; Fan, H.; Ji, W., Diblock Copolymer Templated Nanohybrid Thin Films of Highly Ordered TiO2 Nanoparticle Arrays in PMMA Matrix. *Chem. Mater.* **2006**, *18* (25), 5876-5889.

9. Nie, S.; Emory, S. R., Probing Single Molecules and Single Nanoparticles by Surface-Enhanced Raman Scattering. *Science* **1997**, *275* (5303), 1102-1106.

10. Dick, L. A.; McFarland, A. D.; Haynes, C. L.; Van Duyne, R. P., Metal Film over Nanosphere (MFON) Electrodes for Surface-Enhanced Raman Spectroscopy (SERS): Improvements in Surface Nanostructure Stability and Suppression of Irreversible Loss. *J. Phys. Chem. B* **2002**, *106* (4), 853-860.

11. Sudeep, P. K.; Ipe, B. I.; Thomas, K. G.; George, M. V.; Barazzouk, S.; Hotchandani, S.; Kamat, P. V., Fullerene-Functionalized Gold Nanoparticles. A Self-Assembled Photoactive Antenna-Metal Nanocore Assembly. *Nano Lett.* **2002**, *2* (1), 29-35.

12. Elim, H. I.; Ji, W.; Yuwono, A. H.; Xue, J. M.; Wang, J., Ultrafast optical nonlinearity in poly(methylmethacrylate)-TiO_2 nanocomposites. *Appl. Phys. Lett.* **2003**, *82* (16), 2691.

13. Park, B. J.; Sung, J. H.; Kim, K. S.; Chin, I.; Choi, H. J., Preparation and Characterization of Poly(Methyl Methacrylate) Coated TiO_2 Nanoparticles. *Journal of Macromolecular Science: Physics* **2006**, *45* (1), 53-60.

14. Flynn, C. E.; Lee, S.-W.; Peelle, B. R.; Belcher, A. M., Viruses as vehicles for growth, organization and assembly of materials. *Acta Mater.* **2003**, *51* (19), 5867-5880.

15. Mao, C.; Solis, D. J.; Reiss, B. D.; Kottmann, S. T.; Sweeney, R. Y.; Hayhurst, A.; Georgiou, G.; Iverson, B.; Belcher, A. M., Virus-Based Toolkit for the Directed

Synthesis of Magnetic and Semiconducting Nanowires. *Science* **2004**, *303* (5655), 213-217.

16. Lee, S.-W.; Mao, C.; Flynn, C. E.; Belcher, A. M., Ordering of Quantum Dots Using Genetically Engineered Viruses. *Science* **2002**, *296* (5569), 892-895.

17. T. Douglas, E. S. D. W. A. A. M. L. M. Y., Protein Engineering of a Viral Cage for Constrained Nanomaterials Synthesis. *Adv. Mater.* **2002**, *14* (6), 415-418.

18. Kroger, N.; Deutzmann, R.; Sumper, M., Polycationic Peptides from Diatom Biosilica That Direct Silica Nanosphere Formation. *Science* **1999**, *286* (5442), 1129-1132.

19. Brott, L. L.; Naik, R. R.; Pikas, D. J.; Kirkpatrick, S. M.; Tomlin, D. W.; Whitlock, P. W.; Clarson, S. J.; Stone, M. O., Ultrafast holographic nanopatterning of biocatalytically formed silica. *Nature* **2001**, *413* (6853), 291-293.

20. Sun, Y.; Xia, Y., Shape-Controlled Synthesis of Gold and Silver Nanoparticles. *Science* **2002**, *298* (5601), 2176-2179.

21. Kyung Ju Lee, J. T. P. J. H. G. J. H. K., Synthesis of amphiphilic graft copolymer brush and its use as template film for the preparation of silver nanoparticles. *J. Polym. Sci., Part A: Polym. Chem.* **2008**, *46* (12), 3911-3918.

22. Rifai, S.; Breen, C. A.; Solis, D. J.; Swager, T. M., Facile in Situ Silver Nanoparticle Formation in Insulating Porous Polymer Matrices. *Chem. Mater.* **2006**, *18* (1), 21-25.

23. Andersson, M.; Pedersen, J. S.; Palmqvist, A. E. C., Silver Nanoparticle Formation in Microemulsions Acting Both as Template and Reducing Agent. *Langmuir* **2005**, *21* (24), 11387-11396.

24. He, J.; Kunitake, T.; Watanabe, T., Porous and nonporous Ag nanostructures fabricated using cellulose fiber as a template. *Chem. Commun.* **2005**, (6), 795-796.

25. Hartgerink, J. D.; Beniash, E.; Stupp, S. I., Self-Assembly and Mineralization of Peptide-Amphiphile Nanofibers. *Science* **2001**, *294* (5547), 1684-1688.

26. Naik, R. R.; Stringer, S. J.; Agarwal, G.; Jones, S. E.; Stone, M. O., Biomimetic synthesis and patterning of silver nanoparticles. *Nat. Mater.* **2002**, *1* (3), 169-172.

27. Naik, R. R.; Jones, S. E.; Murray, C. J.; McAuliffe, J. C.; Vaia, R. A.; Stone, M. O., Peptide Templates for Nanoparticle Synthesis Derived from Polymerase Chain Reaction-Driven Phage Display. *Adv. Funct. Mater.* **2004**, *14* (1), 25-30.

28. He, J.; Kunitake, T., Formation of Silver Nanoparticles and Nanocraters on Silicon Wafers. *Langmuir* **2006**, *22* (18), 7881-7884.

29. Deshmukh, R. D.; Composto, R. J., Surface Segregation and Formation of Silver Nanoparticles Created In situ in Poly(methyl Methacrylate) Films. *Chem. Mater.* **2007**, *19* (4), 745-754.

30. Evanoff, D. D.; Chumanov, G., Size-Controlled Synthesis of Nanoparticles. 2. Measurement of Extinction, Scattering, and Absorption Cross Sections. *J. Phys. Chem. B* **2004**, *108* (37), 13957-13962.

31. Balogh, L.; Swanson, D. R.; Tomalia, D. A.; Hagnauer, G. L.; McManus, A. T., Dendrimer-Silver Complexes and Nanocomposites as Antimicrobial Agents. *Nano Lett.* **2001**, *1* (1), 18-21.

32. Jana, N. R.; Sau, T. K.; Pal, T., Growing Small Silver Particle as Redox Catalyst. *J. Phys. Chem. B* **1999**, *103* (1), 115-121.

33. Kang, Y. S.; Kang, S. W.; Kim, H.; Kim, J. H.; Won, J.; Kim, C. K.; Char, K., Interaction with Olefins of the Partially Polarized Surface of Silver Nanoparticles Activated by *p*-Benzoquinone and Its Implications for Facilitated Olefin Transport. *Adv. Mater.* **2007**, *19* (3), 475-479.

34. Thurmond, K. B.; Kowalewski, T.; Wooley, K. L., Water-Soluble Knedel-like Structures: The Preparation of Shell-Cross-Linked Small Particles. *J. Am. Chem. Soc.* **1996**, *118* (30), 7239-7240.

35. Butun, V.; Billingham, N. C.; Armes, S. P., Synthesis of Shell Cross-Linked Micelles with Tunable Hydrophilic/Hydrophobic Cores. *J. Am. Chem. Soc.* **1998**, *120* (46), 12135-12136.

36. Becker, M. L.; Bailey, L. O.; Wooley, K. L., Peptide-Derivatized Shell-Cross-Linked Nanoparticles. 2. Biocompatibility Evaluation. *Bioconjugate Chem.* **2004**, *15* (4), 710-717.

37. Pan, D.; Turner, J. L.; Wooley, K. L., Shell Cross-Linked Nanoparticles Designed To Target Angiogenic Blood Vessels via $\alpha_v\beta_3$ Receptor-Ligand Interactions. *Macromolecules* **2004**, *37* (19), 7109-7115.

Chapter 6

Conclusion

Two types of polymeric nanoparticles, SCKs based on PAA-*b*-PS, and micelle from a hyperbranched star-like amphiphilic poly(acrylic acid)-b-poly(trifluomethyl methacrylate), have been studied as potential diagnosic and therapeutic delivery agents.

Methods have been optimized to develop shell crosslinked nanoparticles bearing cyclic KCRGDC peptide as the nanoscale antagonist to $\alpha_v\beta_3$ integrin, for treatment with acute vascular injuries. Nanoparticles based on PAA-*b*-PS system, labeled with KCRGDC prepared from post-labeling the 5-FAM-KCRGDC peptide onto micelle/SCKs assembled from HOOC-PEG3000$_{4.0}$-*g*-DOTAlysine$_{3.2}$-*g*-PAA$_{58.8}$-*b*-PS$_{71}$ showed significantly improved IC50 values to $\alpha_v\beta_3$ than those nanoparticles prepared from pre-labeling the NH_2-PEG5000-5-FAM-KCRGDC to amphiphilic PAA-*b*-PS block copolymers. It's hypothesized that when the NH_2-PEG5000-5-FAM-KCRGDC was pre-attached to the polymer, the majority of the peptide is buried underneath the shell layer during the course of self-assembly, leading to low accessibility to bind to outer integrins. All the RGD-labeled nanoparticles showed strong specific binding to U87MG glioma cells. A cell-based assay provides further information on binding affinity as well as internalization of these nanoparticles constructs Despite the fact that the

nanoparticles prepared by the post-labeling method having the best IC_{50} values to $\alpha_v\beta_3$, they were less internalized into U87MG glioma cells and showed weaker binding. This discrepancy can be explained by the fact that the isolated integrin binding assay has a constrained geometry and lacks many components found *in vivo*. With the good cell targeting capabilities, good biodistribution been reported, as well as with the DOTAlysine acting as the chelator of radio metals for imaging for PET imaging, these nanoparticles possess good potential to be developed into nanoscale diagnostic and therapeutic agent delivery vehicles.

To the hyperbranched star-like amphiphilic poly(acrylic acid)-*b*-poly(trifluomethyl methacrylate), an F3 peptide, which specifically targets to nucleolin overexpressed in many types of cancer tumor domains, was attached through amidation chemistry in organic solvents. Cascade blue (CB) was also attached to the polymer for imaging purposes by fluorescence. Dialysis of the DMF solutions of the F3 and CB-labeled polymers against water afforded the micelles. Doxorubicin (DOX), a drug widely used in chemotherapy treatments for several types of cancer, such as hematological malignancies and soft tissue sarcomas, was loaded into the core domain. In vitro studies showed the enhanced binding/targeting as a result of the introduction of F3 peptide. In vivo studies with U87MG mice have shown the ability of these micelles to pass the blood-brain barrier and concentrated in the tumor regions. PEGylation was found to enhance the biodistribution of these micelles. Although the DOX release appeared to be

troublesome at this point, this system showed potential to not only provide a novel approach to efficiently deliver therapeutics to the targeted tumor site, it can also potentially attenuate systemic side effects caused by free doxorubicin.

Besides functioning as delivery vehicles, SCK nanoparticles prepared from PAA-*b*-PS have also been studied as nanoscale contrast agents for magnetic resonance imaging, by anchoring a gadolinium complex of DOTAlysine onto the nanoparticles. Methods to achieve clean nanoscale contrast agents (i.e. with no free or loosely bound Gd^{3+} ions) were developed. As expected, compared to the Gd-DOTAlysine small molecule, enhanced relaxivities were achieved by conjugating the small molecule onto SCKs, due to the decreased tumbling rate of the nanoparticles. The relaxivities were found to be increasing with the extents of crosslinking. A reasonable explanation for this is that higher extents of crosslinking makes the environment of Gd-DOTAlysine bound on the SCKs more rigid so that longer rotational correlation time is achieved. With the good blood pool imaging capabilities, and potential for active targeting, as well as the enhanced T_1 relaxivities, SCKs have the potential to serve as a promising candidate for *in vivo* MRI imaging.

Finally, SCKs prepared from poly(acrylic acid)-*b*-poly(methyl acrylate) have been studied as the template to synthesize silver nanoparticles, with silver nitrate as the silver source. The peptide, AG-P35, which binds to the (111) face of silver crystals, was used as a co-templating molecule. The morphology of the silver nanoparticle obtained was

highly dependent on the reaction conditions, such as concentration ratios, reaction durations. At low silver nitrate concentrations, dendritic silver nanoparticles (1-10 μm) consisting of nearly spherical silver nanoparticles (~ 30 nm) were formed in the presence of SCK and the peptide AG-P35. Without AG-P35, flower-like silver nanoparticles were obtained in the presence of SCKs. Self-assembled silver nano-plates were formed at high silver nitrate concentrations. Silver nanoparticles were also formed from aqueous silver nitrate solution, without the use of either SCK or AG-P35. Whether the silver nanoparticles formed in aqueous solution, or on the TEM grids after water evaporation remains unknown. At higher silver nitrate concentrations, silver nano-assembly consists of nano-plates were formed. The presence of the SCKs and AG-P35 contributed to a higher degree of order compared to the nano-plate structures obtained from $AgNO_3$ only.

Appendix

^{1}H NMR, 300 MHz, DMSO-d_6

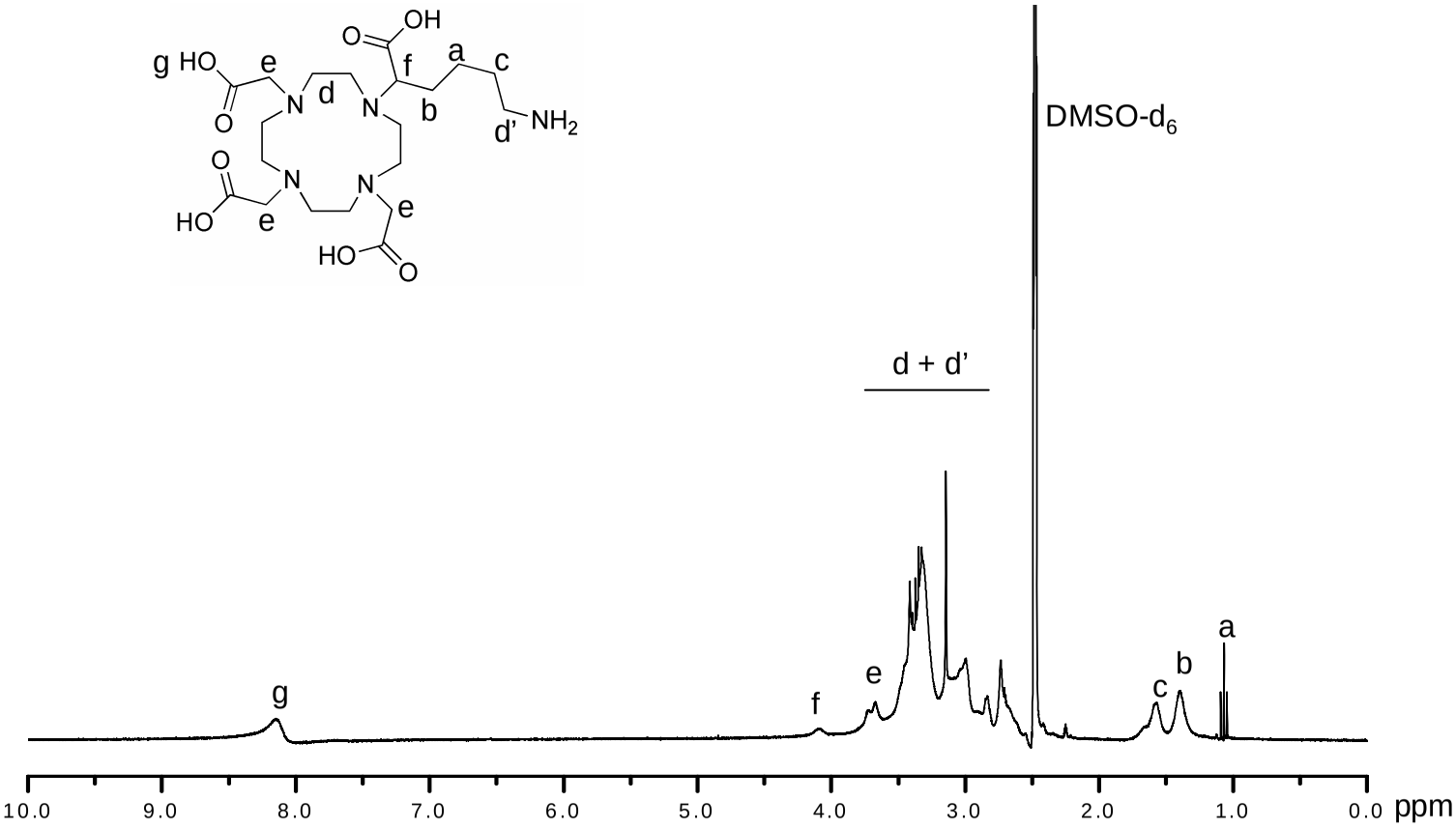

^{1}H NMR, 500 MHz, DMSO-d_6

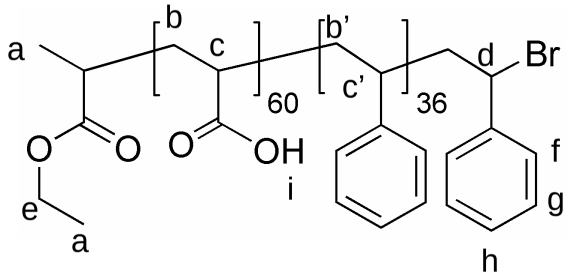

^{1}H NMR, 300 MHz, CD_2Cl_2

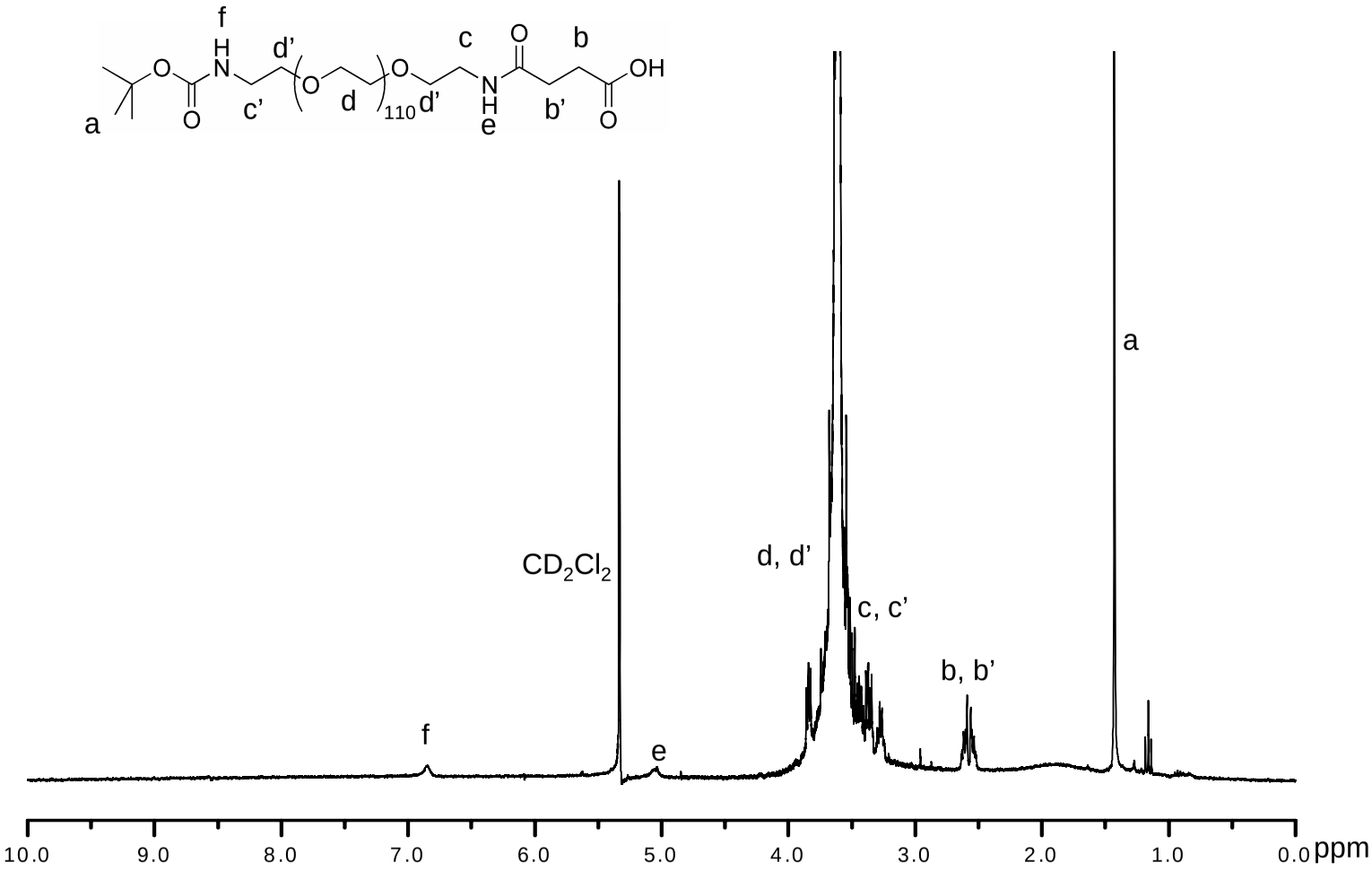

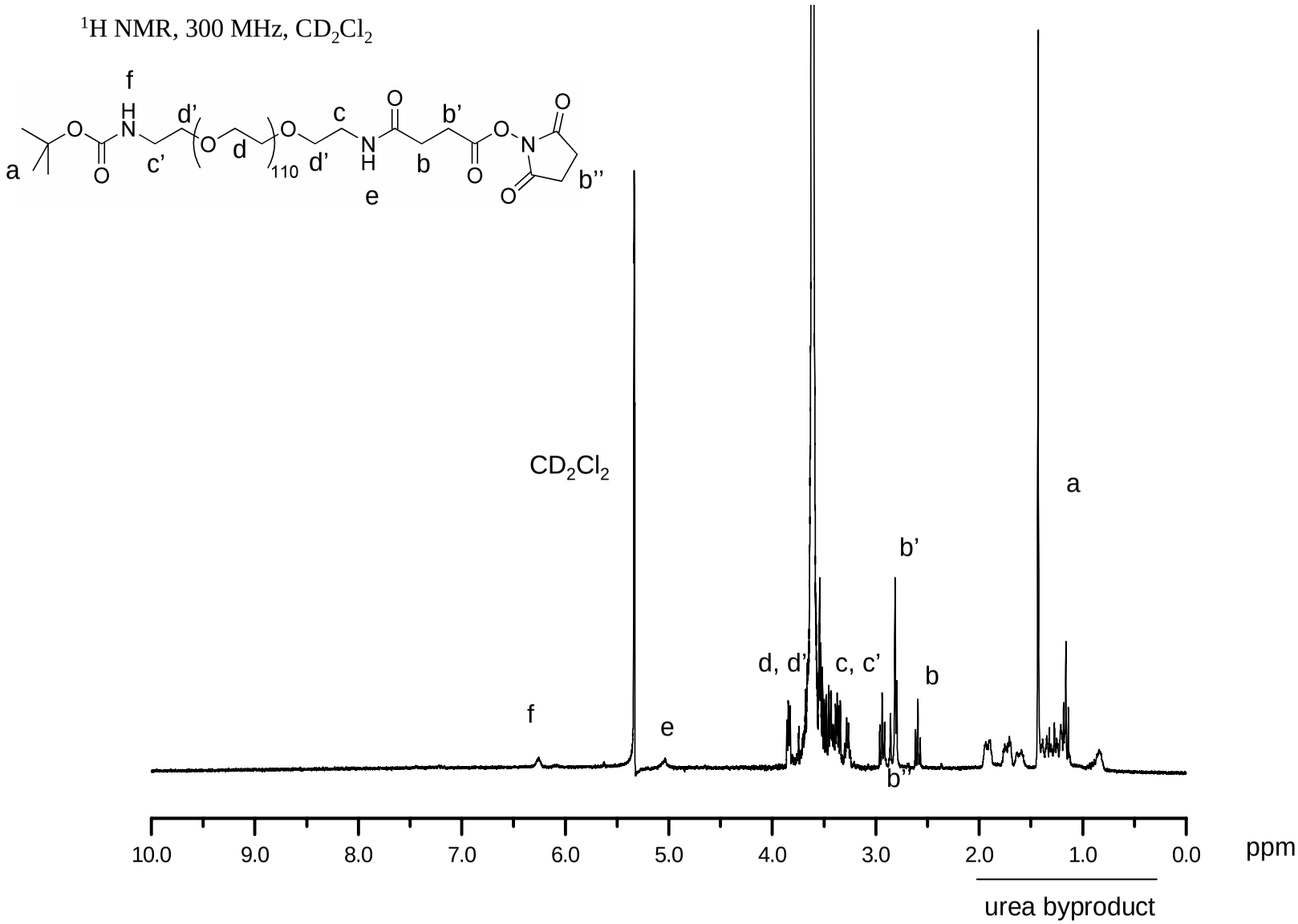
^{1}H NMR, 300 MHz, CD_2Cl_2
f
a
c'
d'
d
110
d'
c
e
b
b'
b''
CD_2Cl_2
f
e
d, d'
c, c'
b
b'
b''
a
10.0
9.0
8.0
7.0
6.0
5.0
4.0
3.0
2.0
1.0
0.0
ppm
urea byproduct

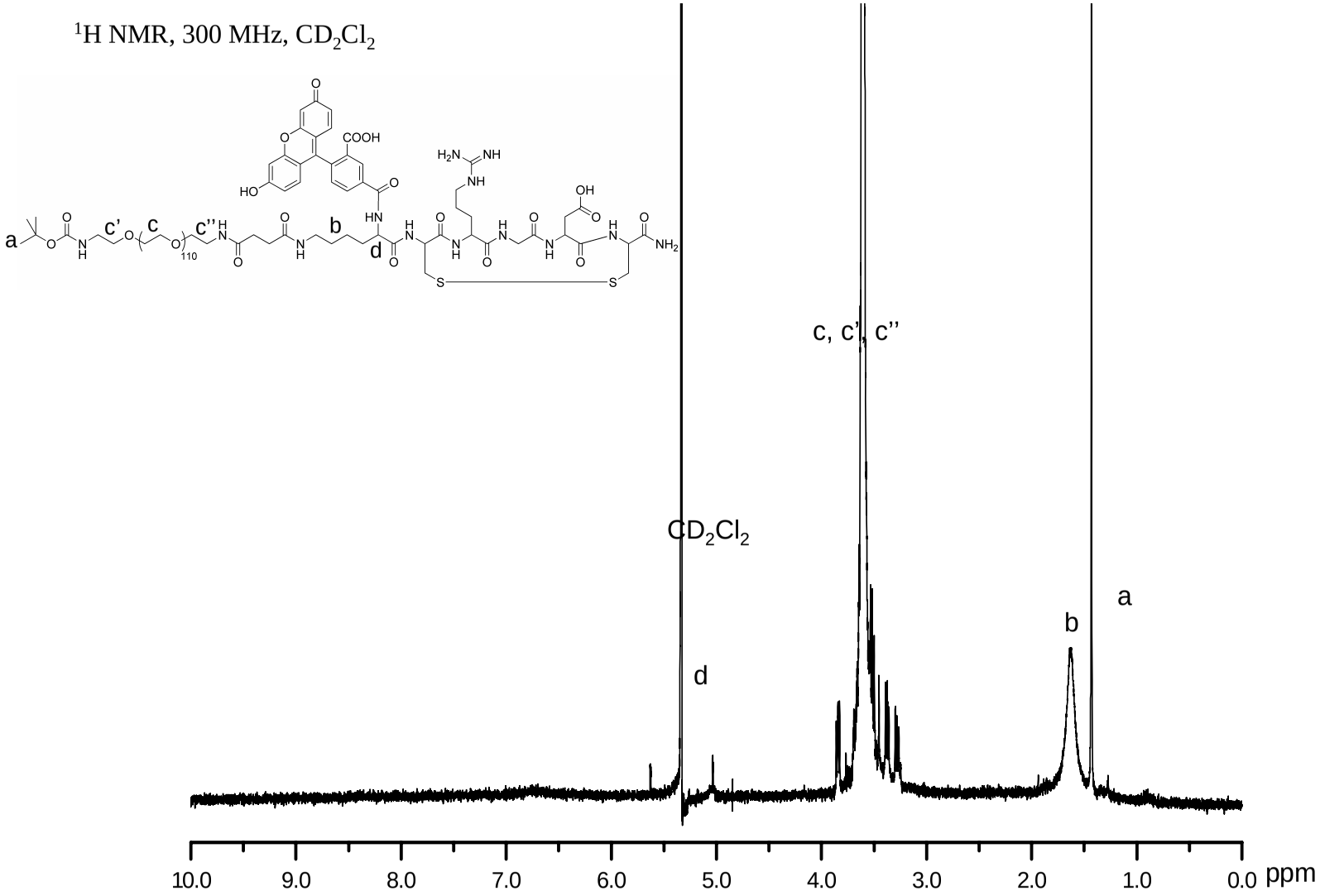
^{1}H NMR, 300 MHz, CD_2Cl_2
a
c'
c
c''
b
d
110
c, c', c''
CD_2Cl_2
d
b
a
10.0
9.0
8.0
7.0
6.0
5.0
4.0
3.0
2.0
1.0
0.0
ppm

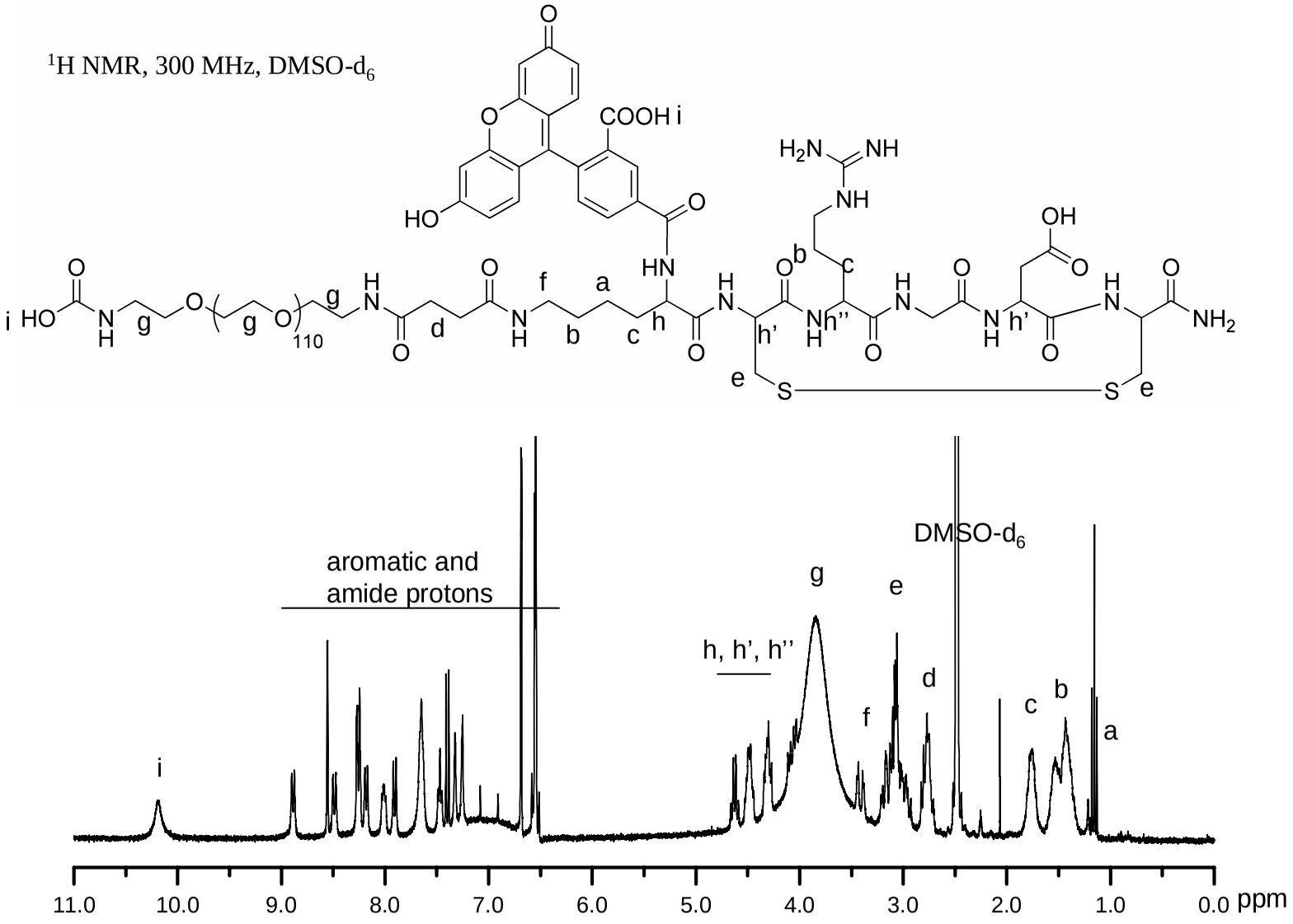
^{1}H NMR, 300 MHz, DMSO-d$_6$
aromatic and
amide protons
h, h', h''
DMSO-d$_6$
i
g
e
d
f
c
b
a
11.0
10.0
9.0
8.0
7.0
6.0
5.0
4.0
3.0
2.0
1.0
0.0
ppm

^{1}H NMR, 500 MHz, DMSO-d_6

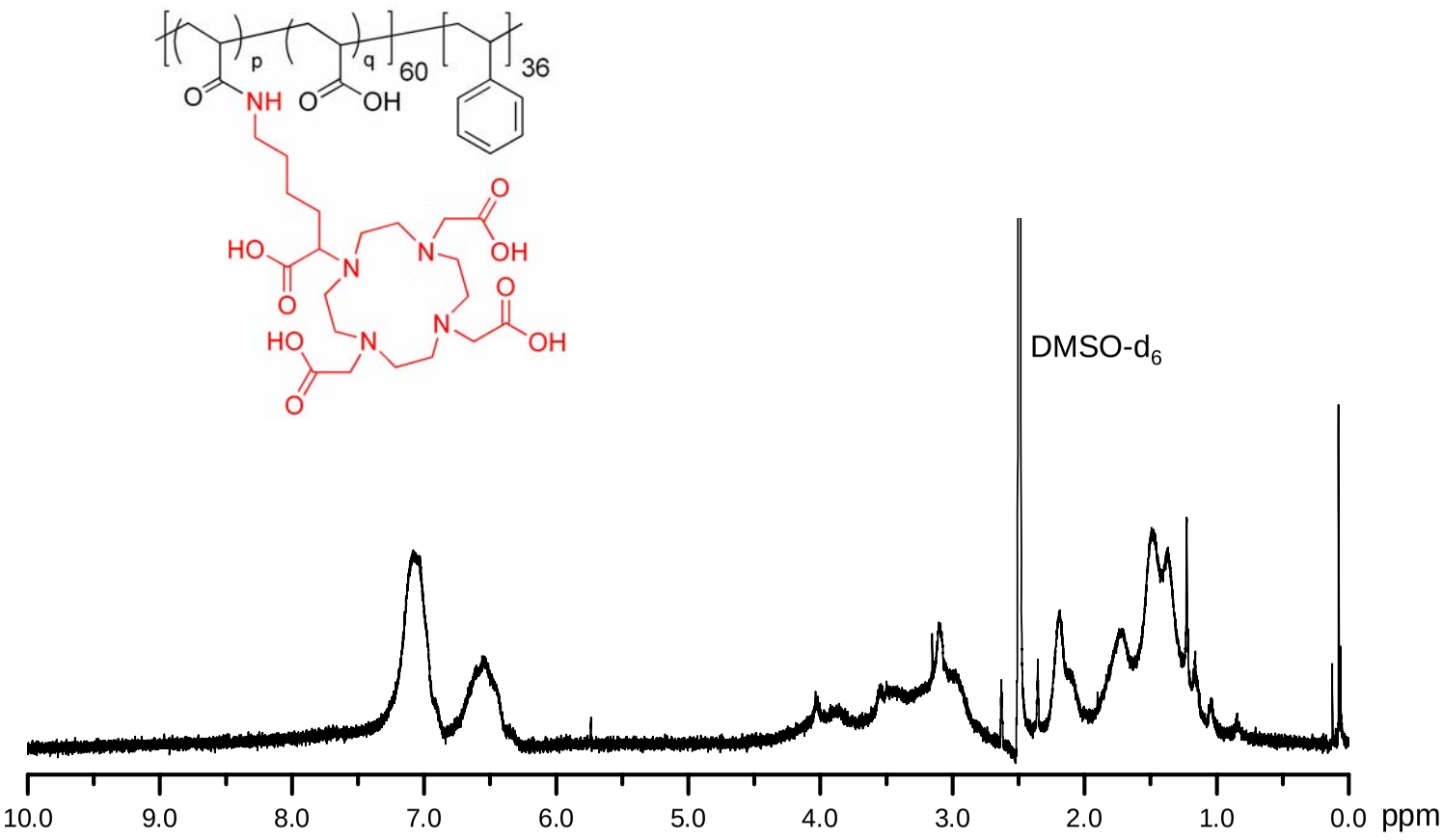

^{1}H NMR, 300 MHz, CD_2Cl_2

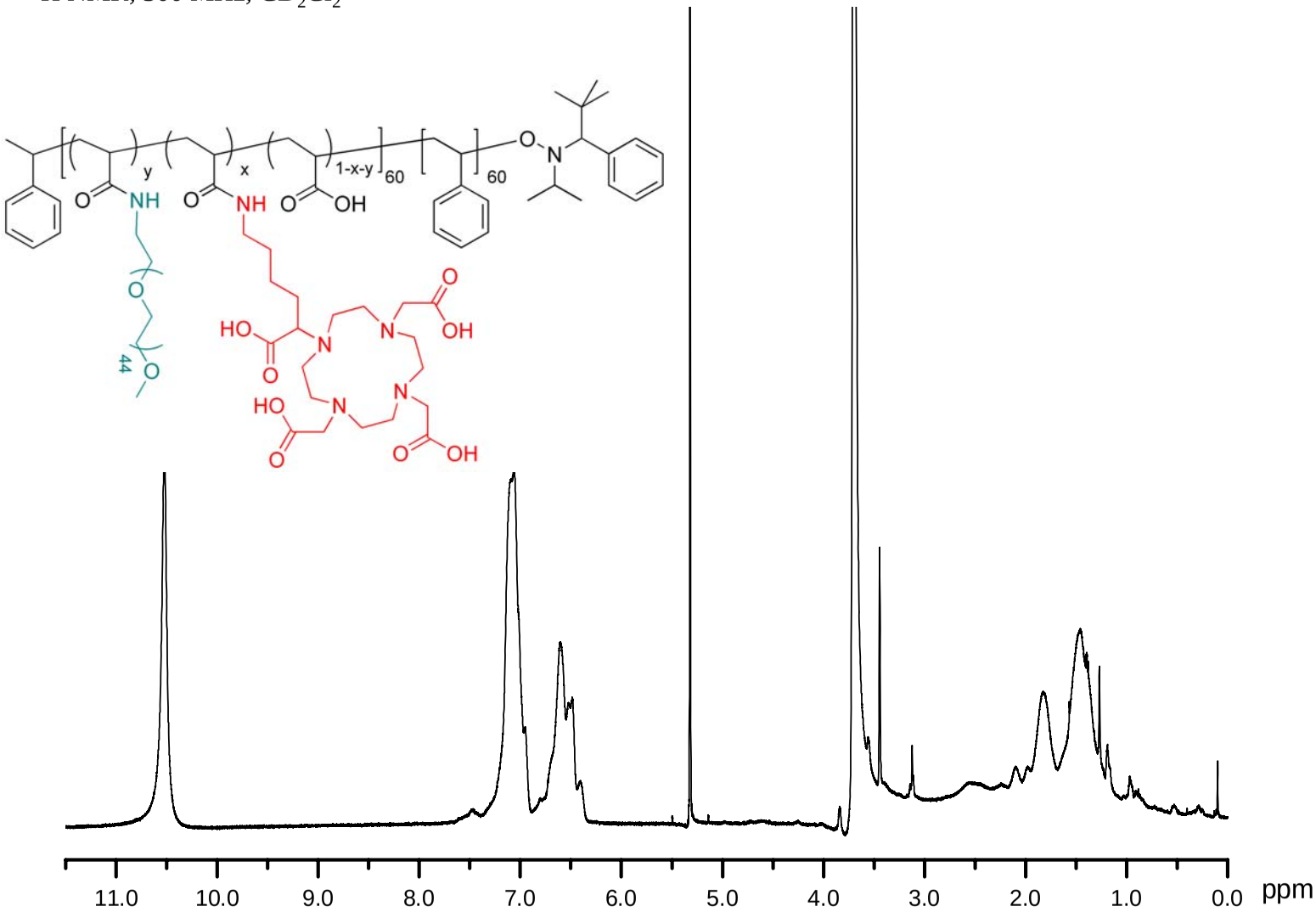

^{1}H NMR, 300 MHz, CD_2Cl_2

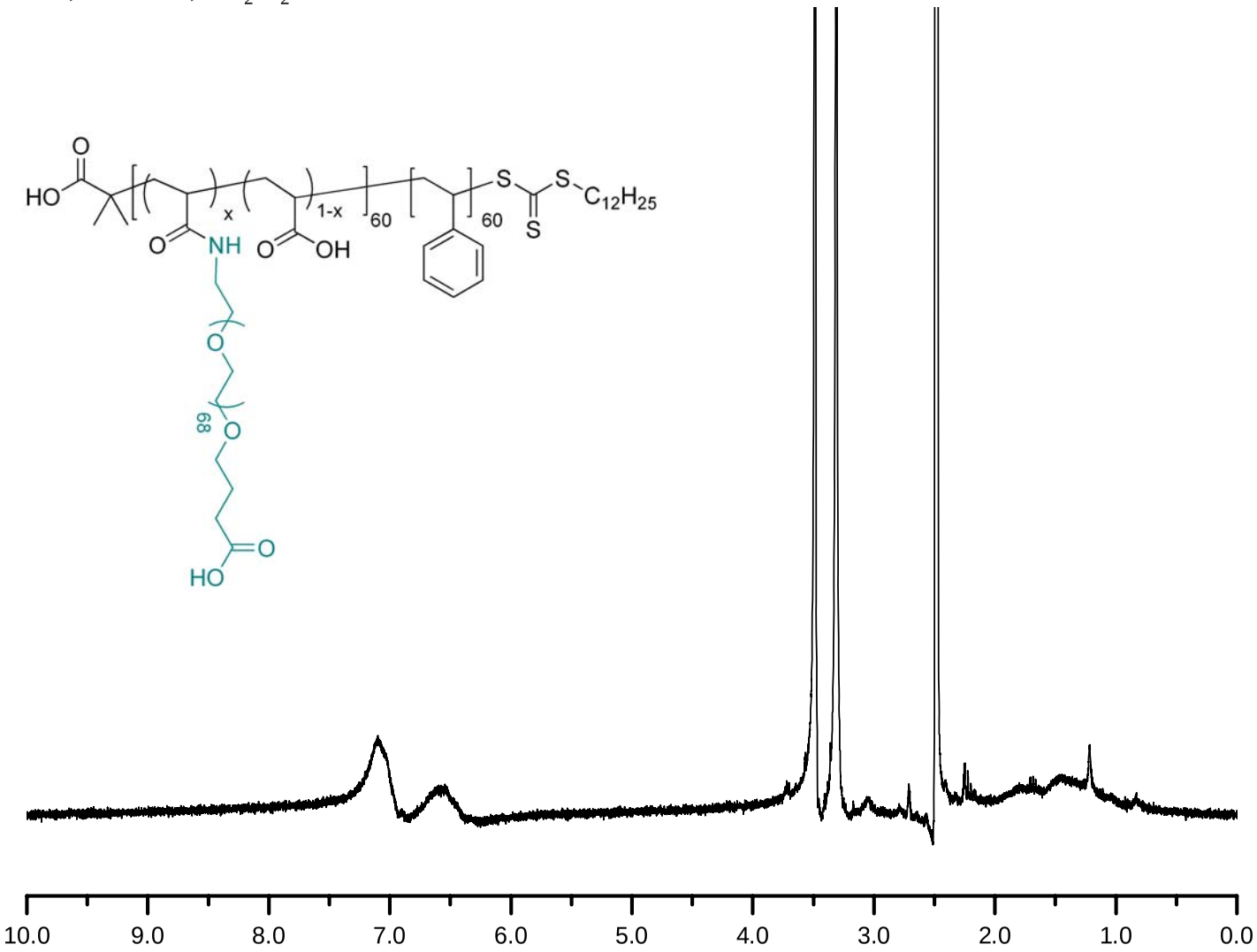

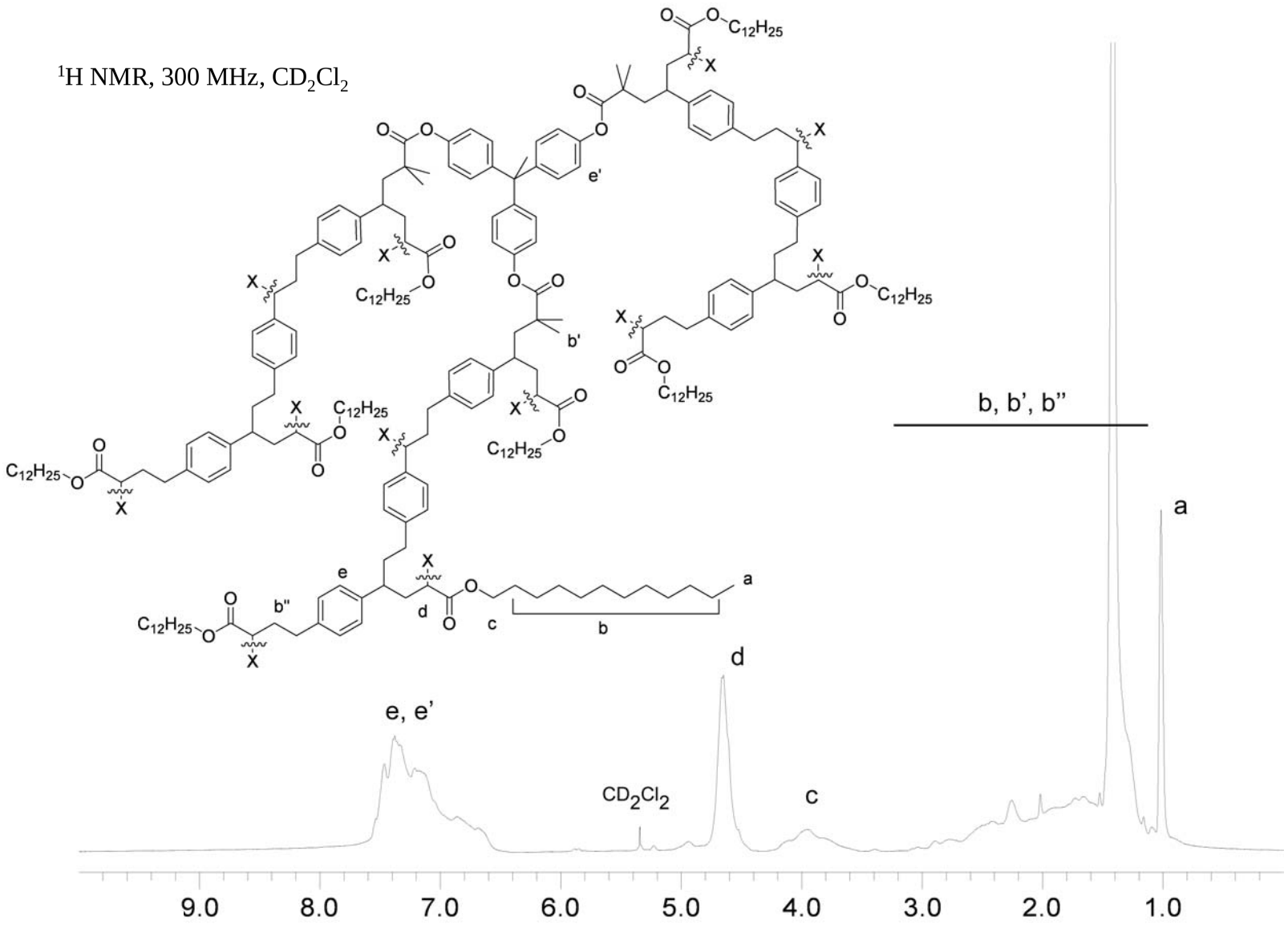
^{1}H NMR, 300 MHz, CD_2Cl_2
b, b', b''
a
d
e, e'
CD_2Cl_2
c
9.0
8.0
7.0
6.0
5.0
4.0
3.0
2.0
1.0

^{1}H NMR, 300 MHz, CD_2Cl_2

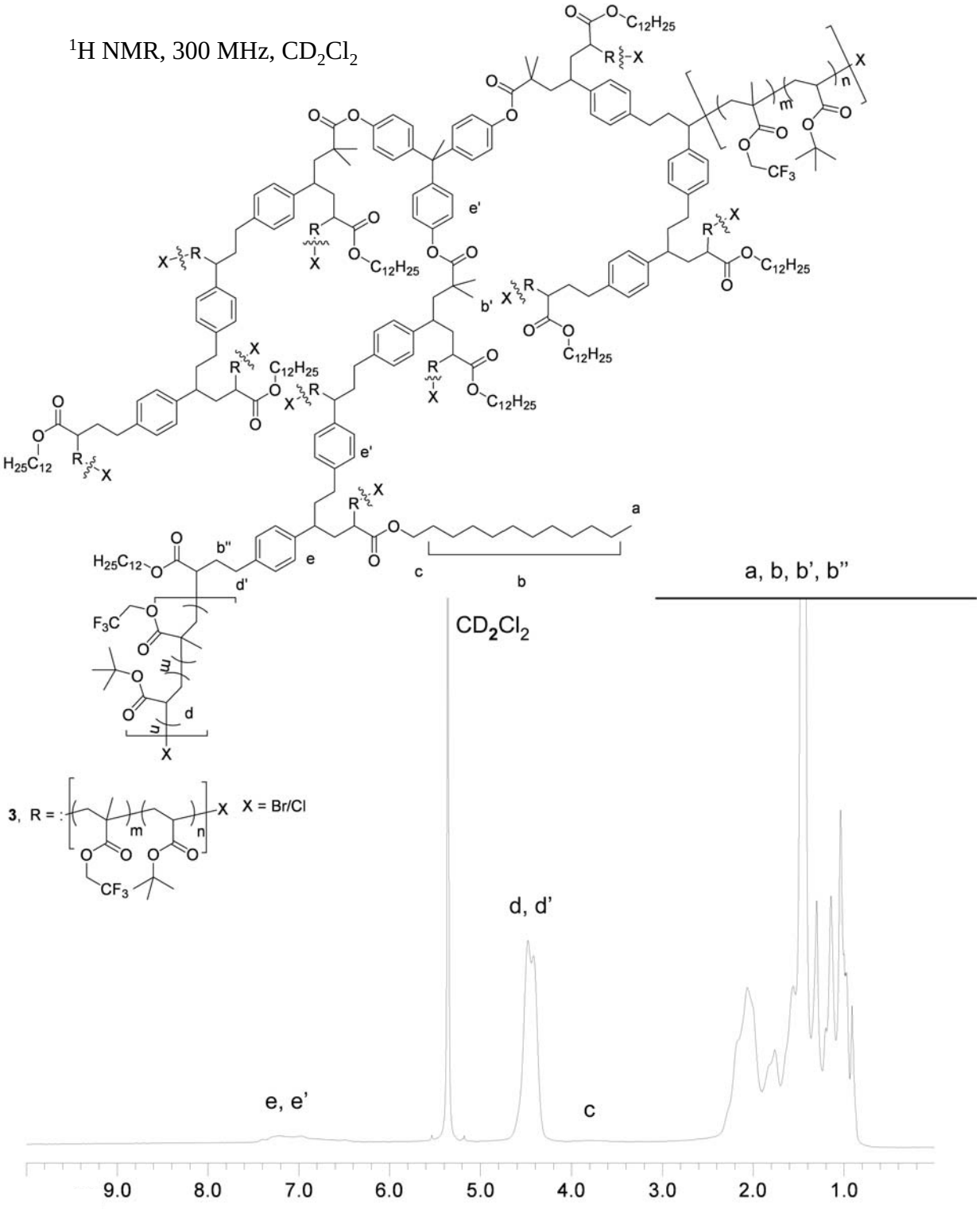

3, R = : X = Br/Cl

^{1}H NMR, 300 MHz, DMSO-d_6

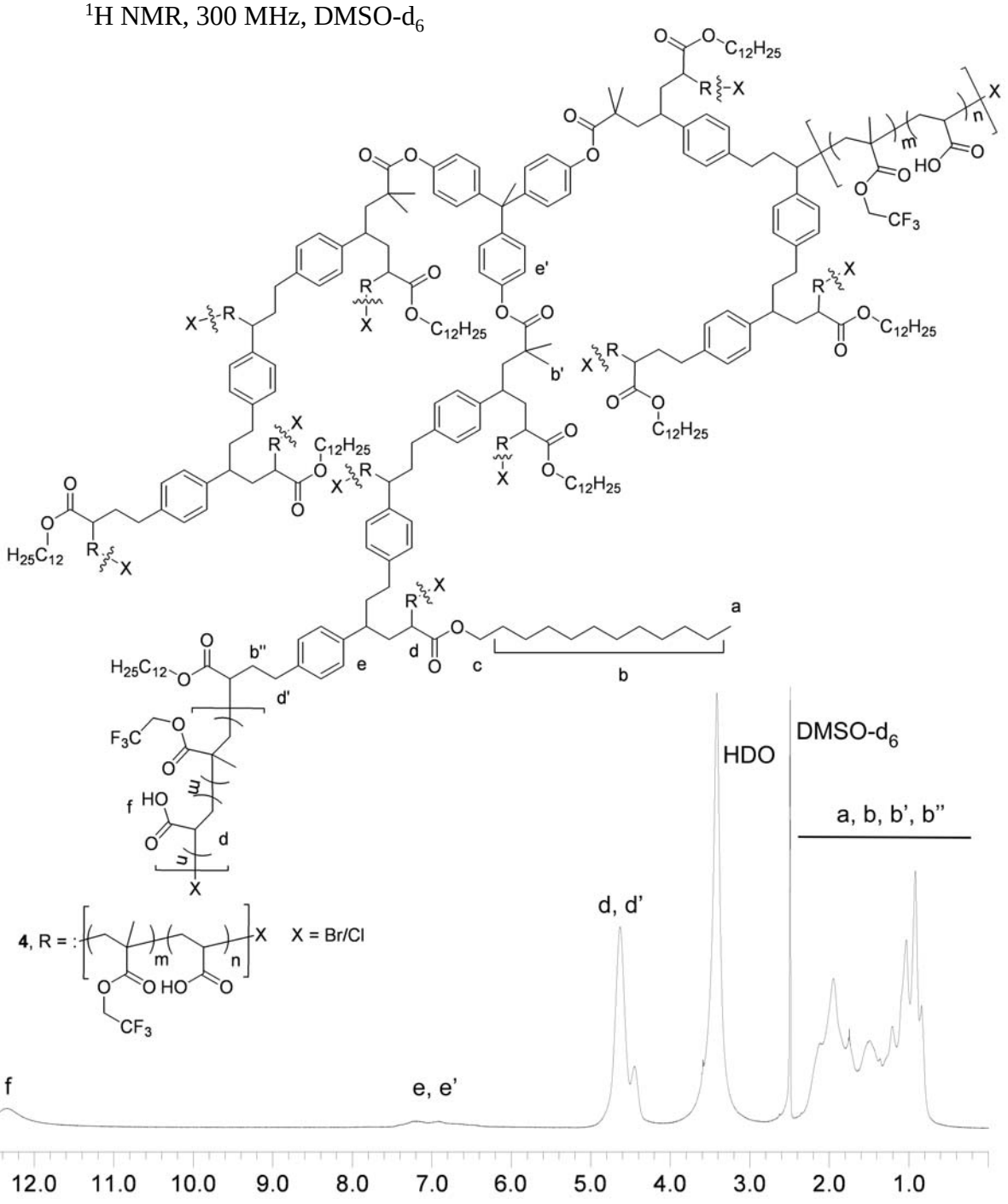

^{1}H NMR, 300 MHz, DMSO-d_6

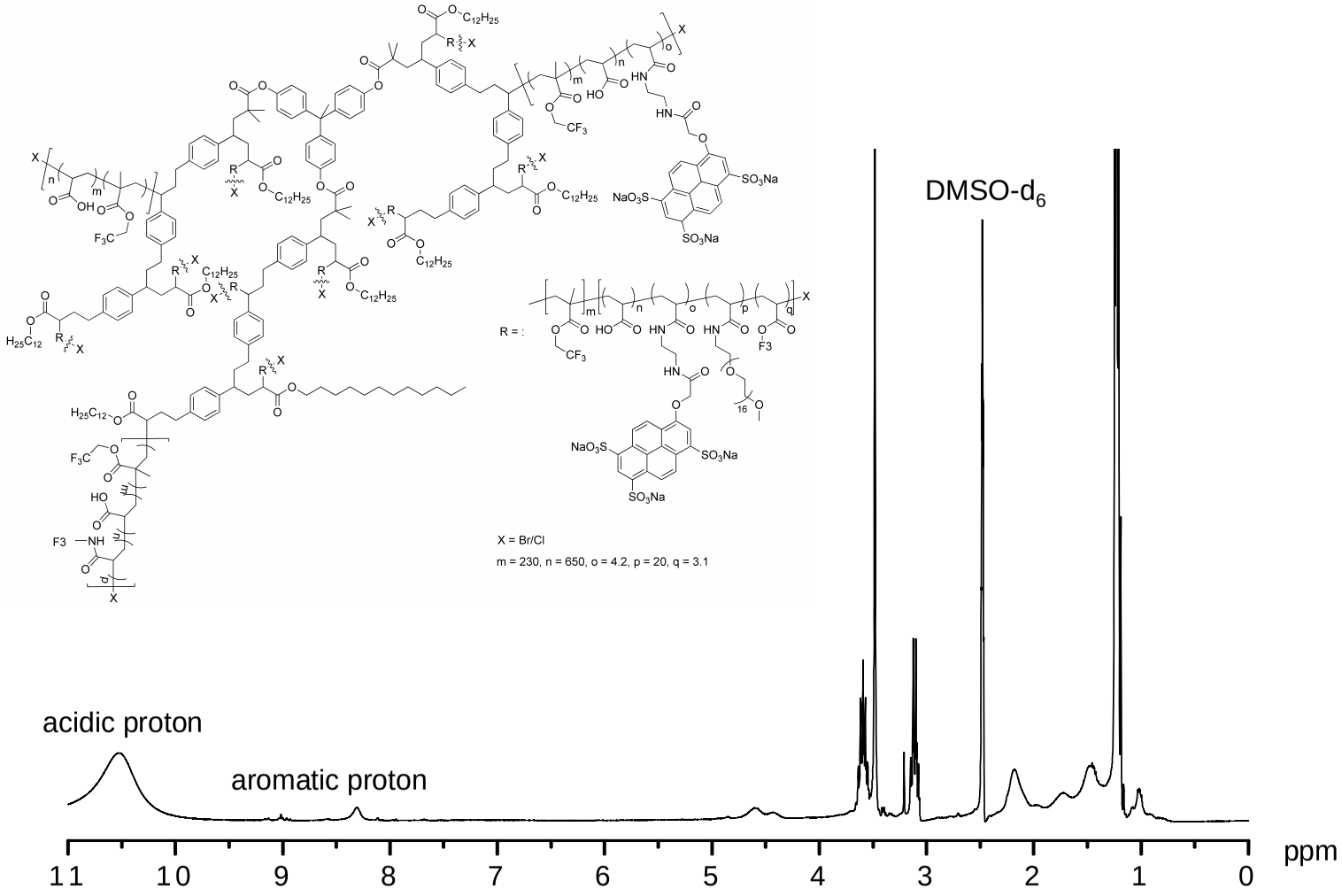

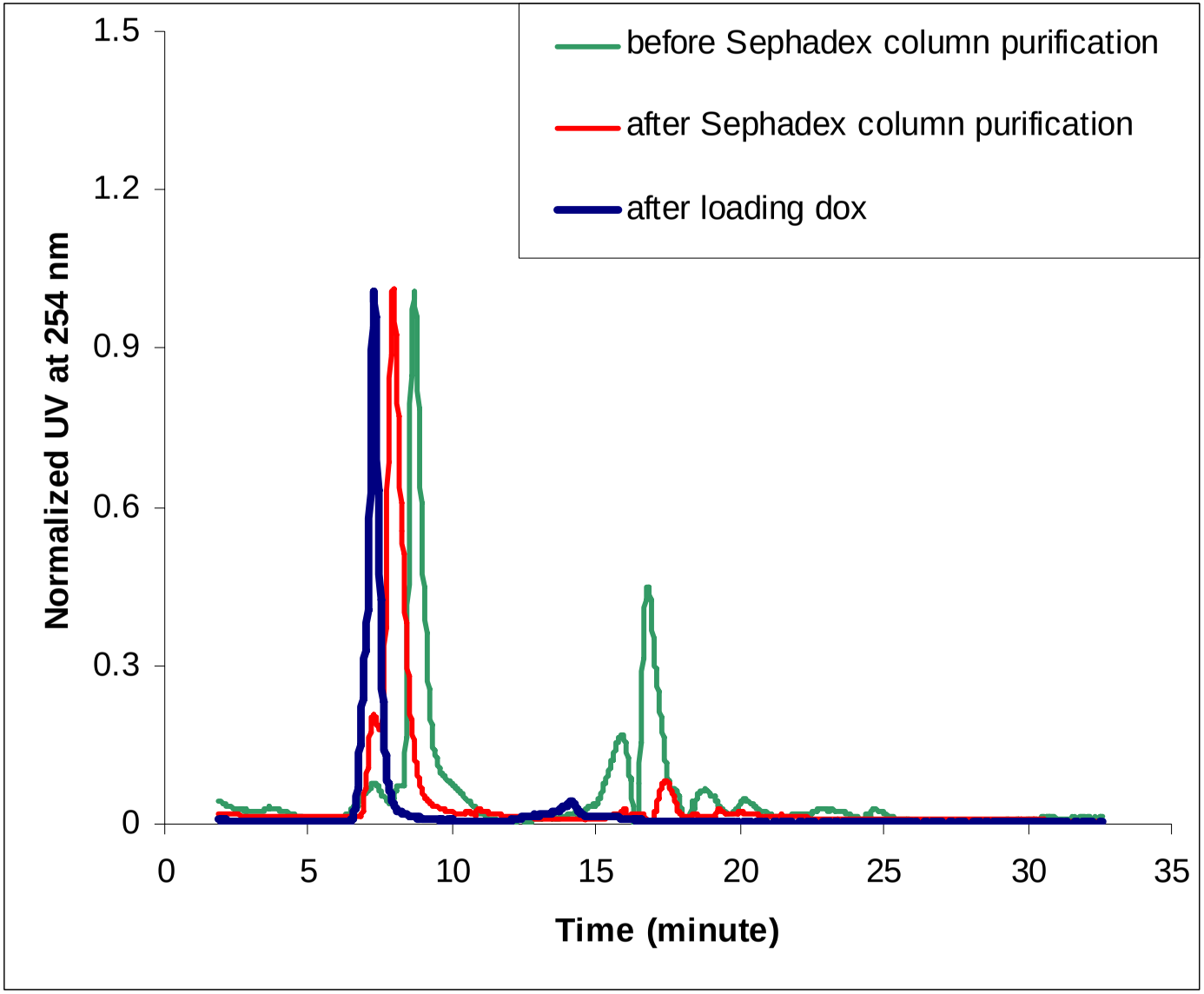
before Sephadex column purification
after Sephadex column purification
after loading dox
Normalized UV at 254 nm
1.5
1.2
0.9
0.6
0.3
0
0
5
10
15
20
25
30
35
Time (minute)

FPLC traces

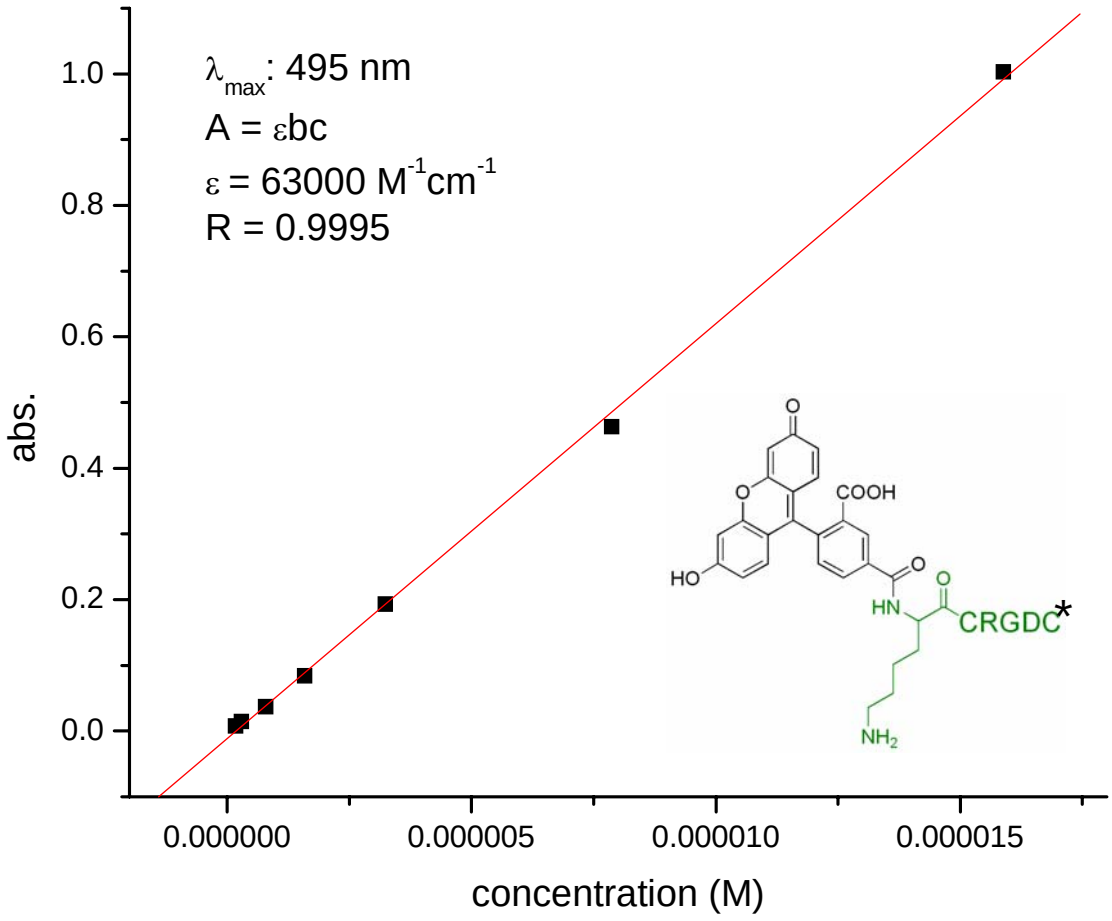

Standard curve of 5-FAM-KCRGDC in 5 mM PBS, pH ~ 7.4.
* For simplicity, the disulfide bond connecting the two cysteines was not shown

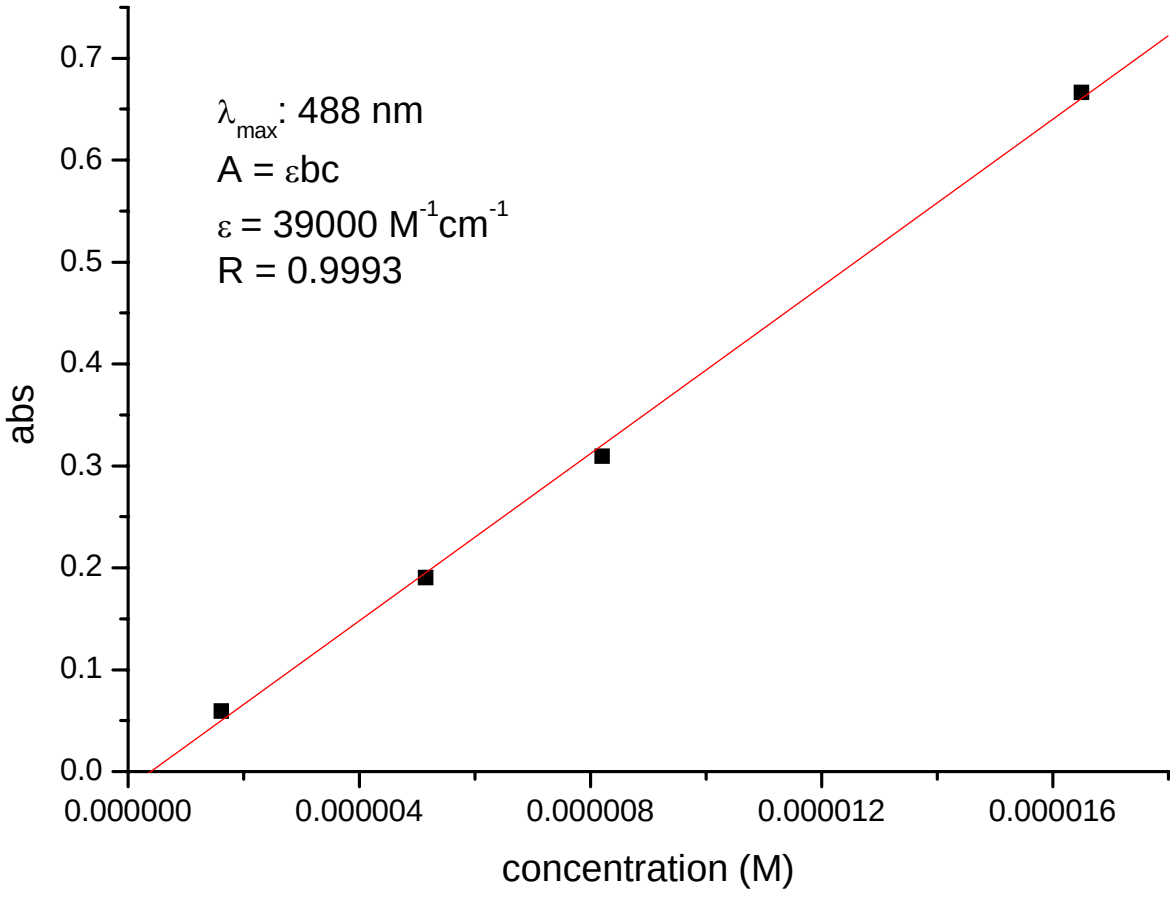

Standard curve of FITC-F3 in 5 mM PBS, pH ~ 7.4